



Application of the DLVO theory for particle deposition problems

Zbigniew Adamczyk*, Paweł Weroński

*Institute of Catalysis and Surface Chemistry, Polish Academy of Sciences, ul. Niezapominajek 1,
30-239 Cracow, Poland*

Abstract

Implications of the DLVO theory for problems associated with colloid particle adsorption and deposition at solid/liquid interfaces were reviewed. The electrostatic interactions between two planar double-layers described by the classical Poisson–Boltzmann (PB) equation were first discussed. Then, the approximate models for calculating interactions of curved interfaces (e.g. spheres) were exposed in some detail, inter alia the extended Derjaguin summation method and the linear superposition approach (LSA). The results stemming from these models were compared with the exact numerical solution for two dissimilar spheres (including the case of sphere/plane interactions) obtained in bispherical coordinate system. The electrostatic interaction energy was used in combination with dispersion interactions for constructing the DLVO energy profiles discussed next. The influence of surface roughness and charge heterogeneity on energy profiles was also discussed. It was demonstrated that in particle deposition problems the monotonically changing profiles determined by the electrostatic interactions played the most important role. In further part of the review the role of these electrostatic interactions in adsorption and deposition of colloid particles was discussed. The governing continuity equation was exposed incorporating the convective transport in the bulk and the specific force dominated transport at the surface. Approximate analytical models aimed at decoupling of these transfer steps were described. It was demonstrated that the surface boundary layer approximation (SFBLA) was the most useful one for describing the effect of electrostatic interaction at initial adsorption stages. A procedure of extending this model for non-linear adsorption regimes, governed by the steric barrier due to adsorbed particles, was also presented. The theoretical results were then confronted with experimental evidences obtained in the well-defined systems, e.g. the impinging-jet cells and the packed-bed columns

* Corresponding author. Tel.: +48-12-425-2841; fax: +48-12-425-1923.

of monodisperse spherical particles. The experiments proved that the initial adsorption flux of particles was considerably increased in dilute electrolytes due to attractive electrostatic interactions. This was found in a quantitative agreement with the convective diffusion theory. On the other hand, the rate of later adsorption stages was diminished by the electrostatic lateral interactions between adsorbed and adsorbing particles. Similarly, the experimental data obtained by various techniques (AFM, reflectometry, optical microscopy) demonstrated that these interactions reduced significantly the maximum monolayer coverages at low ionic strength. This behaviour was found in good agreement with theoretical MC-RSA simulation performed by using the DLVO energy profiles. The extensive experimental evidences seem, therefore, to support the thesis that the electrostatic interactions play an essential role in adsorption phenomena of colloid particles. © 1999 Elsevier Science B.V. All rights reserved.

Keywords: Adsorption of colloid particles; Colloid deposition; Derjaguin method; Electrostatic interactions of colloids; DLVO theory; Particle deposition

Contents

1. Introduction	138
2. Electrostatic interactions between particles	141
2.1. Two planar double-layers	143
2.2. Interactions of spheres and convex bodies	147
2.2.1. The Derjaguin method	147
2.2.2. The linear superposition method	153
2.3. Comparison of exact and approximate results for spheres	160
2.4. Influence of surface roughness and heterogeneity	163
3. The dispersion forces and the energy profiles	166
3.1. Superposition of interactions and the energy profiles	170
4. Role of specific interactions in particle deposition phenomena	174
4.1. The continuity equation	175
4.1.1. Limiting solutions for the perfect sink model	179
4.1.2. The surface force boundary layer approximation	183
4.2. Role of the lateral particle/particle interactions	188
4.2.1. The concept of the steric barrier	193
5. Experimental results	202
5.1. Experimental methods — general remarks	202
5.2. The initial deposition rates	204
5.3. Nonlinear adsorption kinetics	212
5.4. The maximum coverage	217
6. Conclusions	220
Acknowledgement	221
References	221

1. Introduction

Specific interactions among colloid and larger particles in electrolyte solutions

determine the rate of many dynamic phenomena occurring in disperse systems, e.g. aggregation, coagulation, coalescence, flocculation, membrane fouling, phase separation, stress relaxation influencing rheology, etc. Equally important are the interactions of particles with boundary surfaces leading to adsorption, deposition (irreversible adsorption) and adhesion. A quantitative description of these phenomena has implications not only for polymer and colloid science, biophysics and medicine, soil chemistry but also for many modern technologies involving various separation procedures, e.g. water and waste water filtration, membrane filtration, flotation, protein and cell separation, immobilisation of enzymes, etc.

Due to a large significance of the specific interactions numerous attempts have been undertaken in the literature to quantify them, including the pioneering works of Derjaguin and Landau [1,2] and Verwey and Overbeek [3] known as the DLVO theory. The foundation of this theory was the postulate of additivity of the dispersion and electrostatic double-layer interactions. The latter were calculated as pair interactions in an infinite electrolyte reservoir using the Poisson equation with the ion density distribution characterised in terms of the Boltzmannian statistics. In this respect, the DLVO theory can be seen as one of many applications of the Gouy–Chapman–Stern [4–6] electric double-layer model.

This model, and the DLVO theory, was vigorously criticized over the decades from the statistical mechanics viewpoint for not treating the finite ion-size and the self atmosphere effects (ion correlation) in a consistent manner [7–13]. As an alternative, many extensions of the PB equation has been formulated [8–14] by applying the mean-spherical approximation (MSA) and the Ornstein–Zernicke equation for the direct correlation function. This led to non-linear integro-differential equations whose complicated mathematical shape was prohibiting their more widespread applications. Some explicit results were derived using this approach in [15–18] for many-body problems (concentrated colloid suspensions). Both the ion correlation functions and interaction energy profiles were showed to possess an oscillatory character, i.e. at distance comparable with particle diameter the interaction energy was predicted negative (attractive) even for equally charged particles [17]. As pointed out by Ruckenstein [18] this deviation from the DLVO theory was due to the collective Coulomb interactions among all charged species particles and ions (including counterions) becoming more apparent for concentrated systems. This contrasts with the Sogami [19,20] theory who predicted deviation from DLVO even for dilute systems, governed by the ordinary PB equation. As pointed out in Overbeek [21,24], Woodward [22] and Levine [23], however, the Sogami theory proved incorrect and the basic equations of the DLVO remain valid for dilute systems.

Other approaches aimed at improving the PB equation were the phenomenological theories based on the local thermodynamic balance [25–28]. They allowed one to consider the dielectric saturation effect [25,28–33] manifesting itself in the decrease in the medium permittivity at higher field strength or the ion polarisation effect considered in Levine [34].

Other corrections to the PB equation were introduced by Levin et al. [35–37], in particular the image and self-atmosphere effect, cavity potential (another formula-

tion of the ion polarisation effect), medium compressibility (electrostriction effect), discreteness of charge effect, etc. For a dilute electrolyte, the ion density fluctuations in the diffuse part of the double-layer pose an additional complicating factor [38]. It should be remembered, however, that many of these corrections play a significant role under extreme conditions only, rarely met in practice: field strength larger than 10^6 V cm^{-1} , electrolyte concentration above 1 M, etc. Spaarnay [28] showed for instance the polarisation energy of an ion remains of the order of 0.1 kT unit even for maximum field strength occurring at an interface.

It seems that for higher electrolyte concentration the most important corrections should originate from the volume excluded effect [25–28,39–41] which has a direct physical interpretation. Hence, the concentration of counterions accumulating at regions of high potential cannot exceed some limiting value strictly related to the ion hydrated radius. It can be easily estimated that these limiting (maximum packing) values are of the order of 10 M [42]. In principle, the Stern model [3,4] can be treated as the first attempt of considering the volume excluded effect for adsorbing ions. It is obvious, however, that for higher surface charges the excluded volume effect should also affect ion distribution within the diffuse layer. A quantitative phenomenological description of this effect for an isolated double-layer (electrode) was first elaborated in Brodowsky and Strehlow [25] and Wicke [26]. The authors introduced the volume blocking parameter analogous to the van der Waals correction for the self volume. A considerable positive deviation from the Gouy–Chapman theory was predicted for ion concentrations larger than 0.01 M and electrode charge density exceeding $12 \mu\text{C cm}^{-2}$. Hückel and Krafft [7] and Levine and Bell [8] criticized the above approach for not taking into account the ion self-atmosphere and the cavity potential. However, Spaarnay [28], who also considered the excluded volume effect, showed that this critique was irrelevant at least for planar double-layers.

Adamczyk et al. [39–42] studied the influence of the excluded volume effect on potential distribution between two planar double layers. They also calculated the pressure between the plates and the force and interaction energy of two colloid particles of convex shape using the generalised Derjaguin method. It was shown that this effect, although considerably influencing the potential distribution, played rather an insignificant role in particle interactions except for very short separations of the order of 5–10 Å [39–41].

In our opinion all the above mentioned refinements of the PB equation and the DLVO theory lead to second order effects, difficult to be detected in real systems. They will be masked by such primary effects like charge regulation (exchange kinetics), surface roughness and heterogeneity or surface deformations always occurring at short separations. Therefore, we should put forward a thesis that the classical form of the DLVO theory is adequate for interpreting behaviour of colloid systems. This thesis seems to be confirmed by the excellent work [43] concerning the direct force measurements for mica plates in various electrolyte solutions. The goal of this fragmentary review is an attempt to prove this for the particle/solid interface systems.

The organisation of our paper is the following: in Section 2 we discuss elec-

trostatic interactions between two planar double-layers in terms of the classical Poisson–Boltzmann (PB) equation. Then, the approximate models for calculating interactions of curved interfaces (e.g. spheres) are exposed in some detail, with the emphasis on the extended Derjaguin summation method. The results stemming from these models are compared with the exact numerical solution for two dissimilar spheres (including the case of sphere/plane interactions) obtained in bispherical coordinate system. Next, the DLVO energy profiles originating from the superposition of electrostatic and dispersion contributions are discussed together with the influence of surface roughness and charge heterogeneity effects. In further part of our review the role of these interactions in adsorption and deposition of colloid particles on solid surfaces is considered. The governing continuity equation is formulated, incorporating the convective transport in the bulk and the specific force dominated transport at the surface. Approximate analytical models aimed at decoupling these transfer steps are described, in particular the powerful surface boundary layer approximation (SFBLA). A procedure of extending this model to non-linear adsorption regimes, governed by the steric barrier due to adsorbed particles, is also exposed. The theoretical results are then confronted with experimental data obtained in the well-defined systems, e.g. the impinging-jet cells and the packed-bed columns using various experimental techniques of detecting particle monolayers, e.g. AFM, reflectometry, electron and optical microscopy. The significance of the DLVO theory for interpreting these data will be pointed out.

2. Electrostatic interactions between particles

The electrostatic force \mathbf{F} acting between two charged particles immersed in an electrolyte of arbitrary composition can be obtained from the constitutive relationship derived by Hoskin and Levine [44]

$$\mathbf{F} = \iint_S \left[\left(\Delta \mathbf{P} + \frac{\varepsilon}{8\pi} E^2 \right) \hat{\mathbf{n}} - \frac{\varepsilon}{4\pi} (\mathbf{E} \cdot \hat{\mathbf{n}}) \mathbf{E} \right] dS \quad (1)$$

where $\Delta \mathbf{P}(\psi)$ is the osmotic pressure tensor, ψ is the electrostatic potential, $\hat{\mathbf{n}}$ the unit vector normal to the surface S surrounding one of the particles, ε is the dielectric constant of the suspending medium which is assumed a field independent quantity and $\mathbf{E} = -\nabla\psi$ is the field strength.

In the case of anisotropic particles there appears also a torque on particles [45–47] which can be expressed by an equation analogous to Eq. (1).

In the limiting case of a flat geometry (two infinite planar interfaces interacting across electrolyte solution) Eq. (1) reduces to the simple form describing the uniform force per unit area

$$F = \Delta P(x) - \frac{\varepsilon}{8\pi} \left(\frac{d\psi}{dx} \right)^2 = \text{const} \quad (2)$$

where F , P are scalars, x is an arbitrary position between plates, k is the Boltzmann constant and T the absolute temperature.

The interaction energy ϕ can be most directly obtained by integrating Eqs. (1) and (2) along a path starting from infinity [48]. However, in practice, one uses for this purpose the method developed by Vervey and Overbeek [3] based on the Lippmann equation.

As can be noticed, for an explicit evaluation of the interaction force or energy the electrostatic potential distribution in space is needed. This quantity can be calculated after solving the Poisson–Boltzmann equation with appropriate boundary conditions. By neglecting the dielectric saturation and assuming that the electrolyte is composed of N ions of valency z_i (exhibiting ideal bulk behaviour) one can formulate the PB equation in the classical form [48]

$$\nabla^2\psi = -\frac{4\pi e}{\varepsilon} \sum_{i=1}^N z_i n_i^b e^{-z_i e\psi/kT} \quad (3)$$

where e is the elementary charge and n_i^b is the bulk concentration of i -th ion.

Due to non-linearity of the PB equation no analytical solutions were found in the case of multi-dimensional problems, e.g. two spherical particles in space being of primary practical interest. Only recently cumbersome numerical solutions of this problem were reported for dissimilar sphere and sphere/plane geometry as discussed later on.

One of the frequent methods of avoiding mathematical difficulties by solving the PB equation is the linearisation procedure consisting in expansion of the exponential terms and neglecting higher order terms. This procedure, which seems justified for $mx(z_i e\psi/kT) < 1$ (where mx means the maximum term) converts Eq. (1) into the simple form

$$\nabla^2\psi = \kappa^2\psi \quad (4)$$

where

$$\kappa^{-1} = Le = \left(\frac{\varepsilon kT}{8\pi e^2 I} \right)^{1/2}$$

is the Debye screening length, a parameter of primary interest for any particle interaction problem and $I = \frac{1}{2} \sum_{i=1}^N z_i^2 n_i^b$ is the ionic strength of the electrolyte solution.

Accordingly, the osmotic pressure tensor assumes for low potentials the simple form

$$\Delta P = kTI\bar{\psi}^2 \mathbf{I} \quad (5)$$

As discussed in Adamczyk and Warszyński [48] the significance of Eq. (4) is further increased by the fact that it is also applicable for non-linear systems (high

surface charges of particles) at distances large in comparison with Le where the potential decreases to low values due to electrostatic screening. This observation was the basis of the powerful linear superposition approach (LSA) discussed later on.

A remarkably simple analytical solution of Eq. (4) can be derived for an isolated spherical particle immersed in arbitrary electrolyte or for a two plate system. However, an application of Eq. (4) to the two-sphere problem started already by Vervey and Overbeek [3] is leading to complicated iterative or series solutions less useful for practice.

Another method of finding the approximate, closed form solutions for the two-sphere geometry was pioneered by Derjaguin [1,2] who applied the integration procedure exploiting the solution for two flat plates. In Section 2.1 we should discuss in some detail the known results for this geometry including the short and large plate separation cases.

2.1. Two planar double-layers

Let us consider two charged flat plates immersed in an electrolyte solution of arbitrary composition and infinite extension, separated by the distance h apart. Assume that the thickness of the plates is much larger than the screening length Le and that there are no space charges within the plates so the electrostatic potential remains constant there. The PB equation, Eq. (1) assumes for the planar geometry the simpler, one-dimensional form

$$\frac{d^2\bar{\psi}}{d\bar{x}^2} = -\frac{1}{2\bar{I}} \sum_{i=1}^N z_i \alpha_i e^{-z_i e \bar{\psi} / kT} \quad (6)$$

where $\bar{x} = x/Le$ is the dimensionless distance, $\bar{\psi} = \psi e / kT$ is the dimensionless potential, $\bar{I} = I/n_1^b$ and $\alpha_i = n_i^b/n_1^b$.

The general electrostatic boundary conditions for Eq. (6) are

$$\begin{aligned} \frac{d\bar{\psi}}{d\bar{x}} &= -\bar{\sigma}_1^0 \quad \text{at } \bar{x} = 0 \\ \frac{d\bar{\psi}}{d\bar{x}} &= \bar{\sigma}_2^0 \quad \text{at } \bar{x} = \bar{h} \end{aligned} \quad (7)$$

where $\bar{h} = h/Le$ and

$$\begin{aligned} \bar{\sigma}_1^0 &= \sigma_1^0 (4\pi eLe / \varepsilon kT) \\ \bar{\sigma}_2^0 &= \sigma_2^0 (4\pi eLe / \varepsilon kT) \end{aligned}$$

are the dimensionless surface charges at both plates and σ_1^0, σ_2^0 are the surface charges at the plates.

Eq. (7), referred often to as constant charge (c.c) boundary conditions implies

that the charge at each plate remains fixed, irrespective on their separation distance. As discussed in Adamczyk et al. [39–41] this situation seems highly unfavourable thermodynamically at close separations due to considerable increase of the electrostatic potential between plates. Thus, due finite binding energy of ions, the plate charge is expected to change upon their approach. This charge relaxation process can proceed quite slowly as indicated in Frens and Overbeek [49] so a full equilibration of charges is expected under experimental conditions of the direct force measurements [43] only. When the system remains in equilibrium at every separation then the plate charges must change upon approach in order to meet the boundary conditions, expressed by Eq. (7). In this case this equation is formulated in a more convenient way as

$$\begin{aligned}\bar{\psi} &= \bar{\psi}_1^0 \quad \text{at } \bar{x} = 0 \quad (\text{surface of the first plate}) \\ \bar{\psi} &= \bar{\psi}_2^0 \quad \text{at } \bar{x} = \bar{h} \quad (\text{surface of the second plate})\end{aligned}\quad (8)$$

These are the so called constant potential (c.p.) boundary conditions used commonly in the literature starting from the work of Verveij and Overbeek [3]. Sometimes the mixed case is considered when one of the plates is postulated to maintain the c.c. conditions, whereas the second fulfills the c.p. conditions [50]. In the case when the surface charge is due to ionizable (amphoteric) groups the boundary conditions for the PB equation assume the form of non-linear implicit expressions for the surface potential as a function of ionisation constants, pH, etc. [51,52]. Since these boundary conditions are very specific and system dependent they will not be considered in further discussion.

The above boundary conditions should be used for eliminating the constants of integration from the general expression obtained by a twofold integration of the PB equation, Eq. (6), i.e.

$$\int \frac{d\bar{\psi}}{\left[\frac{1}{\bar{I}} \sum_{i=1}^N \alpha_i e^{-z_i \bar{\psi}} + C_1 \right]^{1/2}} = \bar{x} + C_2 \quad (9)$$

Unfortunately, this integral cannot be expressed in any closed form for arbitrary surface charge.

For a symmetric electrolyte Eq. (9) simplifies to the form

$$\int \frac{d\bar{\psi}'}{\sqrt{2 \cosh \bar{\psi}' + C_1}} = \bar{x} + C_2 \quad (10)$$

where $\bar{\psi}' = z\bar{\psi}$.

In this case, the integral can be expressed in terms of the elliptic integral of the first kind as done originally by Verveij and Overbeek [2] who also presented graphical solutions of interaction energy for equally charged surfaces and gave

approximate solutions for large surface potentials. Levine et al. [53–55] formulated approximations valid for small and large distances in the case of an asymmetric electrolyte.

The interactions between identical plates under the c.c. and c.p. boundary conditions were also tabulated by Honig and Mul [56], whereas Devereux and de Bruyn [57] extensively tabulated the interactions for dissimilar plates under the c.p. boundary condition. As pointed out by McCormack et al. [52] some results presented in these tables are charged with considerable errors, especially for extreme values of the surface potential. In the latter work various solutions of Eq. (10) are given in the form of the elliptic integrals and Jacobi elliptic functions for both the c.c., c.p. and mixed boundary conditions. Graphical methods of determining the interaction energy between plates were also presented. Due to recent progress in numerical methods the tabulated and graphical solutions [3,52,56,57] seem less useful than the direct solutions of the non-linear PB equation, Eq. (7), as done for example in Adamczyk et al. [39–41] by applying the Runge Kutta method.

The only exact, analytical solutions of PB equation can be derived for the linear model (Eq. (4)), when the dimensionless potentials (or surface charges) of both plates remain smaller than unity. By assuming this one can easily express the force per unit area of plates (pressure) using Eq. (2) in the form [48]

$$\Delta\Pi = kT n_1^b \bar{I} \left[\pm (\bar{\Psi}_1^{0^2} + \bar{\Psi}_2^{0^2}) \operatorname{cosech}^2 \bar{h} + 2\bar{\Psi}_1^0 \bar{\Psi}_2^0 \frac{\cosh \bar{h}}{\sinh^2 \bar{h}} \right] \quad (11)$$

where the upper sign denotes the c.c. model and the lower sign the c.p. model.

The interaction energy per unit area is accordingly given by

$$\Phi = Le \int_{\infty}^{\bar{h}} \Delta\Pi d\bar{h} = kT Len_1^b \bar{I} \left[\mp (1 - \coth \bar{h}) (\bar{\Psi}_1^{0^2} + \bar{\Psi}_2^{0^2}) + \frac{2\bar{\Psi}_1^0 \bar{\Psi}_2^0}{\sinh \bar{h}} \right] \quad (12)$$

Eq. (12) was first derived for the c.p. case by Hogg et al. [58] and will be referred to as the HHF model. Wiese and Healy [59] and Usui [60] considered the c.c. model, whereas Kar et al. [50] derived analogous formula for the interaction energy in the case of the ‘mixed’ case, i.e. c.p. at one plate and c.c. at the other.

It is interesting to note that the limiting forms of Eq. (12) for short separations, i.e. for $\bar{h} \rightarrow 0$ are

$$\begin{aligned} \Phi &= kT Len_1^b \bar{I} \left[\frac{(\bar{\Psi}_1^0 + \bar{\Psi}_2^0)^2}{\bar{h}} - \bar{\Psi}_1^{0^2} - \bar{\Psi}_2^{0^2} \right] \quad \text{c.c. model} \\ \Phi &= -kT Len_1^b \bar{I} \left[\frac{(\bar{\Psi}_1^0 - \bar{\Psi}_2^0)^2}{\bar{h}} - \bar{\Psi}_1^{0^2} - \bar{\Psi}_2^{0^2} \right] \quad \text{c.p. model} \end{aligned} \quad (13)$$

It can be easily deduced that the interaction energy for the c.c. model diverges to plus infinity (repulsion) for short separations, whereas the c.p. model predicts

diametrically different behaviour, i.e. the interaction energy tends to minus infinity (attraction) for the same combination of surface potentials as for the c.c. case. However, in the case of equal potentials and the c.p. model or opposite potentials and the c.c. model the value of ϕ remains finite, equal $kT Len_1^b \bar{I} (\bar{\psi}_1^{0^2} + \bar{\psi}_2^{0^2})$. The divergence between both models appearing at short separations seems highly unphysical. It is caused by the violation of the low potential assumption. Indeed, in order to observe the c.c. boundary conditions, the surface potential of the plates should tend to infinity when they approach closely each other, even if at large separations these potentials were very low. As a consequence, $\bar{\psi} \gg 1$ for $\bar{h} \rightarrow 0$ and the linear P.B. equation is not valid. Hence, Eqs. (11) and (12) is incoherent for the c.c. model and should not be used for short separations. This was pointed out originally by Gregory [61] who also proposed the approximate ‘compression’ method for analysing plate interactions for the c.c. conditions. However, explicit analytical results were only derived for equal plate charges (potentials).

The deficiency of the linear c.c. model was also demonstrated in Adamczyk et al. [39–41] and Prieve [62] by analysing the asymptotic behaviour of the non-linear PB equation in the limit of small plate separation. It was shown that the force and interaction energy of plates at small separations can be approximated in the c.c. model by the expressions

$$\begin{aligned} \Delta\Pi &= kT n_i^b \bar{I} \frac{2|\bar{\sigma}_1^0 + \bar{\sigma}_2^0|}{|z|\bar{h}} \\ \phi &= kT n_i^b \bar{I} \frac{2|\bar{\sigma}_1^0 + \bar{\sigma}_2^0|}{|z|} \ln \bar{h} \end{aligned} \quad (14)$$

As can be noticed the interaction energy remains positive at short separations and tends to infinity at much slower rate (logarithmically) in comparison to the linear model. It can be easily estimated that for $\bar{h} \ll 0.01$ the differences between the linear and non-linear models increase to an order of magnitude. It is interesting to mention, however, that in the case of the c.p. boundary conditions the asymptotic expression for the interaction energy at short separations remains the same for the linear and non-linear models [39–41] provided that $\bar{\sigma}_1^0 \neq \bar{\sigma}_2^0$.

On the other hand, for larger separations, both models reduce to the same asymptotic form

$$\Phi = kT Len_1^b \bar{I} \bar{\psi}_1^0 \bar{\psi}_2^0 e^{-\kappa \bar{h}} \quad (15a)$$

As one can notice, the interaction energy between plates decreases exponentially at large separations, the rate of decay being proportional to $\kappa = 1/Le$.

It is also worthwhile noting that for equal plate potentials the expressions for the force and interaction energy Eqs. (11) and (12) become,

$$\Delta\Pi = 4kT n_1^b \bar{I} \bar{\psi}^{0^2} \frac{e^{-\bar{h}}}{(1 \mp e^{-\bar{h}})^2}$$

$$\Phi = 4kTLen_1^b \bar{I} \bar{\Psi}^{0^2} \frac{e^{-\bar{h}}}{1 \mp e^{-\bar{h}}} \quad (15b)$$

where the upper sign denotes the c.c. model. Eq. (15b) was derived originally by Derjaguin [1].

All the discussed results are valid for metallic plates or plates of infinite thickness when the inside electric potential remains constant. The influence of the finite plate thickness on their interactions was studied in detail by Oshima [63–66] both under linear and non-linear regimes. It was shown that for situations of practical interest (aqueous solutions) the correction stemming from finite plate thickness remains negligible.

2.2. Interactions of spheres and convex bodies

As mentioned, the analytical and numerical solutions for the plates can be exploited for constructing approximations for the spherical and anisotropic particle interactions. The anisotropic particle systems are of increasing interest considering the fact that the shape of most bioparticles, e.g. bacteria, viruses, proteins deviates significantly from the spherical shape [67]. Other examples of highly anisotropic particles are the red blood cells, blood platelets, pigments and synthetic inorganic colloids: gold, silver iodide, silver bromide, barium sulphate etc. [68,69]. The entire variety of non-spherical particles has been synthesized over decades in the well-known school of Matijević [70–75]. Also, model polymeric colloid system of non-spherical monodisperse particles, e.g. PTFE or polystyrene latexes [76] or silica covered bohemite [77] can now be prepared in a reproducible way.

An exact determination of interaction energy for spherical and anisotropic particle systems and arbitrary electrolyte composition seems prohibitive due to non-linearity of the governing PB equation and lack of appropriate orthogonal coordinate systems, except for the case of two sphere configuration. However, by observing that particle and protein adsorption takes usually place from concentrated electrolyte solutions one can treat the electrostatic interactions as short-ranged (in comparison with particle dimensions). This enables one to avoid the solution of the many-body problem by exploiting the additivity rule and calculating the interparticle energy as sum of contributions stemming from particle pairs. Even if the problem is effectively reduced to a two-particle interactions, it cannot be solved in any exact form. Approximate methods are available only, such as the Derjaguin summation approach exploiting the results for plates discussed next, and the LSA approach discussed later on.

2.2.1. The Derjaguin method

According to the original Derjaguin method [1,2] the interactions of spheres were calculated as a sum (integral) of corresponding interactions of infinitesimal surface elements (rings) having a planar geometry. The summation was carried out in the region close to minimum separation distance h_m by assuming a fast decay of interactions when proceeding further from this region. Thus, the Derjaguin method

is only valid if the radii of the spheres a_1 and a_2 are both much larger than the double-layer thickness, i.e. for κa_1 and $\kappa a_2 \gg 1$. It can be demonstrated that in the Derjaguin method the force \mathbf{F} and interaction energy ϕ of two unequal spheres is given by the relationship

$$\mathbf{F} = 2\pi LeG_D \int_{\bar{h}_m}^{\infty} \Delta\Pi(\bar{h})d\bar{h}\hat{\mathbf{n}} = 2\pi G_D\Phi(h_m)\hat{\mathbf{n}}$$

$$\phi = 2\pi LeG_D \int_{\bar{h}_m}^{\infty} \Phi(\bar{h})d\bar{h} \quad (16)$$

where $\bar{h}_m = \kappa h_m$ and $G_D = a_1 a_2 / (a_1 + a_2)$ is the geometrical Derjaguin factor equal to $0.5a$ for two equal spheres and a for plane/sphere interactions. Note that the force is acting along the vector connecting particle centres.

By using Eqs. (16) and (12) one can derive the explicit expressions for sphere interaction energy in the form

$$\phi = \varepsilon \left(\frac{kT}{2e} \right)^2 G_D \left[\mp (\bar{\psi}_1^{0^2} + \bar{\psi}_2^{0^2}) \ln(1 - e^{-2\kappa h_m}) + 2\bar{\psi}_1^0 \bar{\psi}_2^0 \ln \frac{1 + e^{-\kappa h_m}}{1 - e^{-\kappa h_m}} \right] \quad (17a)$$

where the upper sign denotes the c.c. boundary condition. Note that in contrast to Eq. (12) the interaction energy for spheres does not depend explicitly on I .

Eq. (17a) was first derived by Hogg et al. [58] for the c.c. model and Wiese and Healy [59] and Usui [60] for the c.p. model.

It is interesting to note that in the limit $h_m \rightarrow 0$ Eq. (17a) becomes

$$\phi = \mp \varepsilon \left(\frac{kT}{2e} \right)^2 G_D (\psi_1^0 \pm \psi_2^0)^2 \ln \kappa h_m \quad (17b)$$

where the upper sign denotes the c.c. model.

For equal sphere potential and the c.p. model Eq. (17a) simplifies to the form derived originally by Derjaguin

$$\phi = \varepsilon a \left(\frac{kT}{e} \right)^2 G_D \bar{\psi}^{0^2} \ln(1 + e^{-\kappa h_m}) \quad (18)$$

Eqs. (17a,b) and (18) are commonly used in the literature for determining stability criteria of colloid suspension [58] and for describing the plane/particle interactions in particle deposition problems [58,78].

Due to recent interest in interactions of anisotropic particles mentioned above, the Derjaguin method was generalised by White [79] and Adamczyk et al. [39–41] to convex bodies (see Fig. 1). The first step of these calculations was determining the minimum separation distance h_m of the two surfaces involved (cf. Fig. 1). Then, the local Cartesian coordinate systems (x_1, y_1, z_1) and (x_2, y_2, z_2) are introduced (with the colinear axes z_1 and z_2 and the x_1, x_2 axes forming the angle φ) and four

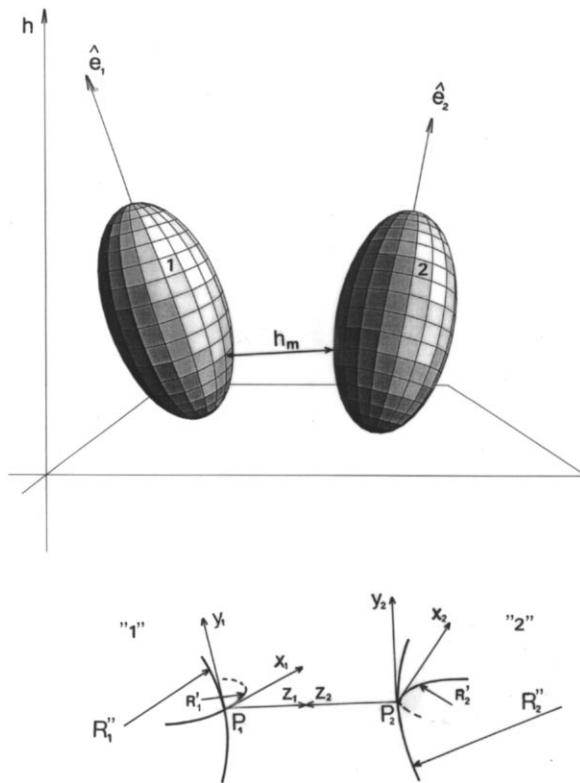


Fig. 1. A schematic representation of the interaction of two convex bodies in space.

principal radii of curvature R_1', R_1'', R_2', R_2'' at these points are evaluated by assuming that the surfaces are quadratically curved in the vicinity at P_1, P_2 . Finally, the interaction energy is calculated as the surface integral of the plate/plate interactions. The generalised Derjaguin factor can be then expressed in the form [79]

$$G_D = \sqrt{\frac{R_1' R_1'' R_2' R_2''}{(R_1' + R_2')(R_1'' + R_2'') + (R_1'' - R_1')(R_2'' - R_2') \sin^2 \varphi}} \quad (19)$$

In the case of particle/plane or two coplanar particle configurations one has $\varphi = 0$ and Eq. (19) simplifies to the form derived by Adamczyk et al. [39–41].

Despite apparent simplicity, it is very inconvenient to apply Eq. (19) for three-dimensional situations except for the crossed-cylinder problem when G_D can be expressed for orientations close to 90° as

$$G_D = \frac{1}{\sin \beta} \sqrt{R_1 R_2} \quad (20)$$

where β is the angle formed by cylinder axes and R_1, R_2 are the radii of the cylinders.

The main problem when using Eq. (19) is finding the points of the minimum separation of the two bodies involved as a function of their mutual orientation and consequently to determine h_m . Even for such simple particle shape as spheroids, one has to solve a high order non-linear trigonometric equations which can only be done in an efficient way by iterative methods [80,81]. However, analytical results can be derived, for limiting orientations of prolate and oblate spheroids as shown in Table 1. It is interesting to observe that the ratio between the Derjaguin factors (and hence of the interaction energy) for the parallel and perpendicular orientations of prolate spheroid (against a planar boundary) equals $1/As^2$ (where $As = b/a$ is the shorter to longer axis ratio). This means that the electrostatic attraction will be much higher for the parallel orientation (at the same separation distance h_m) so the particles will tend to adsorb parallel.

In the case of electrostatic repulsion (adsorption against an electrostatic barrier) the particles will preferably adsorb under the perpendicular orientation. The same concerns the oblate spheroid adsorption.

It is interesting to note that in the case of spheroid/plane interactions the Derjaguin factor can be evaluated analytically as a function of the orientation angle α . For prolate spheroids one has

$$G_D = a \frac{As^2}{As^2 \cos^2 \alpha + \sin^2 \alpha} \quad (21a)$$

whereas for the oblate spheroids the solution is

$$G_D = a \frac{As}{As^2 \cos^2 \alpha + \sin^2 \alpha} \quad (21b)$$

The dependence of G_D/a on α determined from these equations is shown in Fig. 2 for prolate spheroids and in Fig. 3 for oblate spheroids. In accordance with a previous discussion, the differences between the perpendicular ($\alpha = 90^\circ$) and parallel ($\alpha = 0^\circ$) orientations increase when the parameter A becomes small, e.g. for very elongated or flattened particles. Note also that the most significant changes in G_D (for particle/wall interactions) occur around $\alpha = 0^\circ$, i.e. a slight deviation from the parallel orientation will result in an abrupt change of interactions.

The situation becomes more complicated in the case of particle/particle interactions, occurring for example during slow aggregation, since the Derjaguin factor will depend (for a fixed h_m) not only on two relative orientation angles but also on the relative position of the spheroids in space. This makes it difficult to present the results graphically in the general case. However, some limiting cases can be visualised, e.g. for the coplanar orientation of spheroids (when the symmetry axes are parallel to the common adsorption plane) and the crossed-orientation (one particle above the other).

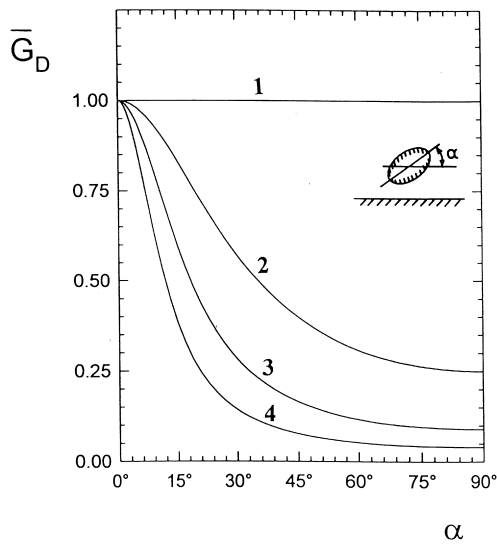


Fig. 2. The dependence of the dimensionless Derjaguin geometrical factor $\bar{G}_D = G_D / a$ on the angle α for prolate spheroid/plane interactions. (1) $As = 1$ (spheres); (2) $As = 0.5$; (3) $As = 0.3$; (4) $As = 0.2$.

In Fig. 4 the interactions between spheroids are visualised in such a way that the length of the line normal to the spheroid surface, connecting the contour represents the Derjaguin factor at this point for a given orientation. As can be easily

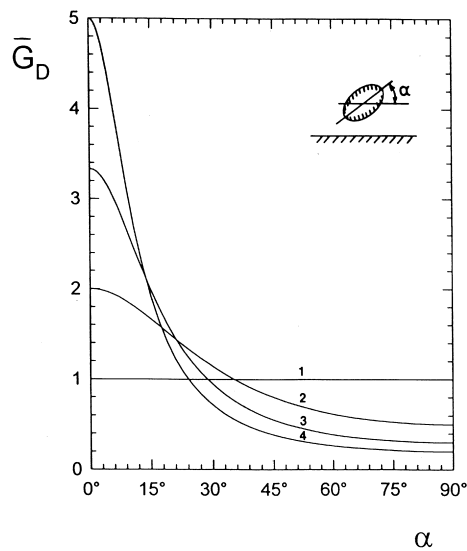


Fig. 3. Same as in Fig. 2 but for oblate spheroids.

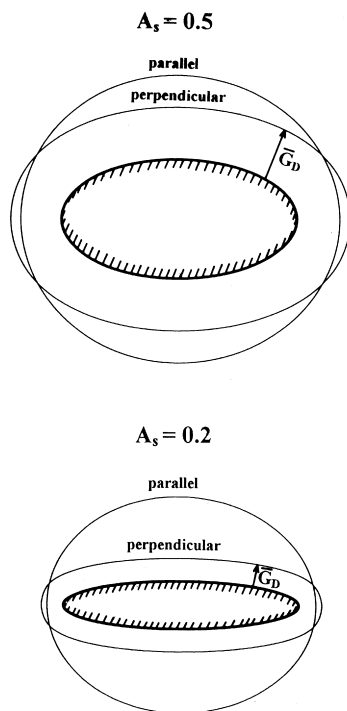


Fig. 4. Graphical representation of the spheroid/spheroid interactions (coplanar orientation); the contours give the geometrical Derjaguin factor G_D/a at the given position of the two spheroids for parallel and perpendicular orientations, respectively.

deduced from Fig. 4, the repulsive interactions will be the smallest for the edge-to-edge orientation.

Another limiting case of the two spheroid interactions is the crossed particle configuration when the particle centres are above each other and the symmetry axes form the angle β (see Fig. 5). For comparison the results for the cylinder are shown as well. It can be observed that a considerable change in the orientation angle β (crossed particles) is predicted to influence little the particle interactions which quantitatively confirms the usefulness of the crossed cylinder configuration in the direct force measurements technique [43].

It should be mentioned that the Derjaguin method and in consequence all the data shown in Table 1 are not limited to electrostatic interactions but also to other interactions whose range remains smaller than particle dimension (e.g. the van der Waals interactions). However, a serious limitation of the method is that it breaks down at larger particle/particle or particle/wall separations. This leads to an overestimation of the interactions and to a wrong asymptotic dependence of ϕ on the distance h_m . Recently, Bhattacharjee and Elimelech [82] have undertaken an attempt to remove this deficiency by developing the so called surface element

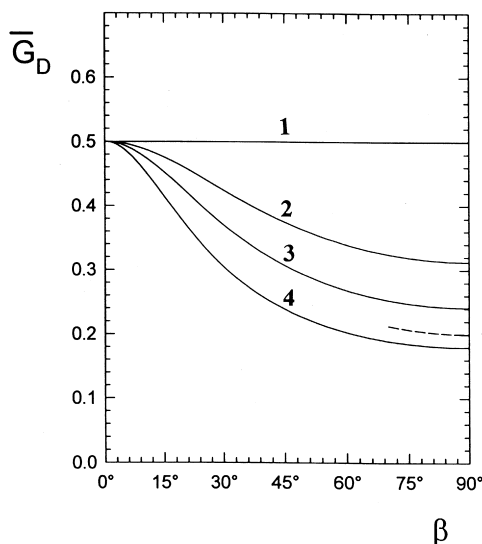


Fig. 5. The Derjaguin factor $\bar{G}_D = G_D / a$ for two crossed spheroids whose symmetry axes form the angle β . (1) $As = 1$ (spheres); (2) $As = 0.5$; (3) $As = 0.3$; (4) $As = 0.2$; the broken line denotes the results for crossed cylinders.

integration (SEI) procedure. Their approach is similar to the Derjaguin method, but the integration domain extends over the entire surface of the interacting particle, including the region opposite to the interface, where the sign of interactions is assumed to change. It was demonstrated in Bhattacharjee and Elimelech [82] that the method predicts results which are in good agreement with the numerical solution of the linearised PB equation for κa as low as 0.3, in contrast to the Derjaguin method which fails as expected for this κa range. Also, the method is claimed to reflect properly the van der Waals interaction between a sphere and a plane which is rather surprising in view of the fact that these interactions are always attractive, whereas in the SEI method the sign of interactions is reversed for the opposite part of the particle.

It seems that despite some sporadic success, the usefulness of every integration method, and the SEI approach in particular for $\kappa a < 1$ seems rather doubtful because the surface elements cannot be treated as isolated entities in this case.

2.2.2. The linear superposition method

The basic assumption of the LSA method introduced originally by Bell et al. [83] is that the solution of the PB equation for the two particle system can be constructed as a linear superposition of the solutions for isolated particles in an electrolyte of infinite extension. This is justified because due to electrostatic screening, the electrostatic potential at separations larger than Le drops to very small values and its distribution can be described by the linearised version of the

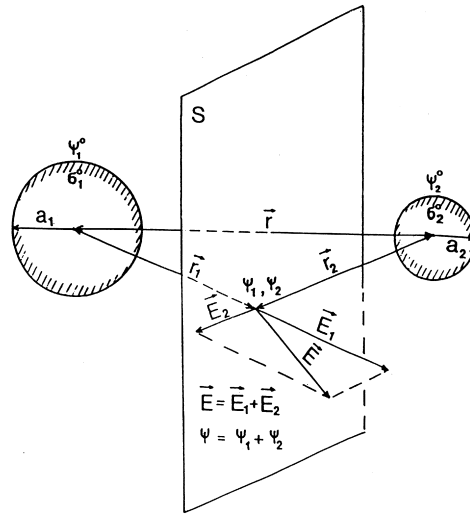


Fig. 6. The linear superposition approach (LSA) for two unequal spheres.

PB, i.e. Eq. (4). As a consequence, the solution of the PB equation in this region can be obtained by postulating the additivity of potentials and fields stemming from the isolated particles (see Fig. 6), i.e.

$$\begin{aligned}\psi &= \psi_1 + \psi_2 \\ \mathbf{E} &= \mathbf{E}_1 + \mathbf{E}_2\end{aligned}\quad (22)$$

where ψ_1 and ψ_2 are the solutions of the PB equation derived for isolated particles.

The LSA method can, in principle be applied for arbitrary particle shape provided the solution of the PB for isolated particle exists. At present, however, such solutions are known for a sphere in a simple 1–1 electrolyte only when the potential distribution is governed by the equation

$$\psi = \bar{Y}^0 \frac{A}{\bar{r}} e^{-(\bar{r}-A)} \quad (23)$$

where $A = \kappa a$, a is the sphere radius, $\bar{r} = \kappa r$ is the dimensionless distance from the sphere centre and \bar{Y}^0 is the ‘effective’ surface potential which can be approximated by Oshima et al. [84]

$$\bar{Y}^0 = 8 \tanh(\bar{\psi}^0/4) \frac{1}{1 + \left[1 - \frac{2A + 1}{(A + 1)^2} \tanh^2(\bar{\psi}^0/4) \right]^{1/2}} \quad (24a)$$

For $A \rightarrow \infty$ (planar interface) Eq. (24a) reduces to

$$\bar{Y}^0 = 4 \tanh(\bar{\psi}^0/4) \quad (24b)$$

It should be mentioned that Eq. (24b), in contrast to Eq. (24a), represents exact result derived by analytical solution of the PB equation [4,5]. It has been shown in Oshima et al. [84] that the deviation of Eq. (24a) from exact, numerical results of Loeb et al. [85] is confined to within a few percent for $A > 0.1$ and $\bar{\psi}^0 < 5$.

On the other hand, Chew and Sen [86] derived the asymptotic expression for \bar{Y}^0 in the form

$$\bar{Y}^0 = 4 \tanh(\bar{\psi}^0/4) + 2 \tanh^3(\bar{\psi}^0/4)/A \quad (25)$$

By applying the LSA method with Eq. (23) for the potential distribution, Bell et al. [83] derived the following analytical expressions for the force and energy of interaction for two dissimilar spheres configuration

$$\mathbf{F} = \phi_0 \kappa A_1 \frac{1 + \bar{R}}{\bar{R}^2} e^{-\kappa h_m} \frac{\mathbf{r}}{|\mathbf{r}|} \quad (26a)$$

$$\phi = \phi_0 \frac{A_1}{\bar{R}} e^{-\kappa h_m} \quad (26b)$$

where $\phi_0 = \varepsilon a_2 (kT/e)^2 \bar{Y}_1^0 \bar{Y}_2^0$, $\bar{R} = \kappa a_1 + \kappa a_2 + \kappa h_m = A_1 + A_2 + \bar{h}_m$ is the dimensionless distance between particle centres and $\mathbf{r} = \mathbf{r}_1 - \mathbf{r}_2$.

Eq. (26a) indicates that the force vector is acting along the direction of the relative position vector $\bar{\mathbf{r}}$, i.e. along the line connecting the sphere centres.

On the other hand, the LSA expression for interaction energy, Eq. (26b) assumes a simple two parametric form, analogous to the Yukawa potential used widely in statistical mechanics [87,88]. It remains valid for arbitrary surface potentials and the double layer thickness at distances $\kappa h_m \gg 1$. An additional advantage of this formula is that, unlike the HHF expression, Eq. (17a), it never diverges to infinity in the limit $h_m \rightarrow 0$ but approaching the constant value, which can be treated as the energy at contact. For colloid particles, the value of the contact energy is usually varying between 10 and 100 kT units. Due to the simple mathematical shape, (Eqs. 26a,b) are extensively used in numerical simulations of colloid particle adsorption problems.

It seems that the use of the LSA method is equivalent to acceptance of the energy additivity principle, i.e. the interactions in the multiparticle systems can be calculated as the sum of contributions stemming from particle pairs (including the limiting case of particle/wall interactions). Indeed, Oberholtzer et al. [89] have proven this for the three-body system consisting of two particles at a planar interface.

It should be mentioned, however, that the LSA method and the additivity rule is expected to break down for values of $\kappa a < 1$, especially for the particle/wall configuration when the electric field from the interface is penetrating through adsorbed particles. Moreover, due to the large field prevailing in the gap between

the particle and the interface the charge migration effects are likely to appear. Due to mathematical problems in finding appropriate coordinate systems, the true many-body problems have not been treated yet in a consistent way.

Another limitation of the LSA method is that it can only be used in the original form for spherical particles. Due to increasing importance of non-spherical particle interactions, an approximate method, being in principle a mutation of the LSA has been proposed in Adamczyk and Weroński [80,81] to deal with this problem. The essence of this model (referred to as the equivalent sphere approach, ESA) consists of replacing the interactions of convex bodies by analogous interactions of spheres having appropriately defined radii of curvature (see Fig. 7). As postulated in Adamczyk and Weroński [80,81] these radii should be calculated as the geometrical means of the principal radii of curvature evaluated at the point of minimum separation between the bodies, i.e.

$$R_1 = \frac{2R'_1 R_1''}{R'_1 + R_1''}$$

$$R_2 = \frac{2R'_2 R_2''}{R'_2 + R_2''} \quad (27)$$

The advantage of the ESA consists in the fact that the known numerical and analytical results concerning sphere interactions can directly be transferred to non-spherical particles. Thus, the LSA results, Eq. (26b) can be generalised for spheroidal particles to the form

$$\phi = \phi_0 \frac{R_1 R_2}{a(R_1 + R_2 + h_m)} e^{-\kappa h_m} = \phi_0 \frac{\bar{G}_e^0}{1 + \bar{G}_e \frac{h_m}{a}} e^{-\kappa h_m} \quad (28)$$

where $\phi_0 = \varepsilon a(kT/e)^2 \bar{Y}_1^0 \bar{Y}_2^0$ and

$$\bar{G}_e^0 = \frac{R_1 R_2}{a(R_1 + R_2)} = \frac{2R'_1 R_1'' R'_2 R_2''}{a[R'_1 R_1'' (R'_2 + R_2'') + R'_2 R_2'' (R'_1 + R_1'')]}$$

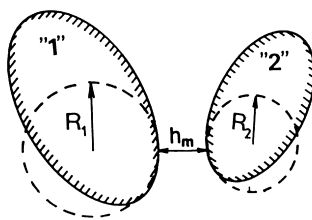


Fig. 7. A schematic representation of the equivalent sphere approach (ESA) for two convex particles in space.

$$\bar{G}_e = \frac{a}{(R_1 + R_2)} = \frac{a(R'_1 + R_1'')(R'_2 + R_2'')}{2[R'_1 R_1''(R'_2 + R_2'') + R'_2 R_2''(R'_1 + R_1'')]} \quad (29)$$

are the two geometrical correction factors, a is the longer spheroid semiaxis.

Although Eq. (28) possesses the simple Yukawa-type form, its application in the general case of spheroid interaction in space is not straightforward due the necessity of a numerical evaluation of the geometrical functions \bar{G}_e^0 and \bar{G}_e [80,81]. However, analogously as for the Derjaguin model, these functions can be evaluated analytically for some limiting orientations collected in Table 1.

It is interesting to note that for the spheroid/plane interactions, due to the fact that $\bar{G}_e = 0$, the energy is described by the equation analogous to the Derjaguin formula, Eq. (18) (at large separations), i.e.

$$\phi = \phi_0 \bar{G}_e^0 e^{-\kappa h_m} \quad (30)$$

where the geometrical factor \bar{G}_e^0 can be evaluated analytically for prolate spheroids in terms of the inclination angle α as [48]

$$\bar{G}_e^0 = 2As \frac{(G_D/a)^{3/2}}{G_D/a + As^2} \quad (31)$$

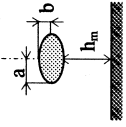
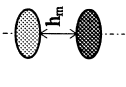
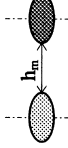
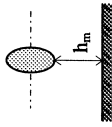
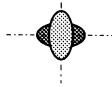
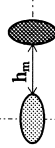
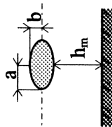
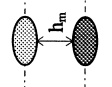

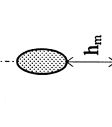
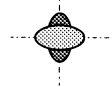
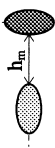
and G_D is the Derjaguin factor given by Eq. (21a) (see Table 1).

The dependence of G_e^0/a and G_D/a on α is plotted in Fig. 8. As can be seen, for α approaching 90° (perpendicular orientation of prolate spheroids) both the Derjaguin and the ESA give similar results and since \bar{G}_e^0 and G_D/a tend to the same limiting value equal to $(b/a)^2$. Significant deviations occur, however, in the limit of $\alpha \rightarrow 0^\circ$ (parallel orientation) when the Derjaguin model predicts $G_D = a$ and the ESA, $G_e^0 = 2b/[1 + (b/a)^2]$. As discussed in Adamczyk and Warszyński [48] this discrepancy, increasing for $b/a \rightarrow 0$, suggests that both models give rather inaccurate results for very elongated particles, when $As < 0.2$. Similar calculations performed for the oblate spheroid are plotted in Fig. 9.

As mentioned, in the case of arbitrary orientation of spheroids, one has to use numerical methods for evaluating the minimum separation distance and calculating the radii of curvature [80,81]. The use of efficient iterative schemes makes this task quite simple, so tedious simulations for spheroids become feasible [81]. Even with this complication, the use of the ESA seems considerably more efficient than any attempt of solving the PB equation for the anisotropic particle case.

Another approximation which can be used for modelling electrostatic interactions of anisotropic particles in the case of large κa values is the effective hard particle (EHP) concept introduced originally by Barker and Henderson [90]. According to this method, the true interaction potential between particles is replaced by the hard wall potential. Physically this means that the interacting particles can be treated as hard ones having the equivalent dimensions increased over the true geometrical dimensions by the small value h^* (skin), which can be treated as the effective interaction range. It was demonstrated in Adamczyk and

Table 1
The Derjaguin (\bar{G}_D) and the ESA (\bar{G}_e^0, \bar{G}_e^0) geometrical factors for limiting spheroid orientations

<p>OBLATE</p>		$\bar{G}_D = \bar{G}_e^0 = \frac{1}{A}$		$\bar{G}_D = \bar{G}_e^0 = \frac{1}{2A}$ $\bar{G}_e = \frac{1}{2A}$		$\bar{G}_D = \frac{1}{2}A$ $\bar{G}_e^0 = \frac{A^2}{A^2+1}$ $\bar{G}_e = \frac{A^2+1}{4}$
<p>SPHEROIDS</p>		$\bar{G}_D = A$ $\bar{G}_e^0 = \frac{2A^2}{A^2+1}$		$\bar{G}_D = \bar{G}_e^0 = \frac{A^2}{A^2+1}$ $\bar{G}_e = \frac{A^2+1}{4}$		$\bar{G}_D = \frac{A}{\sqrt{(A^3+1)(A+1)}}$ $\bar{G}_e^0 = \frac{2A^2}{2A^3+A^2+1}$ $\bar{G}_e = \frac{A^2+1}{A^3+A+2}$
<p>PROLATE</p>		$\bar{G}_D = 1$ $\bar{G}_e^0 = \frac{2A}{A^2+1}$		$\bar{G}_D = \frac{1}{2}$ $\bar{G}_e^0 = \frac{A}{A^2+1}$ $\bar{G}_e = \frac{A^2+1}{4A}$		$\bar{G}_D = \bar{G}_e^0 = \frac{1}{2}A^2$ $\bar{G}_e = \frac{1}{2A^2}$
<p>SPHEROIDS</p>		$\bar{G}_D = \bar{G}_e^0 = A^2$		$\bar{G}_D = \bar{G}_e^0 = \frac{A}{A^2+1}$ $\bar{G}_e = \frac{A^2+1}{4A}$		$\bar{G}_D = \frac{A^2}{\sqrt{(A^3+1)(A+1)}}$ $\bar{G}_e^0 = \frac{2A^2}{A^3+A+2}$ $\bar{G}_e = \frac{A^2+1}{A^4+A^2+2A}$

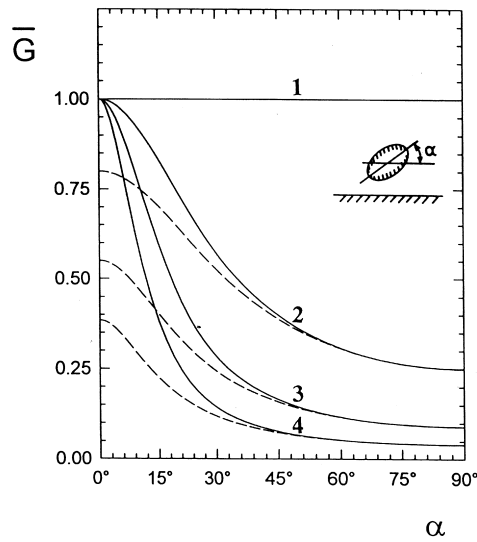


Fig. 8. Comparison of the Derjaguin and ESA (depicted by broken lines) geometrical factors for prolate spheroid/plane interactions. (1) $As = 1$ (spheres); (2) $As = 0.5$; (3) $As = 0.3$; (4) $As = 0.2$.

Weroński [81] by performing extensive Monte-Carlo type calculations that h^* is proportional to the Le parameter with the proportionality constant equal approximately $2 \div 3$ for colloid particles. However, this approach seems more suitable for

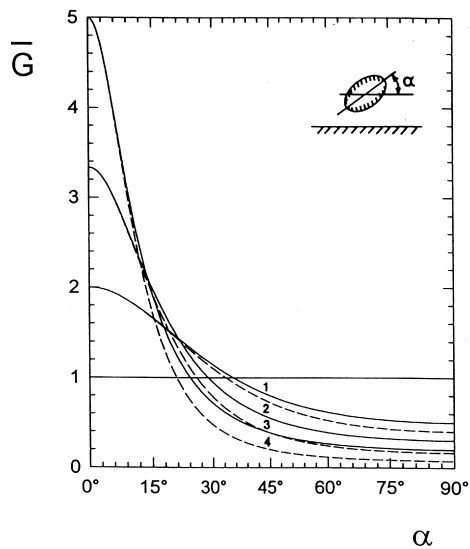


Fig. 9. Same as in Fig. 8 but for oblate spheroids.

characterizing the lateral particle/particle interactions than the particle/interface interactions.

2.3. Comparison of exact and approximate results for spheres

It is not a trivial task to estimate the range of validity of the approximate approaches discussed above because of the inherent difficulty in finding analytical solutions of the non-linear PB equation for the sphere/sphere geometry.

As mentioned, the approximation often used for describing interactions of spheres consists in linearisation of the PB equation which is then solved for two equal spheres by the perturbation techniques as shown by Levine et al. [91–94], Verveij and Overbeek [3] and Oshima et al. [95–98] for ion penetrable spheres. The resulting analytical expressions are too cumbersome for direct use, however. McCartney and Levine [99], developed the approximate surface dipole integration method which was extended by Bell et al. [83] and Sader et al. [100] to a dissimilar sphere system. The disadvantage of the analytical solutions valid for low surface potentials is that the geometrical and electrostatic factors stemming from surface potentials are coupled in a non-linear way. In Bhattacharjee and Elimelech [82], the finite element method exploiting the cylindrical coordinates was used to obtain the numerical solution of the linearised PB equation for the sphere/plane geometry.

Probably Hoskin [101] and Carnie et al. [102] were the first who solved the non-linear PB equation for two equal sized spheres in an exact way using the finite difference method. They applied the orthogonal, bispherical coordinate system whose advantage was that the boundary conditions could be accurately expressed. This coordinate system (with more mesh points) was subsequently used by Carnie et al. [102] who performed calculations of interaction force for two spherical particles in a 1–1 electrolyte. Taking into account in a rigorous manner the electrostatic field distribution within the particles the authors proved that this exerted a negligible effect on interaction force of particles characterised by $\varepsilon < 5$, e.g. polystyrene latex particles. Performing numerical calculations the authors also determined the range of validity of the Derjaguin and the linear HHF approaches as a function of κa and particle surface potentials. The interaction energy was not calculated in their work.

The electrostatic potential distribution and the energy of interaction for the dissimilar sphere system (including the important subcase of sphere interaction with a plane) was calculated in Warszyński and Adamczyk [103] using also the bispherical coordinates with the fine grid of 150 per 120 mesh points. The calculations were performed for a 1–1 electrolyte, κa changed between 0.25 and 10 and a dimensionless surface potential reaching 4.

The distribution of the potential in the electrolyte and within a particle adsorbed at a solid interface is shown in Fig. 10. The parameter set for which the calculations were performed ($\bar{\psi}_1^0 = -1.5$, $\bar{\psi}_2^0 = 3$, $\varepsilon = 2.5$) was chosen to mimic a polystyrene latex particle adsorbed at silanized mica [67]. In Fig. 10a the potential distribution is shown for $\kappa a = 5$ (which should correspond to a particle of

micrometer size range) whereas in Fig. 10c the situation more likely for a nanoparticle ($\kappa a = 0.25$) is presented. As can be seen, the exact potential distribution within the electrolyte can well be reflected by the LSA distribution, postulating simple additivity of the potentials stemming from the particle and the interface. It can also be seen in Fig. 10 that for microparticles the electrostatic field of the interface penetrates little the adsorbed sphere whose surface potentials remains negative, except for a small region at the point of contact. Qualitatively, one can expect that adsorption of further particles, due to lateral repulsion, should occur at the interface only, so a monolayer adsorption is expected. In contrast, for $\kappa a = 0.25$ (nanoparticles) the interface electric field causes an inversion of the surface potential of the adsorbed sphere over a considerable area. This suggests that adsorption of new particles can occur at preadsorbed particles which can lead to bilayer or multilayer adsorption. However, an exact description of this many-body problem (two particles at the interface) poses insurmountable difficulties at the present time.

A quantitative comparison of numerical results obtained in Warszyński and Adamczyk [103] with various approximate expressions is shown in Figs. 11 and 12 where the normalised interaction energy is plotted as a function of $\bar{h} = \kappa h_m$ both for the two particle systems $\bar{\phi}_{pp} = \phi/(\epsilon a \psi_2^0/2)$, upper part of Figs. 11 and 12 and the particle-interface system $\bar{\phi}_{pi} = \phi/(\epsilon a |\psi_1^0 \psi_2^0|/2)$, lower parts of these figures. The exact numerical data obtained in Warszyński and Adamczyk [103] were compared with the LSA model (given by Eq. (26b)), the linear HHF model (Eq. (17a)) both for the c.c., c.p. and the mixed case. As can be seen in Fig. 11 the particle/particle energy interaction profile is well reflected by the LSA model whereas the HHF model shows a definite tendency to overestimate the interactions for the c.c. boundary conditions. Also the particle/interface energy profiles are fairly well reflected by the LSA model with slightly smaller accuracy for the c.p. boundary conditions. Similar conclusions can be drawn from a comparison of the data shown in Fig. 12 collected for $\kappa a = 0.25$ although much higher deviations of the HHF model from the exact data are predicted at all distances for the c.c. model with the LSA model performing again very well.

An interesting feature of the exact numerical results shown in Figs. 11 and 12 is that the c.c. and c.p. model give very similar interaction energy values for the particle/particle case (identical surface potentials), except for very short distances $\kappa h_m < 0.25$. Moreover, in the c.c. model, the exact energy value remains finite in the limit $\kappa h_m \rightarrow 0$ which sharply contrasts with the linear HHF model predicting a logarithmically diverging interaction energy in the limit $h_m \rightarrow 0$ [cf. Eq. (17b)]. In view of these results, the long lasting controversy in accepting the c.c. or c.p. models seems rather immaterial.

It should be mentioned, however, that the accuracy of the LSA approximation is strongly influenced by the surface potential asymmetry in the case of particle/wall interactions. This is illustrated in Fig. 13 where one can see that the LSA reflects the exact results well if the absolute values of the surface potentials of particle and the interface do not differ too much. For the potential asymmetry exceeding 2:1 the LSA overestimates the attraction energy for distances $\kappa a < 1$.

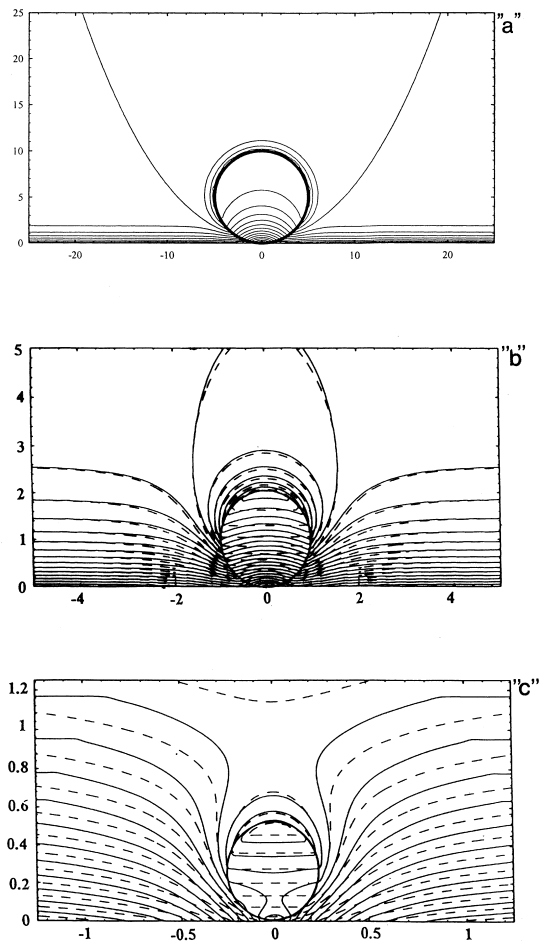


Fig. 10. Distributions of the electrostatic potential in the electrolyte and within a colloidal particle adsorbed at a solid/liquid interface. The solid lines denote the exact results obtained by solving the non-linear PB equation in bispherical coordinates for [103] $\varepsilon = 78$ (water), $\varepsilon_p = 2.5$ (polystyrene), $\psi_1^0 e/kT = 3$, $\psi_2^0 e/kT = -1.5$, $\kappa a = 5$, the broken lines represent the LSA results; part 'a' for $\kappa a = 5$, part 'b' for $\kappa a = 1$, part 'c' for $\kappa a = 0.25$.

It may be concluded from the data presented in Figs. 11–13 and similar results for the interaction force discussed in Carnie et al. [102] that significant differences between the LSA and the exact results occur at distances smaller than κa only where the interaction energy assumes very large absolute values either positive (similar surface potentials) or negative (opposite surface potentials). In both cases a relatively large uncertainty in ϕ can be tolerated. Moreover, the surface deformation, roughness and charge heterogeneity effects are expected to play a decisive role at such small separations as discussed in Section 2.4.

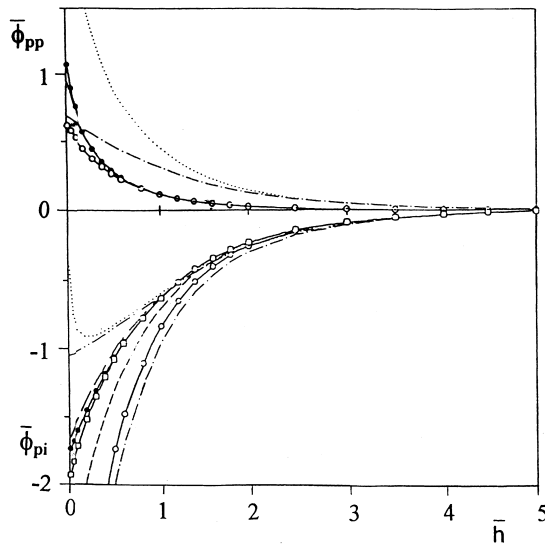


Fig. 11. The dimensionless electrostatic interaction energy between two particles $\bar{\Phi}_{pp} = (2/\varepsilon a \psi_2^{02})\phi$ (upper part) and for particle/interface $\bar{\Phi}_{pi} = (2/\varepsilon a |\psi_1^0 \psi_2^0|)\phi$ (lower part) calculated from various models ($\psi_1^0 e/kT = 3$, $\psi_2^0 e/kT = -1.5$, $\kappa a = 5$) [103]: - · - ·, exact numerical solution for the c.c. model; - · · - ·, exact numerical solution for the c.p. model; - □ - exact numerical solution for the mixed model (c.c. at the particle, c.p. at the surface); · · · ·, the linear HHF model at c.c.; - ● - ·, the linear HHF model for c.p.; —, the LSA model [analytical, Eq. (26b)]; - - - -, the LSA model (numerical); and - · · · ·, Kar et al. model [50].

2.4. Influence of surface roughness and heterogeneity

The above results are valid for idealised systems of perfectly smooth surfaces characterised by uniform charge distribution and lack of deformations upon approach. When dealing with real systems, e.g. colloid suspensions, these assumptions are likely to be violated since many complicating effects will appear such as:

1. heterogeneity of charge distribution at interacting surfaces which can be of a microscopic scale (of chemical origin) or macroscopic, patchwise scale; also considerable differences within particle populations are expected to appear with respect to, e.g. average charge (zeta potential);
2. surface roughness, either due to isolated, well defined asperities of different shape or of a statistical nature when the regular particle profile is perturbed;
3. surface deformations upon approach which seem particularly important for polymeric colloids (latexes) characterised by a low Young modulus value; and
4. dynamic relaxation phenomena of the double layer upon contact (ageing effects) due to ion migration along the surface or from one surface to another and eventually due to ion transfer into the bulk; these processes are again expected to appear for polymeric colloids having the random coil structure.

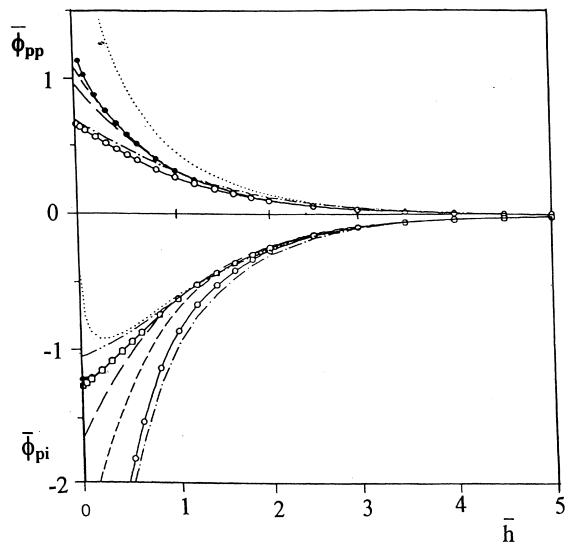


Fig. 12. Same as for Fig. 11 but for $\kappa a = 0.25$.

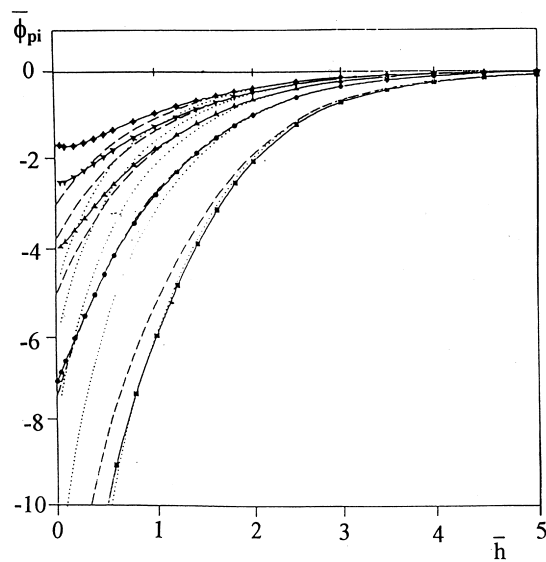


Fig. 13. The dimensionless particle/interface energy $\bar{\phi}_{pi}$ determined for $\varepsilon = 78$, $\varepsilon_p = 2.5$, $\kappa a = 1$ and $\bar{\psi}_1^0 e/kT = 3$ [103]. The full symbols denote the exact numerical solutions for the c.c. model for $\bar{\psi}_2^0 = -3$ (squares); $\bar{\psi}_2^0 = -1.5$ (circles); $\bar{\psi}_2^0 = -1$ (triangles); $\bar{\psi}_2^0 = -0.75$ (reversed triangles); and $\bar{\psi}_2^0 = -0.6$ (diamonds). Dotted curves show the numerical LSA model and dashed curves the analytical LSA.

Despite the great practical significance of these dynamic phenomena surprisingly little effort has been devoted to quantify them by developing theoretical approaches. The effect of microscopic non-uniformity of charge distribution (discrete charge effect) was studied by Levine [37]. A similar problem was considered by Richmond [104,105] where the interaction energy between parallel plates with a discrete charge distribution forming two-dimensional lattices was studied using the linearised PB equation. It was found that the discrete charges generated a larger interaction potential in comparison with uniformly charged surfaces.

The effect of heterogeneity of charge distribution on particle/surface interactions was studied by Song et al. [106] by considering two simple models of a macroscopic, patchwise heterogeneity and the microscopic model when the charge distribution was described by the Gaussian probability distribution. The interactions were simply calculated from the usual expressions stemming from the DLVO theory by introducing the local values of the surface potential. A similar approach was used by Adamczyk [78] by postulating that the surface charge (characterised by zeta potential) of particles is described by a Gaussian distribution. It was shown in both works that the initial particle flux under the barrier transport conditions will be increased by orders of magnitude when the charge distribution heterogeneity appears.

The effect of geometrical surface roughness was studied in more detail. Krupp [107] was probably the first who qualitatively consider the effect of a hemispherical asperity on the adhesion force of a smooth colloid particle. It was concluded that the attractive electrostatic interactions will be decreased to a lesser extent than the dispersion forces so the net adhesion force should be determined by the electrostatic component. A similar model was used by Adamczyk [78] to determine graphically the maximum size of a rough particle which can adhere to an interface under hydrodynamic shearing forces. Elimelech and Melia [108] used an analogous model for simulating the interaction of a smooth particle with a flat plate containing a single hemispherical asperity. The electrostatic interaction energy was calculated using the Derjaguin method as a sum of particle/smooth wall and particle/asperity contributions.

Czarnecki [109] and Czarnecki and Warszyński [110] used the additivity principle for modelling the interaction of a smooth sphere with a heterogeneous (rough) planar surface. The rough surface was generated by distributing at random over a smooth surface a number of small spherical particles having various size and charge distribution governed by the Gaussian law. Considerable differences in the interaction energy of the sphere were predicted at various spots of the interface which could explain the appearance of specific tangential interactions in particle deposition processes.

The energy additivity rule was also exploited by Herman and Papadopolous [111,112] who determined the effect of conical and hemispherical asperities on the van der Waals and electrostatic interaction between flat plates using the LSA approach combined with the Derjaguin summation method. It was demonstrated that due to asperities, the repulsive interaction energy was increased over the smooth plate case, especially for large κa values. This approach was generalised to

the rough colloid particle/smooth surface case [113,114]. The following formula for the electrostatic interaction energy based on the LSA/Dejaguin approach was derived

$$\phi = \phi_0(1 - \theta)e^{-\kappa h_m} + \phi'_0\theta e^{-\kappa(h_m - a_s)} \quad (32)$$

where $\phi_0 = \varepsilon a (kT/e)^2 \bar{Y}_1^0 \bar{Y}_2^0$ as previously defined, $\phi'_0 = (2\varepsilon a/\kappa a_s)(kT/e)^2 \bar{Y}_1^0 \bar{Y}_s^0$, $\theta = \pi a_s^2 N$ is the surface coverage of the asperities, a_s is the asperity radius and N is their surface concentration, $\bar{Y}_1^0, \bar{Y}_2^0, \bar{Y}_s^0$ and are the effective surface potentials of the interface, particle and asperity, respectively.

This model is applicable for high electrolyte concentration when $\kappa a_s \gg 1$ and for low coverages θ when the number of asperities within the contact area remains low so the uncovered surface areas can be treated as isolated patches.

It can be deduced from Eq. (32) that due to asperities the repulsive interaction energy is much higher (at the same distance between the smooth surface and the plate) than in the case of smooth objects. On the other hand, when defining h_m as the distance between the asperity surface and the smooth boundary (which has a more natural physical interpretation in the case of attractive interactions leading to adsorption and adhesion) one can deduce from Eq. (32) that the absolute value of ϕ should become much smaller than for bare particles at the same separation.

In an attempt to develop improved modes, Kostaglou and Karabelas [115] treated the problem of electrostatic interactions of two infinite surfaces exhibiting periodic (sinusoidal) surface roughness. The linear PB equation was applied which was then solved by the perturbation, boundary collocation, and boundary integral methods. It has been found that the interaction energy of rough surfaces is at all separations larger than that for smooth surfaces. However, it was claimed that the theory predicts a decrease in the electrostatic interaction energy upon contact. Obviously, further studies using more realistic surface roughness distributions (e.g. of a stochastic nature) are needed to resolve this discrepancy.

Apparently, the effect of surface deformations has not been treated in the literature. One may suppose that in the case of repulsive interactions, ϕ is expected to increase over the values for perfectly rigid bodies as a result of surface deformations. This would be so because the radius of curvature around the minimum separation area increases due to a surface flattening effect. On the other hand, in the case of attraction, the absolute value of the interaction energy will decrease due to a decrease in the curvature radius. As discussed by Krupp [107], however, upon making a physical contact, the adhesion energy will likely be larger due to flattening of the surfaces involved. In any case, due to unequivocal definition of the separation distance in the case of deformable bodies, producing a coherent theory of electrostatic interactions seems difficult.

3. The dispersion forces and the energy profiles

Since the dispersion (van der Waals) interactions have been treated extensively

in excellent monographs and reviews [116–118], in our paper we shall invoke some selected results only, pertained to particle adsorption problems.

Generally, there exist two methods of calculating the dispersion interactions:

1. the microscopic approach exploiting the energy additivity principle to derive solutions for more complex geometries from known solutions for atoms and molecules [119,120]; and
2. the macroscopic approach [121] treating the interacting body as a continuum and exploiting the imaginary part of the dielectric constant expressed as a function of the radiation frequency for determining the material constants characterizing the magnitude of the interactions [107].

The shortcoming of the microscopic approach is that in condensed phases the atoms and molecules may undergo structural changes so the additivity principle is violated and the interaction constant known for isolated species is no longer valid. On the other hand, a great advantage of this approach treated exclusively in our review, is that analytical formulae can be derived for complicated geometries of the interacting particles, including the case of rough surfaces. In contrast, it is very difficult to go with the macroscopic approach beyond the case of two half-space interactions.

The interaction of two different atoms across a vacuum is described by the expression, first derived by Lodon [122]

$$\phi_a = -\frac{3}{2}\hbar\alpha_1\alpha_2\frac{\omega_1\omega_2}{\omega_1+\omega_2}\frac{1}{r^6} = -\frac{\beta_{12}}{r^6} \quad (33)$$

where ω_1, ω_2 are the characteristic oscillation frequencies, α_1, α_2 are the polarisabilities of the atoms, β_{12} is the London constant and r the distance between the atom centres.

Due to omission of the retardation effect, Eq. (33) is only valid for distances between atoms shorter than the characteristic wavelength λ , being of the order 10–15 nm. It was shown by Schenkel and Kitchener [123] that by considering the retardation effect the interaction energy of atoms is given by the approximate expression valid for $2\pi r/\lambda > 0.5$

$$\phi_a = -\frac{\beta_{12}}{r^6} \left[\frac{2.45\lambda}{2\pi r} - \frac{2.17\lambda^2}{4\pi^2 r^2} + \frac{0.59\lambda^3}{8\pi^3 r^3} \right] \quad (34)$$

At larger distances the leading term obviously dominates and one recovers the formula derived originally by Casimir and Polder [124].

The force of interactions between atoms can be directly obtained from the above formulae by a simple differentiation with respect to r .

Using Eqs. (33) and (34) one can derive the expressions for macroscopic bodies of arbitrary shape by calculating the volume integral

$$\phi = \int_{v_1} \int_{v_2} \phi_a q_1 q_2 \, dv_1 \, dv_2 \quad (35)$$

where q_1, q_2 are the number density of atoms in the two bodies involved, and v_1, v_2 are the volumes of the bodies.

Applying Eq. (35) with ϕ_a given by Eq. (33) to the two halfspaces case one obtains the expression for the unretarded interaction energy per unit area in the form

$$\phi = -\frac{A_{12}}{12\pi h^2} \quad (36)$$

where $A_{12} = \pi^2 \beta_{12} q_1 q_2$ is the Hamaker constant.

For the retarded case using Eq. (34) (with the leading term only) one obtains [113,114]

$$\phi = -\frac{A_{12}}{\pi^2 h^3} \left[\frac{2.45\lambda}{60} - \frac{2.17\lambda^2}{240\pi h} + \frac{0.59\lambda^3}{840\pi^2 h^2} \right] \quad (37)$$

Because the dispersion interactions are usually of much shorter range than colloid particle dimensions one can use Eqs. (36) and (37) in conjuncture with the generalised Derjaguin method to derive the expressions for ϕ in the case of arbitrary convex bodies (whose radius of curvature is larger than approx. 10 nm). In this way one obtains

$$\phi = -G_D \frac{A_{12}}{6h_m} \quad (38)$$

where G_D is the generalised Derjaguin factor given by Eq. (19) and shown in Table 1 for limiting configurations of spheroids.

On the other hand, the exact result which can be derived by evaluating the volume integral, Eq. (35) for two spherical particles in the non-retarded case is [117]

$$\phi = -\frac{A_{12}}{6} \left[\frac{2a_1 a_2}{h_m(h_m + 2a_1 + 2a_2)} + \frac{2a_1 a_2}{(h_m + 2a_1)(h_m + 2a_2)} + \ln \frac{h_m(h_m + 2a_1 + 2a_2)}{(h_m + 2a_1)(h_m + 2a_2)} \right] \quad (39)$$

In the case of retarded interactions the Derjaguin expression reads

$$\phi = -G_D \frac{A_{12}}{\pi h_m^2} \left[\frac{2.45\lambda}{60} - \frac{2.17\lambda^2}{360\pi h_m} + \frac{0.59\lambda^3}{1680\pi^2 h_m^2} \right] \quad (40)$$

For this geometry the exact results are too cumbersome and are not presented here.

For the sphere/plane interactions the exact results can be derived by substituting $a_1 = a$ and letting $a_2 \rightarrow \infty$. In this way one obtains for the non-retarded and retarded interactions, respectively [109]

$$\begin{aligned} \phi &= -\frac{A_{12}}{6} \left[\frac{a}{h_m} + \frac{a}{2a + h_m} + \ln \frac{h_m}{2a + h_m} \right] \\ \phi &= -\frac{A_{12}}{\pi h_m^2} \left\{ \frac{2.45\lambda}{60} \left[(a - h_m) + \frac{(h_m + 3a)}{(h_m + 2a)^2} \right] \right. \\ &\quad - \frac{2.17\lambda^2}{720\pi} \left[\frac{2a - h_m}{h_m} + \frac{(h_m + 4a)h_m^2}{(h_m + 2a)^3} \right] \\ &\quad \left. + \frac{0.59\lambda^3}{5040\pi^2} \left[\frac{3a - h_m}{h_m^2} + \frac{(h_m + 5a)h_m^2}{4(h_m + 2a)^4} \right] \right\} \end{aligned} \quad (41)$$

Since the expression for the retarded interactions are rather cumbersome for direct use, Suzuki [125] derived an approximate equation having the simpler form

$$\phi = -\frac{A_{12}}{6} \frac{a}{h_m \left(1 + 11.11 \frac{\lambda}{h_m} \right)} \quad (42)$$

Obviously, the Derjaguin model, Eqs. (38) and (40) still holds for the sphere/plane geometry with $G_D = a$.

The corresponding expressions for the force of interaction can easily be derived from the above formulae by a simple differentiation with respect to the distance h_m .

The above presented expressions are strictly valid for atom interactions in a vacuum only. As shown in [120], however, the analogous interactions across a continuous medium can be characterised by the same functional dependencies with the ‘composite’ Hamaker constant, A_{102} denoting interactions between particles of material 1 interacting with particles of material 2 across the intervening medium 0. Obviously, when the medium 0 is a liquid phase, its composition may change at the liquid/solid boundaries due to, e.g. electrolyte concentration changes. This is expected to influence to some extent the value of the Hamaker constant. Thus, in the general case, the electrostatic and dispersion interactions are coupled in a complex, non-linear way which violates the basic assumption of the DLVO theory. Due to the lack of appropriate theories we should accept the hypothesis that this coupling is not too significant ([117], p. 224).

In contrast to double-layer interactions, the case of dispersion interaction of rough particles has been well treated in the literature [109,110,126,127]. Although exact results for arbitrary statistical distribution of microroughness were found to be rather complicated [126], Czarnecki and Dąbroś [127] and Czarnecki [109] have derived a simple interpolating function for ϕ_r , valid both for sphere/sphere and sphere/plane interactions

$$\phi_r = \phi_s \left(\frac{h_m}{S} \right)^c \quad (43)$$

ϕ_s is the energy for the smooth particle interface, the distance h_m is now measured between the two outermost points at the particle surfaces, $S = h_m + (b_1 + b_2)/2$ and b_1, b_2 is the thickness of the rough layer at particles 1 and 2, respectively and c is the exponent, close to one for the unretarded case [109] and 1.5 for the retarded case [127]. Thus, in the limit $h_m \rightarrow 0$, Eq. (43) reduces to the simple form (for unretarded interactions)

$$\phi_r = \phi_s H \quad (44)$$

where $H = 2h_m/(b_1 + b_2)$ is the scaled distance between particle surfaces.

It can be easily deduced from Eq. (43) that, in accordance with intuition, the dispersion interactions between rough bodies are substantially reduced at all separations in comparison with smooth particles.

3.1. Superposition of interactions and the energy profiles

Since for most known cases the Hamaker constant assumes a positive value (with the exception for liquid helium [118]) one can deduce from Eqs. (37)–(44) that the dispersion contribution to the interaction energy is negative (attraction) at all interparticle separations. Moreover, due to insensitivity of the Hamaker constant on material properties (except for metals it is usually confined within the range $5 \times 10^{-14} \div 2 \times 10^{-13}$ ergs), the range of dispersion interactions is fairly fixed, equal to 10–20 nm.

In contrast, the electrostatic interactions can be either positive or negative depending on surface potentials and separation distance. Additionally, their range can be varied between broad limits (1–1000 nm) by simply changing the ionic strength of electrolyte solutions. As a result, the superposition of the dispersion and electrostatic interaction may lead to complicated energy profiles discussed first by Verwey and Overbeek [3] and classified by Rajagopalan and Kim [128,129].

Of most pertinence to the particle adsorption problem is the energy profile of type I shown in Fig. 14a when the interaction energy decreases monotonically when $h_m \rightarrow 0$ (the bulk energy level is assumed conveniently to be zero). This profile appears in systems when particle and interface bear opposite surface charges. In order to simplify the mathematical analysis of particle transport phenomena this energy profile is often idealised by introducing the perfect sink (PS) model, as done

originally by Smoluchowski [130] in his fast coagulation theory. According to this approach, the interaction energy remains zero up to a small distance δ_m where it becomes minus infinity (see Fig. 14a).

Obviously, both the energy profile of type I and the PS model should be treated as an idealisation of any real situation because at very small separations the interaction energy must become positive due to the Born repulsion preventing particle/wall penetration. In the DLVO theory, these repulsive interactions were not considered. Even at present no quantitative theory of these interactions for macroscopic objects has been developed. Assuming that the repulsive part of the potential is described for atoms and molecules by the 6–12 power law one may expect that for the particle/wall interactions $\phi \sim r^{-7}$. These interactions seem, therefore, very short ranged, probably not exceeding 0.5–1 nm.

In any case, the appearance of the repulsive interactions fixes the minimum value of the interaction energy which remains finite in accordance with intuition. This minimum energy value is often referred to as the primary minimum denoted by ϕ_m and the distance where it appears as δ_m (see Fig. 14a). One may expect that δ_m is of the order of the range of the Born repulsive forces, i.e. 0.5–1 nm. However, the extension of the region where the interaction energy assumes a negative value can be much larger, comparable with the Debye screening length, i.e. approximately 100 nm for a 10^{-5} M electrolyte solution.

Since for a type I profile the energy assumes large negative values around δ_m , the probability of finding a colloid particle within this region will be considerably larger than the uniform probability in the bulk of the suspension. This will result in particle accumulation around δ_m leading to a particle concentration increase. Under equilibrium, the resulting particle concentration profiles can be described by the Boltzmannian distribution, i.e. $n = n_b e^{-\phi/kT}$ as shown in the upper part of Fig. 14a. It should be remembered, however, that particle accumulation can proceed to some limiting value when the volume exclusion effects start to play the decisive role as discussed later.

Therefore, the existence of the energy minimum would physically explain adsorption of colloid particles, at least under static, no flow, conditions. For a flowing colloid system, as is the case for most practical applications, the situation becomes conceptually more complicated because neither the classical DLVO, nor the theory with inclusion of Born repulsion would explain particle immobilisation under vigorous shearing forces [131–133]. Thus, the particles accumulated at the interface would easily be removed by the tangential fluid flow. One has to accept somehow ad hoc the appearance of strong tangential interactions most probably due to short-ranged geometrical and charge heterogeneities [131–133]. It is difficult to estimate the magnitude of the local energy sinks arising due to the tangential interactions although it can be predicted that their depth will be a fraction of ϕ_m . As discussed by Adamczyk [78] these tangential interactions exert a rather minor influence on adsorption kinetics of colloid particles. They are expected, however, to influence considerably the maximum size of particle attached to the surface under given flow shear rate.

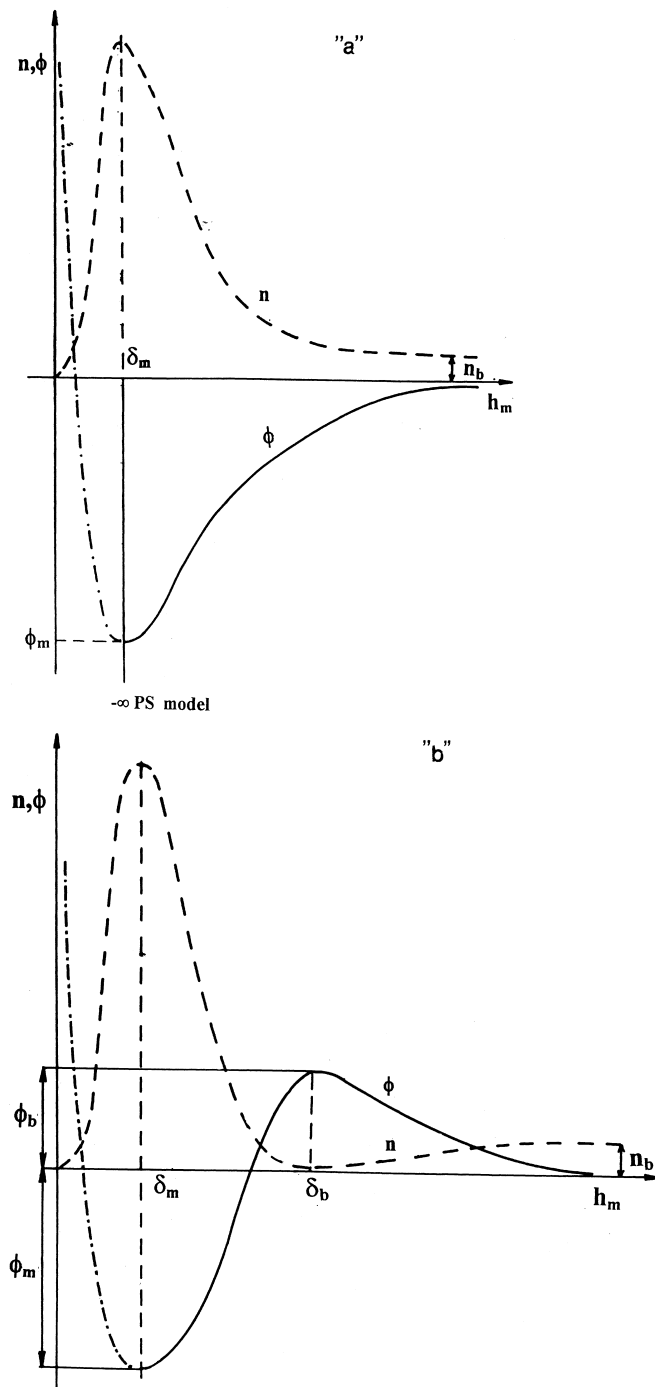


Fig. 14. Part 'a' the Type I energy profile (no energy barrier) and the corresponding particle concentration profile at equilibrium (schematic view). Part 'b' the Type II energy profile (energy barrier) and the corresponding particle concentration profile at equilibrium.

To simplify our considerations we assume in due course that these interactions are strong enough to keep adsorbed particles fixed at a given position (localised adsorption postulate).

Since for the type I energy profile the attractive specific forces appear over distances comparable with particle dimensions (for low electrolyte concentration) it can be deduced that particle transport from flowing systems will be significantly accelerated as discussed quantitatively later on.

In the case when the interface and particle are likely charged, the energy profile of type II is likely to appear (see Fig. 14b). The characteristic feature of the profile is the appearance of a maximum energy barrier of height ϕ_b at the distance δ_b . The corresponding Boltzmannian distribution under equilibrium is presented in the upper part of Fig. 14b. This energy profile corresponds to the activated transport conditions in the chemical kinetics. In the case of two colloid particles, this profile would correspond to the slow coagulation conditions. Obviously, the height of the barrier is very sensitive to the electrolyte concentration and composition (presence of polyvalent ions). Much effort in the literature was devoted to derive, starting from the DLVO theory, functional dependencies (known empirically as the Schultz–Hardy rule ([117] p. 421) connecting the critical coagulation concentration with the Hamaker constant, electrolyte concentration, valence and the size of the particles [3].

On the other hand, when the barrier height assumes large values (as is the case for lower electrolyte concentration) the system is kinetically frozen, in the sense that particle aggregation is proceeding at much slower rate than the usual observation time. In particle adsorption experiments the existence of an energy barrier would also reduce the particle adsorption rate considerably which will be inaccessible for accurate measurements. Therefore, a compromise is usually sought in this kind of experiment characterised by a negligible aggregation rate of the suspension and measurable rate of particle adsorption. It should also be expected that due to large transport resistance due to barrier, the bulk transport conditions will be less important in this case.

For low electrolyte concentration and large particles (micrometer size range) a situation may arise when the so called secondary minimum appears at the distance δ_{sm} much larger than δ_m . Obviously, this minimum is more shallow than the primary minimum due to smaller dispersion energy contribution at this distance. This type of energy profile will be referred to as IIa. Fundamentally, there is not much difference in the II and IIa energy profiles. In the latter case, additional accumulation of particles around δ_{sm} is expected which could influence particle adsorption kinetics. However, due to flow the concentration peak within this region does not become significant [131,132].

As this fragmentary analysis suggests it is generally much more efficient to analyse the influence of the energy profile on particle adsorption phenomena than to analyse the influence of numerous physicochemical parameters influencing ϕ_m , δ_m , ϕ_{sm} , δ_{sm} . This approach will be generally adopted in later parts of our work dealing with quantitative analysis of adsorption kinetics.

4. Role of specific interactions in particle deposition phenomena.

The specific interactions discussed in previous sections are expected to significantly influence colloid particle deposition at solid/liquid interfaces not only by regulating the transport rate through the diffusion boundary layer but also by controlling the adhesion force necessary for localisation of particles. Depending on the magnitude of the specific interactions one can distinguish the two main categories of particle deposition regimes [67]:

- (i) the barrierless deposition when the particle/interface specific interaction profile is of type I and that of particle/particle of type II;
- (ii) the barrier-controlled deposition when both energy profiles are of type II with the barrier for particle deposition significantly lower than for particle aggregation.

Note that in both cases the suspension is stable in a kinetic sense only, which means that a noticeable aggregation may occur within the timescale of particle deposition experiments, in the case of higher electrolyte concentration.

Whereas in case (i) the system is usually well behaved (in the sense that surface heterogeneities and natural distribution of particle charge density exert little effect on particle deposition kinetics), the deposition regime of type (ii) is usually ill-defined. This means that deposition rate and mechanism is very sensitive to the specific details of surface topology, e.g. presence of isolated patches or surface roughness, characterised by different surface properties. Also the particles which have favourable surface properties will selectively be deposited from a suspension characterised by a spread of, e.g. surface charge.

Due to these complications, the barrier-controlled deposition regime (ii) has sporadically been studied in comparison with regime (i), treated extensively in the literature both theoretically and experimentally (see the reviews [48,67,78,128,133]).

Even for the barrierless deposition, however, the linear transport conditions are relatively short-lasting, especially when concentrate suspensions are involved. The deviations from linearity stem from the presence of particles accumulated at the interface which disturb locally fluid flow and exert additional forces on adsorbing (flowing) particles. This leads to surface blocking effects (called also surface exclusion effects) which are responsible for the reduction in particle deposition rate at higher coverage. As pointed out by Adamczyk [67] a rigorous theoretical analysis of these many-body phenomena seems difficult without introducing rather drastic simplifications concerning the hydrodynamic and electrostatic interactions. In the literature, these surface blocking effects are introduced somehow ad hoc, usually in the form of flux correction function $B(\theta)$ (where $\theta = NS_g$ is the fractional surface coverage, N is the surface concentration and S_g is the characteristic particle cross-section area) which depends solely on the surface coverage of deposited particles. $B(\theta)$ is traditionally referred to as the blocking function, whereas in the physical literature the more accurate notion of available surface function (ASF) is used [134,135].

The most obvious, but rather ill founded for continuous surfaces, seems the

Langmuir model based on the assumption that $B(\theta) = 1 - \theta/\theta_L$, where θ_L is the ‘saturation’ coverage to be determined empirically. With this function in hand the actual adsorption flux j is expressed as

$$j = j_0 B(\theta) \quad (45)$$

where j_0 is the initial particle flux (if it can be defined).

The definition of the blocking function $B(\theta)$, inherent to Langmuir and other models as a ‘surface’ quantity, independent on the distance from the interface and particle distribution seems conceptually wrong as pointed out [134,135]. The deficiency of this model becomes apparent when realizing that at the same coverage (e.g. $\pi/8 = 0.39$) the adsorbed particles can either block the entire surface, when forming a regular layer, or approximately 0.43 of the available surface only, when forming a two-dimensional hexagonal crystalline phase.

To avoid these limitations, we shall accept in our work a more general approach in which the effect of adsorbed particles is treated as additional transport resistance which depends not only on particle coverage but also on the structure of the adsorbed layer. Physically this means that due to the presence of deposited particles an energy barrier is formed (hereafter referred to as the steric barrier) whose magnitude is growing with particle coverage. Analogously as for the electrostatic interactions, this barrier has some spatial extension (width) which is close to particle diameter. The repulsive interactions due to this barrier are incorporated in an exact way in the particle continuity (mass conservation) equation as discussed next.

4.1. The continuity equation

Our considerations presented hereafter are in principle valid for spherical particles only since due to insurmountable mathematical difficulties no exact solutions of the continuity equation for anisotropic particles have been derived. However, the results obtained for spheres may be exploited as useful reference system for other particle shapes, especially when the steric barrier for these particles is estimated.

Assuming that the colloid particle suspension can be treated as a stable, well defined phase one can write down the expression for the mass flux vector for quiescent (no flow) systems in the usual form

$$\mathbf{j} = -(\mathbf{M} \cdot \nabla \tilde{\mu})n = -\mathbf{M} \cdot (\nabla \mu + \nabla \phi)n = -\mathbf{D} \cdot (\nabla \mu/kT + \nabla \phi/kT)n \quad (46)$$

where \mathbf{M} is the mobility matrix, $\tilde{\mu}$ the total potential of a particle, μ the chemical part of the potential, ϕ the external force potential, n is the local value of particle concentration and $\mathbf{D} = kT\mathbf{M}$ the diffusion matrix.

It should be mentioned that the potential ϕ contains the contribution stemming from external sources, e.g. gravity, magnetic fields, electrostatic interactions due to the interface, etc., whereas the specific interactions between particles are contained in the chemical part of the potential, μ . Hence, by formulating Eq. (46) one

assumes implicitly that there is no coupling between external and chemical interactions.

For dilute systems, as is usually the case in the bulk of the suspension during deposition experiments, the chemical potential simply becomes $\mu = \mu_0 + kT \ln n$ (where μ_0 is some reference value of the potential). This case would correspond to the ideal bulk behaviour of the suspension. In the general case, however, e.g. in the regions where local particle concentration increases, the deviations from the ideality may become significant.

It is not conceptually simple to generalize Eq. (46) to flowing systems due to appearance of inertia forces for high Re flows (where Re is the Reynolds number) and the inherent non-potential nature of viscous flows. It has been postulated, however, that for colloid particles the local flows are practically inertialess and of a quasistatic nature [132]. Assuming additionally that there is no coupling between hydrodynamic and specific interactions one can formulate the flux expression in the form

$$\mathbf{j} = -\mathbf{D} \cdot (\nabla\mu/kT + \nabla\phi/kT)n + \mathbf{V}_p n \quad (47)$$

where $\mathbf{V}_p = \mathbf{M} \cdot \mathbf{F}_h + \mathbf{M}_r \cdot \mathbf{T}_h$ is the particle velocity vector due to the hydrodynamic force \mathbf{F}_h and torque \mathbf{T}_h , and \mathbf{M}_r is the rotational mobility matrix. It should be mentioned that by formulating Eq. (47) all the hydrodynamic particle/particle interactions were neglected as well as all flow disturbances due to the presence of particles.

For a suspension exhibiting an ideal bulk behaviour by neglecting specific and external forces, and assuming that particle velocity coincides with the fluid velocity (as is the case far from boundary surfaces) one can simplify Eq. (47) to the form

$$\mathbf{j} = -D_z \nabla n + \mathbf{V}_p n \quad (48)$$

where D_z is the diffusion coefficient (position-independent scalar quantity) and \mathbf{V} is the fluid velocity vector fulfilling the continuity equation $\nabla \cdot \mathbf{V} = 0$.

Eq. (48), being the starting point of the convective diffusion theory [136] is usually referred to as the Smoluchowski–Levich (SL) approximation.

Let us now consider transport of colloid particles in the vicinity of an interface. Assume that after approaching the interface close enough the particles become immobilised due to the presence of above mentioned tangential interactions whose range is infinitesimal in comparison with particle dimension. Thus, upon contact, the particles do not move along the surface although they can occasionally escape from the primary minimum region. Using the flux expression, Eq. (47), one can formulate the non-stationary continuity equation as

$$\frac{\partial n}{\partial t} = -\nabla \cdot \mathbf{j} = \nabla \cdot [(\mathbf{D} \cdot \nabla\mu/kT + \mathbf{D} \cdot \nabla\phi/kT - \mathbf{V}_p)n] \quad (49)$$

where t is the time.

The mass conservation equation for the immobile phase can be formulated by

observing that the increase in the surface concentration of the immobilised particles N is due to the normal component of particle flux at the interface j (more correctly at the surface surrounding the boundary at the distance which can be identified with the primary minimum distance δ_m), i.e.

$$\frac{dN}{dt} = \mathbf{j}(\delta_m) \cdot \hat{\mathbf{n}} = k_a n(\delta_m) - k_d N \quad (50)$$

where $\mathbf{j}(\delta_m)$ is the local flux vector given by the expression

$$\mathbf{j}(\delta_m) = (\mathbf{D} \cdot \nabla \mu / kT + \mathbf{D} \cdot \nabla \phi / kT - \mathbf{V}_p) n|_{\delta_m} \quad (51)$$

where $\hat{\mathbf{n}}$ is the unit normal pointing outwards from the interface, k_a is the adsorption rate constant characterizing the transfer rate from mobile to immobilised phase and k_d is the desorption rate constant describing particle escape rate from the immobilised phase.

Using Eqs. (50) and (51) one can formulate the general kinetic boundary condition for the bulk phase in the form

$$k_a n(\delta_m) - k_d N = [\mathbf{D} \cdot \nabla \mu / kT + \mathbf{D} \cdot \nabla \phi / kT - \mathbf{V}n] \cdot \hat{\mathbf{n}} \quad \text{at } \delta_m \quad (52)$$

Eq. (52) indicates that the bulk and surface continuity equations are coupled and cannot be solved independently. However, when one assumes the perfect sink behaviour, i.e. when the transfer rate from mobile into immobile phase k_a becomes infinite (due to presence of infinite energy sink) and $k_d = 0$, then the boundary condition for the bulk phase assume the particularly simple form

$$n = 0 \quad \text{at } \delta_m \quad (53)$$

This type of boundary condition has been used in the Smoluchowski–Levich theory in conjuncture with the bulk transport equation derived by exploiting the flux expression, Eq. (48), i.e.

$$\frac{\partial n}{\partial t} = D_\infty \nabla^2 n - \mathbf{V} \cdot \nabla n \quad (54)$$

Later on, the PS boundary conditions, Eq. (53) have extensively been exploited in numerical calculations of particle deposition rate at various surfaces [67,133].

The boundary value problem expressed by the mass conservation equations, Eqs. (49) and (50) and the boundary condition, Eq. (52) is complemented by the bulk boundary condition which usually assumes the form

$$n \rightarrow n_b \quad \text{at large distances from the interface} \quad (55a)$$

On the other hand, for adsorption from a finite volume the symmetry boundary conditions are appropriate [137]

$$\nabla n = 0 \quad \text{at the symmetry plane} \quad (55b)$$

It should be remembered that due to the presence of adsorbed particles, the chemical potential entering Eq. (49) is modified in the vicinity of the interface. One can postulate that the modified potential can be expressed as

$$\mu = \mu_0 + kT \ln fn = \mu_0 \mathbf{V} + kT \ln n + kT \ln f \quad (56)$$

where f is the activity coefficient which is supposed to depend not only on the distribution and surface concentration of deposited particles but also on particle/particle interactions. Note also that f is a spatial variable having the property

$$f = 1 \quad \text{at distance} > 2a + \delta^* \quad (57)$$

where δ^* is the range of particle/particle interactions.

Since the coefficient f as defined by Eq. (56) is dependant on particle configuration which in turn is determined by the particle transport mechanism in the bulk (flow, diffusion, external force), both the bulk and surface continuity equations become coupled in a complicated, non-linear way which prohibits any general solution of the boundary value problem expressed by Eqs. (52)–(54). Therefore, simplified models are usually considered like the above SL approximation (Eqs. (53) and (54)) or the linear model assuming an ideal behaviour in the bulk and neglecting the influence of deposited particles, when $f = 1$. In the latter case the non-stationary bulk transport equation becomes

$$\frac{\partial n}{\partial t} = \nabla \cdot [\mathbf{D} \cdot \nabla n + (\mathbf{D} \cdot \nabla \phi / kT - \mathbf{V}_p) n] \quad (58a)$$

with the PS boundary conditions

$$n = 0 \quad \text{at } \delta_m \quad (58b)$$

$n = n_b$ far from the interface

A particularly attractive from the theoretical viewpoint situation arises when the normal component of the flow and the external force are independent of coordinates tangential to the interface. Then Eq. (58a) can be converted into the simple one-dimensional form [131–133]

$$\frac{\partial n}{\partial t} = \frac{\partial}{\partial h} \left\{ D(h) \left[\frac{\partial n}{\partial h} + n \frac{\partial \phi / kT}{\partial h} \right] \right\} + Q(h) \quad (59)$$

where h is the separation between particle and the interface and $Q(h) = -n \nabla \cdot \mathbf{V}_p - \mathbf{V}_p \cdot \nabla n$.

The advantage of Eq. (59) (being from a mathematical viewpoint a parabolic partial differential equation) is that it can exactly be solved by standard numerical techniques, e.g. by the finite-difference Crank–Nicholson scheme [131,132] under

transient (non-stationary) conditions. The surfaces for which Eq. (59) is fulfilled are usually referred to in the literature as the uniformly accessible surfaces [67,133].

Eq. (59) can further be simplified when assuming that the steady-state conditions are established. As demonstrated in Adamczyk [138], this is a valid assumption for a broad class of practically important situations when the duration of the transient regimes is of the order of seconds. One of a few exceptions is particle sedimentation against an energy barrier [139] or particle accumulation at a secondary minimum of a considerable depth [131,132]. When the steady-state is postulated, Eq. (59) simplifies to the form

$$\frac{d}{dh} \left[D(h) \left(\frac{dn}{dh} + \frac{d\phi/kT}{dh} n \right) \right] + Q(h) = 0 \quad (60)$$

This is an ordinary one-dimensional differential equation, which can be efficiently solved by the standard numerical method (e.g. the Runge–Kutta method).

A number of important solutions to Eqs. (59) and (60) have been derived in the literature for barrier-less and barrier-controlled transport conditions. Since these solutions are also important for many practical applications we shall briefly discuss some representative results in Section 4.1.1.

4.1.1. Limiting solutions for the perfect sink model

The solutions of quite general validity can be derived analytically for the Smoluchowski–Levich approximation. Physically, this model works best for suspensions of small colloid particles and not too vigorous flows. Then, the diffusion boundary-layer thickness remains much larger than particle dimension so the effect of specific and external force fields become negligible as well as the diffusion coefficient changes due to the presence of interfaces. The simplest situation of this kind arises for a larger sphere of radius R (collector) placed in an otherwise quiescent suspension of particles having the radius a . In this case the SL equation, Eq. (52) can be solved analytically giving the expression for the particle flux in the form [130]

$$j = \frac{D_{12}}{R} \left(\frac{1}{\sqrt{\pi\tau}} + \frac{1}{1 + As} \right) n_b \quad (61)$$

where $D_{12} = D_1 + D_\infty$ (D_1 , D_∞ are the diffusion coefficients of the collector and the colloid particle, respectively), and $As = a/R$, $\tau = tD_{12}/R^2$.

It should be mentioned that we have accepted hereafter the convection of expressing fluxes to the interface as positive quantities (adsorption rates).

The first term on the r.h.s. of Eq. (61) describes the transient particle flux which becomes negligible when $\tau \gg 1$. Then, after this transition time, the stationary j_0 flux becomes

$$j_0 = \frac{D_{12}}{R} \frac{1}{1 + A_s} n_b. \quad (62)$$

The number of particles deposited on the surface of larger sphere per unit time is according Eq. (62) equal to

$$N_p = 4\pi(a + R)^2 j_0 = 4\pi(D_1 + D_\infty)(a + R)n_b \quad (63)$$

Eq. (63) was first derived by Smoluchowski [130] in his fast coagulation theory.

In the case when $A_s \rightarrow 0$ (colloid particle size much smaller than collector dimension), the stationary flux becomes $D_\infty n_b / R$.

It should be remembered, however, that in this case, the collector size should be small enough so the inequality $D_\infty t / R^2 \gg 1$ is fulfilled. Otherwise, for large collector radius, the first term on the r.h.s. of Eq. (61) dominates and particle flux remains non-stationary for $t < R^2 / D_{12}$, i.e.

$$j = \sqrt{\frac{D_{12}}{\pi t}} n_b \cong \sqrt{\frac{D_\infty}{\pi t}} n_b \quad (64)$$

Such situation occurs, e.g. for a planar interface.

Eq. (61) has an important meaning because it represents the only analytical solution of the SL equation under transient conditions when no flow occurs. For flowing systems, analytical solutions are only feasible under stationary conditions. Thus, in the case of a sphere placed in uniform suspension stream V_∞ (or the analogous case of a sphere sedimentation with the steady velocity V_∞ throughout a quiescent suspension of infinite extension) particle flux in the vicinity of the flow symmetry line is given by the expression [67]

$$j_0 = 0.88 \frac{D_\infty^{2/3} V_\infty^{1/3}}{R^{2/3}} n_b \quad (65)$$

Note, that this stationary value of the flux (often referred to as the limiting or initial flux) is proportional to $D_\infty^{2/3}$ rather than D_∞ as was the case for no flow conditions. It is also interesting to observe that j_0 is rather insensitive to the fluid velocity V_∞ .

A formula analogous to Eq. (65) with the proportionality coefficient 0.98 was derived for the cylinder placed in the uniform [67]. Similarly, for the circular impinging jet cells one formulated the expressions [140]

$$j_0 = 0.78 \bar{\alpha}^{1/3} \frac{D_\infty^{2/3} V_m^{1/3}}{R^{2/3}} n_b \quad (66)$$

where $\bar{\alpha}$ is the dimensionless flow intensity function of $Re = V_m R / \nu$ (V_m is the mean linear velocity in the cell, R is the capillary radius, ν is the fluid kinematic viscosity). For $Re > 10$, $\bar{\alpha}$ can well be approximated by $C Re^{1/2}$ where C is the dimensionless constant of the order of unity [141,142].

For the slot impinging jet (SIJ) the expression for j_0 is analogical to Eq. (66) [143] with the $\bar{\alpha}$ function determined numerically in Adamczyk et al. [144]. For $Re < 40$ it can be approximated by the interpolating polynomial

$$\bar{\alpha} = 0.424 + 0.822Re + 0.0013Re^2 \quad (67a)$$

For $Re > 10$ one has a simpler expression for $\bar{\alpha}$ [144]

$$\bar{\alpha} = 0.92Re^{1/2} - 1.71 \quad (67b)$$

Analytical expression for j_0 was derived by Levich in the case of the rotating disc [136]

$$j_0 = 0.616D_\infty^{2/3} \frac{\omega^{1/2}}{\nu^{1/6}} n_b \quad (68)$$

where ω is the disc angular velocity.

It should be mentioned that in this case the limiting flux j_0 is uniform over the entire surface, whereas for all previous cases the flux remained constant within a small region in the vicinity of the symmetry line. This can be deduced from the exact expressions derived for a sphere [136] or cylinder [145] placed in an uniform flow, i.e.

$$j_0 = f_s(\vartheta) \frac{A_f^{1/3} D_\infty^{2/3} V_m^{1/3}}{R^{2/3}} n_b \quad (69)$$

where $f_s(\vartheta) = 0.78\sin\vartheta / (\vartheta - 1/2\sin 2\vartheta)^{1/3}$ for the sphere,

$$f_c(\vartheta) = 0.85 \frac{\sqrt{\sin\vartheta}}{\left(\int_0^\vartheta \sqrt{\sin\xi} d\xi \right)^{1/3}}$$

for the cylinder, ϑ is the angular coordinate measured from the flow symmetry line or plane (for cylinder), and A_f is the flow model parameter.

It was shown in Adamczyk et al. [144] by performing numerical calculations that a quite analogous dependence of j_0 on the tangential coordinate is expected for the SIJ cell.

As can be deduced from Eq. (69) and the graph shown in Adamczyk et al. [67] the flux does not change appreciably for angles smaller than 90° , i.e. in the front part of the collector. The flux uniformity is markedly more uniform for the cylindrical collector [67].

A different situation occurs for other non-uniformly accessible surfaces like the parallel-plate or cylindrical channel used widely for colloid deposition studies. For

these collectors the flux tends to infinity at the entrance part, according to the analytical expressions derived in [146]

$$j_0 = 0.78 \frac{D_\infty^{2/3} V_m^{1/3}}{b^{1/3} x^{1/3}} n_b \quad (70a)$$

where x is the distance measured from the inlet region, $2b$ is the depth of the channel and V_m is the mean fluid velocity in the channel.

For the cylindrical channel one has [146]

$$j_0 = 0.86 \frac{D_\infty^{2/3} V_m^{1/3}}{R^{1/3} x^{1/3}} n_b \quad (70b)$$

where R is the radius of the channel.

Obviously, for any practical situation the flux will remain finite (although large) in the limit $x \rightarrow 0$ due to the tangential diffusion which was neglected by derivation of Eqs. (70a,b).

Except for predicting particle deposition rate for the initial conditions (low coverage regime), Eqs. (62)–(67), (67b)–(70) and (70b) have a significance for testing the accuracy of numerical solutions of the exact continuity equation, Eq. (59). These solutions, discussed extensively in previous reviews [48,67,78,133], demonstrated that the above limiting solutions can be useful for predicting deposition rate of particles smaller than $0.5 \mu\text{m}$ in diameter when the specific interaction energy was characterised by the Type I profile. For larger particle sizes, the coupling between specific and hydrodynamic interactions is causing a significant deviation of exact flux from the Smoluchowski–Levich theory [67]. In this case only the numerical solution of the exact continuity equation assure a sufficient accuracy of the limiting flux estimation. However, for particle sizes $> 1 \mu\text{m}$, and Type I profile dominated by strong electrostatic attraction, one can derive limiting, analytical expressions for j_0 which can well approximate the exact numerical results. The derivation is based on the effective hard particle concept [90], i.e. the geometrical radius of particle a is replaced by the effective radius a^* increased by the effective interaction range h^* . Thus, a^* is calculated for the HHF model from the formula [147]

$$a^* = a \left[1 + \overline{Le} \xi - 2 \overline{Le} \ln(1 + \overline{Le} \xi) \right] = a f_i \quad (71)$$

where $\overline{Le} = Le/a$, $\xi = \ln(2\epsilon a |\psi_1^0 \psi_2^0| / kT \overline{Le} Pe)$ $Pe = 2V_{ch} a/D$ is the dimensionless Peclet number characterizing the ratio of convection to diffusion effects [67,133] and V_{ch} is the characteristic convection velocity at the distance a^* from the interface. Eq. (71) is valid for $Pe > 1$ [147]. It can be deduced from Eq. (71) that a significant increase in the effective interaction range is expected for high surface potentials and κa values < 10 .

By introducing the concept of the effective interaction radius one can properly describe the interception effect, dominating for large particles, which is proportio-

nal to a^{*2} . As a consequence the limiting particle flux is approximated by the expression [147]

$$j_0 = \frac{1}{2} Pe \frac{D_\infty}{a} f_i^2 n_b \quad (72)$$

One can formulate Eq. (72) explicitly using the Pe definitions given in Adamczyk et al. [67]. In this way, one obtains for the spherical collector (in the region close to the flow stagnation point) the expression

$$j_0 = 1.5 A_f \frac{V_\infty}{R^2} a^{*2} n_b = 1.5 A_f \frac{V_\infty}{R^2} a^2 f_i^2 n_b \quad (73)$$

For the impinging jet and the slot impinging jet cell one has analogously

$$j_0 = \bar{\alpha} \frac{V_m}{R^2} a^2 f_i^2 n_b \quad (74a)$$

$$j_0 = \bar{\alpha} \frac{V_m}{d^2} a^2 f_i^2 n_b \quad (74b)$$

where $2d$ is the slot width.

As can be seen from Eqs. (72)–(74b), the flux increases proportionally to the mean flow rate V_m and to the square of the effective particle radius a^* . Since, according to Eq. (71) the effective interaction radius increase considerably with the decrease in κa , one can deduce from Eqs. (72)–(74b) that the appearance of attractive electrostatic interactions could enhance manifold particle deposition rate [147].

A quite opposite situation is met when the electrostatic interactions are of repulsive character leading to Type II energy profile, characterised by the presence of an energy barrier. Due to its practical significance this case will be discussed separately in Section 4.1.2.

4.1.2. The surface force boundary layer approximation

As mentioned, the specific interactions described by Type II energy profile are very short ranged in comparison with the diffusion boundary layer thickness. This leads to large potential gradients at the interface which makes exact numerical solution of the mass transfer equations, Eq. (59) rather cumbersome [131,132]. However, the barrier dominated transport of colloid particles can effectively be treated by the approximate method developed originally by several authors [148–151]. The method, referred to as the surface boundary layer approximation (SFBLA), is based on the assumption that the particle transport through the thin surface force layer can be treated as a process independent of bulk transport. As a result, fluid convection is neglected within the surface layer of thickness δ , whereas the specific interactions are assumed negligible outside δ . We shall formulate the

SFBLA in a more general form, suitable for treating the problem of the steric barrier arising due to deposited particles.

The starting point of the approach would be Eq. (47) formulated, by neglecting fluid convection and using Eq. (56), in the more concise form

$$\mathbf{j} = -\mathbf{D} \cdot [\nabla \ln n + \nabla \Phi/kT]n \quad (75)$$

where the function $\Phi = \phi + kT \ln f$ can be treated as the generalised potential. Because, according to the SFBLA, the thickness of the surface layer is very small in comparison with the interface dimensions (curvature) one can treat particle transport through this layer as a one-dimensional problem. As a consequence, Eq. (75) can be expressed as

$$j(h,t) = -D(h) \left[\frac{\partial \ln n}{\partial h} + \frac{\partial \Phi/kT}{\partial h} \right] n = -D(h) e^{-\Phi/kT} \frac{\partial}{\partial h} e^{\Phi/kT + \ln n} \quad (76)$$

Considering that the relaxation time of establishing the quasi stationary transport conditions through this layer $\tau = \delta^2/D(h) \sim \delta^2/D_\infty$ is very short, one can treat j as a quasi-stationary variable, independent of time and the distance h . Then, Eq. (76) can easily be integrated within the domain $\delta_m < h < \delta$ which gives the general expression (positive flux convention used) [135]

$$j_b = \frac{n(\delta) e^{\Phi(\delta)/kT} - n(\delta_m) e^{\Phi(\delta_m)/kT}}{R_b} \quad (77)$$

where $n(\delta_m)$, $n(\delta)$ is the particle concentration at the PM and at the edge of δ , respectively, and

$$R_b = \int_{\delta_m}^{\delta} \frac{e^{\Phi/kT}}{D(h)} dh = R_{\text{exc}} + R_0 \quad (78)$$

can be treated as the static resistance due to the presence of the barrier.

Moreover,

$$R_0 = \int_{\delta_m}^{\delta} \frac{dh}{D(h)} \quad (79a)$$

and

$$R_{\text{exc}} = \int_{\delta_m}^{\delta} \left[\frac{e^{\Phi/kT} - 1}{D(h)} \right] dh \quad (79b)$$

is defined as the excess resistance.

Spielman and Friedlander [149] assumed that the diffusion coefficient is independent of the distance h so the appear integration limit in Eq. (79a) could be extended to infinity.

One can derive from Eq. (77) several interesting cases. For the interaction energy Type II profile (characterised by deep PM potential and $\phi \rightarrow 0$ outside the surface layer) and no steric barrier (when $f = 1$) Eq. (77) reduces to

$$j_b = \frac{n(\delta)}{R_b} = \frac{n(\delta)}{R_{\text{exc}} + R_0} = k'_a n(\delta) \quad (80)$$

where $k'_a = 1/R_b$ is the rate constant of particle deposition.

Eq. (80) can be treated as the generalised boundary condition for the bulk transport [148–151].

For energy profiles characterised by the presence of the secondary minimum the expression for the flux becomes

$$\frac{n(\delta_{\text{sm}})e^{\phi_{\text{sm}}/kT}}{\int_{\delta_m}^{\delta_{\text{sm}}} \frac{e^{\phi/kT}}{D(h)} dh} = \frac{n(\delta_{\text{sm}})}{\int_{\delta_m}^{\delta_{\text{sm}}} \frac{e^{\phi'/kT}}{D(h)} dh} \quad (81)$$

where $\phi' = \phi - \phi_{\text{sm}}$, and ϕ_{sm} is the secondary minimum depth.

Eq. (81) indicates that for calculating the static resistance R_b one should use the SM potential as the reference value. In other words, the barrier height should be measured relative to the SM rather than to the bulk zero value as usually done. This prediction was confirmed by numerical results discussed in Dąbróś and Adamczyk [152].

Knowing j_b one can derive a general expression for the overall flux due to barrier and bulk transport. In general, for the non-uniformly accessible surfaces this requires the bulk transport equation to be solved with the boundary conditions expressed by Eq. (80). Such solutions were derived in the case of the spherical and cylindrical collectors by Spielman and Friedlander [149] and for the parallel plate and cylindrical channel by Boven et al. [150] and Ruckenstein [151]. Unfortunately, explicit evaluation of the overall deposition rate as a function of parameters characterizing surface interactions can only be carried out numerically.

However, useful analytical expressions for the overall flux can be derived in the case of uniformly accessible surfaces. This can be done by exploiting the flux continuity condition $j_b = j$ (where j is the flux due to bulk transport through the macroscopic layer) from which it follows that

$$\frac{n(\delta)}{R_b} = \frac{n_b - n(\delta)}{R'_{\text{conv}}} \quad (82)$$

where R'_{conv} is the static resistance of the diffusion boundary layer (up to the point $h = \delta$). By eliminating $n(\delta)$ from Eq. (82) one obtains the explicit expression for

the overall flux in the form

$$j = n(\delta)/R_b = \frac{1}{R_b + R'_{\text{conv}}} n_b = \frac{1}{R_{\text{exc}} + R_{\text{conv}}} n_b \quad (83)$$

where $R_{\text{conv}} = R'_{\text{conv}} + R_0$ is the static resistance of the overall boundary layer in the absence of the energy barrier. R_{conv} can be estimated from previous expressions for the limiting flux since $j_0 = n_b/R_{\text{conv}}$. Using this expression one can transform Eq. (83) into the form

$$j = j_0 \frac{1}{1 + \frac{j_0}{n_b} R_{\text{exc}}} = j_0 \frac{1}{1 + \frac{j_0}{n_b} \int_{\delta_m}^{\delta} \frac{e^{\phi/kT} - 1}{D(h)} dh} \quad (84)$$

The use of Eq. (84) requires evaluation of the definite integral which can be cumbersome. However, explicit results of quite general validity can be derived for energy profiles exhibiting well defined maxima. Then, expanding the energy distribution around the maximum in Taylor series one can derive in the case of a symmetric maximum the formula [148,150,151]

$$R_{\text{exc}} \cong R_b \cong \left(\frac{2\pi kT}{\gamma_b} \right)^{1/2} \frac{e^{\phi_b/kT}}{D(\delta_b)} \quad (85)$$

where $\gamma_b = - \left(\frac{d^2\phi}{dh^2} \right)_{\delta_b}$.

Eq. (85) can further be simplified by realizing that $\gamma_b \sim \phi_b/\delta^2$ and $D \sim D_{\infty}\delta/a$ [133]. In this way Eq. (85) can be expressed as

$$R_b \cong \frac{a}{D_{\infty}} \left(\frac{2\pi kT}{\phi_b} \right)^{1/2} e^{\phi_b/kT} \quad (86)$$

For a strongly asymmetric barrier, e.g. of a triangular shape one can analogously express R_b as

$$R_b \cong \frac{a}{D_{\infty}} \frac{kT}{\phi_b} e^{\phi_b/kT} \quad (87)$$

Substituting this expression into Eq. (83) one obtains

$$j = j_0 \frac{1}{1 + \frac{j_0 a}{D_{\infty} n_b} \frac{kT}{\phi_b} e^{\phi_b/kT}} = \frac{1}{1 + Sh_0 \frac{kT}{\phi_b} e^{\phi_b/kT}} \quad (88)$$

where $Sh_0 = j_0 a/D_{\infty} n_b$ is the dimensionless flux (Sherwood number). The dependence of the relative flux j/j_0 on the triangular barrier height ϕ_b calculated

from Eq. (88) is shown in Fig. 15. As one can notice, the effect of the barrier height is the largest for large Sh values, i.e. high particle deposition rate (larger particle sizes). Then, for $\phi_b > 5kT$, the relative flux decreases exponentially with increasing barrier height since

$$j/j_0 \cong \frac{1}{Sh_0} \left(\frac{\phi_b}{kT} \right) e^{-\phi_b/kT} \quad (89)$$

On the other hand, for low Sh_0 values (which physically corresponds to the small colloid particles under low Re flows), the relative flux is insensitive to barrier height if the inequality is met

$$\phi_b/kT < -\ln Sh_0 + \ln|\ln Sh_0|$$

where $Sh_0 \ll 1$.

It is interesting to mention that Eqs. (88)–(90) and the results shown in Fig. 15 are of an universal validity and can be used for flux estimation for any kind of a barrier.

The role of specific interactions and estimations of the range of validity of the analytical approximations discussed in the last sections have been determined theoretically in numerous works concerning the barrier-less [67,78,133,147,153–156] and barrier-controlled deposition regimes [78,128,132,133,152]. It has been predicted that the limiting flux can be increased considerably by the attractive electrostatic interactions (barrier-less transport), especially in the case of larger Pe number (large particle sizes and high Re flows) [147,156] in accordance with Eqs.

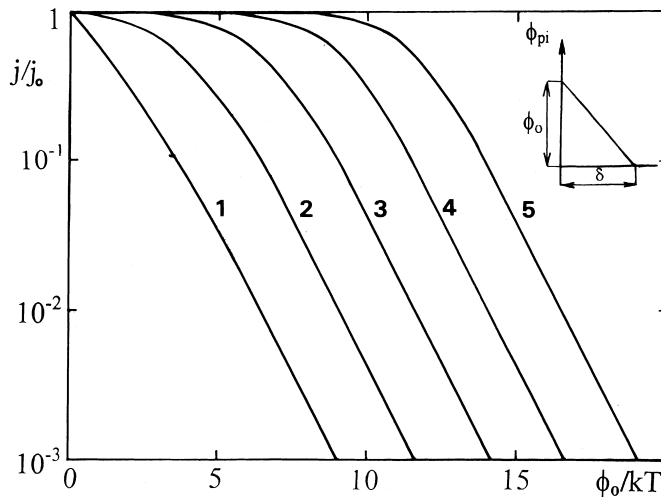


Fig. 15. The influence of the triangular barrier height ϕ_0/kT (for definition see the inset) on the relative particle flux j/j_0 (where j_0 is the flux when no barrier is present); the curves were calculated from Eq. (88) for (1) $Sh_0 = 1$; (2) $Sh_0 = 10^{-1}$; (3) $Sh_0 = 10^{-2}$; (4) $Sh_0 = 10^{-3}$; (5) $Sh_0 = 10^{-4}$.

(71)–(73). The influence of the double layer model and the surface potentials of particle and the interface was found to be minor, the κa parameter played a decisive role [78,147,156]. It was so, however, for collectors placed in stagnation flows, like the impinging jet cell [147], cylindrical [154] and spherical collectors either isolated or forming packed bed columns [155,156]. For the parallel and cylindrical channel [153] the flux enhancement due to attractive double-layer interactions was found less significant, except in the region close to the suspension inlet point.

The role of the dispersion interactions was also extensively studied for various collectors. In accordance with previous discussion, the dispersion interactions, due to their fairly limited range (especially when the retardation effect is concerned) increased the predicted initial flux very moderately. For $Pe \gg 1$ (large particle limit) the flux increase was found proportional to $A_{102}^{1/3}$ [157,158]. From these numerical calculations one can draw the conclusion that, in general, for a particle size below $0.5 \mu\text{m}$ the attractive specific interactions exert no appreciable effect on particle deposition rate which can accurately be determined from the SL approximation [Eqs. (62)–(67), (67b)–(70), (70b)].

A more complicated situation arises for the barrier controlled deposition regime discussed extensively by several authors [78,128,152]. As expected, the calculated flux values were found very sensitive to the double-layer model, surface potential, double layer thickness and the Hamaker constant, since all these parameters influence significantly the energy barrier height. However, when the deposition flux is correlated with the interaction energy profile rather than with the above physicochemical parameters, some conclusions of general validity could be formulated. Thus, it has been found in Dąbroś and Adamczyk [152] that the SFBLA works well for deposition regimes characterised by $Pe < 0.1$ (which again would correspond to particle sizes below $0.5 \mu\text{m}$) provided that the energy barrier is measured relative to the SM depth (cf. Eq. (81)). For larger particles ($Pe \gg 0.1$), the calculated flux values under barrier controlled regime are much larger than the SFBLA predicts [152] which is due to flow-induced transport of particles through the energy barrier.

4.2. Role of the lateral particle / particle interactions

The results discussed above concerning particle deposition at the initial, linear stages may be useful for basic studies of the dynamic interactions in the colloid particle/solid interface system. Since particle deposition in this case can be treated as the limiting form of heterocoagulation one can draw important clues about the stability of colloid mixtures just by measuring particle deposition rate at appropriately chosen surfaces. Also the validity of the DLVO theory for describing particle/wall interactions can be tested with a good accuracy by performing well designed deposition experiments.

However, as mentioned before, the linear transport conditions are usually short-lasting, especially for concentrate colloid suspensions. The deviation from linearity is due to the presence of particles accumulated at the interface during the

course of deposition process. The resulting surface blocking effects are very complex for interacting colloid particles which prohibits any exact mathematical treatment of these phenomena. Usually drastically simplified models are introduced like the Langmuirian approach discussed above when all hydrodynamic and electrostatic interactions are neglected and topology of particle distribution is not considered. Another disadvantage of this model is that the saturation coverages cannot be determined a priori, not even as crude estimations. This can only be done experimentally which is bound to large uncertainty due to long deposition times needed for approaching maximum coverages.

A more realistic description of particle adsorption can be attained using the random sequential adsorption (RSA) approach developed originally for hard (non-interacting) particles [159–172] and extended later on for interacting particles [80,81,173].

The RSA model is based on the main assumptions:

1. Particles are placed at random (shot) over a target, every position on the target is accessible with equal probability.
2. If the trial (virtual) particle overlaps with any of previously adsorbed particles it is removed with unit probability.
3. Otherwise the particle is placed with unit probability (hard sphere model) or with the probability calculated from the Boltzmann distribution by taking into account the pairwise electrostatic interactions (interacting sphere model). Once the particle is adsorbed its position is permanently fixed (localised adsorption called deposition as above).
4. The process is continued until the entire surface is completely covered and no more particles can be accommodated thus the maximum (jamming) coverage θ_∞ is attained.

The jamming coverages for particles of various geometrical shape adsorbing flat (side on) on planar interfaces were determined numerically using the Monte-Carlo simulation technique [163,167–170]. For hard spheres (more precisely disks) θ_∞ was found to be 0.547 [160,163]. For spheroidal particles adsorbing flat, this value does not change appreciably with the elongation parameter As [169]. However, for the unoriented adsorption (when particles can adsorb perpendicularly) the saturation coverages were found much larger, increasing proportionally to $1/As$ for higher elongations [172].

The RSA model can also be applied for determining the surface blocking parameter $B(\theta)$ and for modelling adsorption kinetics of both spherical [164–167] and non-spherical particle, e.g. cylinders, spherocylinders and spheroids [167–172]. It was found that in all cases and not too high surface coverages the blocking function can well be approximated by the polynomial expansion [164,168,172]

$$B(\theta) = 1 - \sum C_n \theta^n \quad (90)$$

where the coefficients $C_1 \div C_3$ were determined for spheres [164], hard (noninteracting) spheroids (ellipses) [168], cylinders and spherocylinders [168–170].

For hard spheres, using the analytical values for $C_1 \div C_3$ given in Schaaf and Talbot [164], one can evaluate Eq. (90) explicitly as

$$B(\theta) = 1 - 4\theta + \frac{6\sqrt{3}}{\pi}\theta^2 + \left(\frac{40}{\pi\sqrt{3}} - \frac{176}{3\pi^2} \right)\theta^3 + O(\theta^4) \quad (91)$$

For low θ one can arrive apparently at the Langmuirian model since

$$B(\theta) \cong 1 - 4\theta = 1 - \theta/\theta_L \quad (92)$$

where $\theta_L = 0.25$

One can easily notice, however, that this θ_L value deviates from the above mentioned jamming value of $\theta_\infty = 0.547$. This proves that approximating the blocking function by Langmuir model with the θ_L coefficient calculated from the saturation coverage is rather inaccurate. Similar situation arises for other particle shapes as well, i.e. the C_1 coefficient never agrees with the $1/\theta_\infty$ value. This can be observed in Fig. 16 where the exact numerical simulations (points) are compared with the limiting analytical expansion, Eq. (90) and the Langmuirian model, Eq. (92). As one can observe, the low coverage expansion works well for $\theta < 0.3$ both for spheres and spheroids (ellipses). On the other hand, the Langmuir model gives poor approximation of exact data, especially for non-spherical (elongated) particles.

The deviation from the Langmuir model becomes also pronounced for larger θ

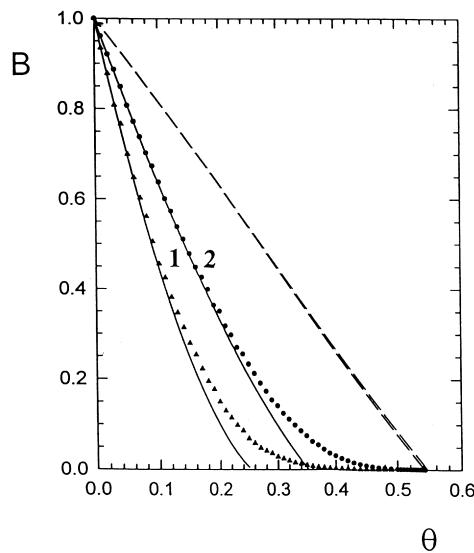


Fig. 16. $B(\theta)$ for spheres and spheroids (side on adsorption), the points denote the exact MC stimulation results, the continuous line represents the low-coverage approximation Eq. (90) and the dashed lines show the Langmuirian model, when $B(\theta) = 1 - \theta/\theta_\infty$. (1) $As = 0.2$; (2) $As = 1$ (spheres).

close to the jamming limit, when the blocking parameter can be approximated by the formula [164,166,170,171]

$$B(\theta) \approx (\theta_\infty - \theta)^m \quad (93)$$

where m is an integer equal to 3 for sphere adsorption [164], equal to 4 for a side on adsorption of anisotropic particles [166,169] and equal to 5 for unoriented adsorption of spheroids [172]. One can deduce from Eq. (93) that the blocking effects predicted in the RSA model are considerably more pronounced than in the Langmuirian model. This originates from the fact that due to topological constraints only a small fraction of the free surface $1-\theta$ is available for particle adsorption, i.e. in the later adsorption stages most of the unoccupied surface fragments (targets) are too small to accommodate additional particle [67].

Similar results as that expressed by Eqs. (90)–(93) can also be derived for interacting particle adsorption provided that the effective interaction range remains much smaller than particle dimensions [80,81,173]. Then, the many-body electrostatic interactions between adsorbed and adsorbing particles can be approximated by the sum of interactions between particle pairs. The electrostatic energy of the interaction of the pair is calculated from the above discussed double-layer models using the LSA for spherical particles [173] and the Derjaguin and ES approaches for anisotropic particles [80,81]. In practice the RSA modelling for interacting particles can only be performed in terms of time consuming MC numerical simulations [48,67,80,81,173]. It was demonstrated, however, that the limiting expressions, Eqs. (91) and (93) retain their validity if the interacting particle is replaced, in accordance with the EHP concept [90], by the effective hard particle having the size increased by the effective interaction range h^* . As demonstrated in Adamczyk and co-workers [81,173] h^* is proportional to Le both for spheres and spheroids. This can be seen in Fig. 17 where the dependence of $H^* = h^*/a$ on $\overline{Le}(\kappa a)$ is plotted for spheres, and prolate spheroids having the axis ratio As equal to 0.5 and 0.2, respectively. Thus, H^* can well be approximated by the relationship analogous to Eq. (71)

$$H^* = \frac{1}{2} L e \ln \frac{\phi_0}{\phi_{ch}} \quad (94a)$$

where ϕ_0 is given according to the LSA model by $\varepsilon a(kT/e)^2 \overline{Y}_1^{02}$ and ϕ_{ch} is the characteristic energy close to a kT unit [81].

In terms of H^* , the $C_1 \div C_3$ constants in Eq. (91) scale up as

$$\begin{aligned} C_1^* &= C_1(1 + H^*)^2 \\ C_2^* &= C_2(1 + H^*)^4 \\ C_3^* &= C_3(1 + H^*)^6 \end{aligned} \quad (94b)$$

Analogously, the θ_∞ for interacting particles is given by the simple expression (referred to as the maximum coverage θ_{mx})

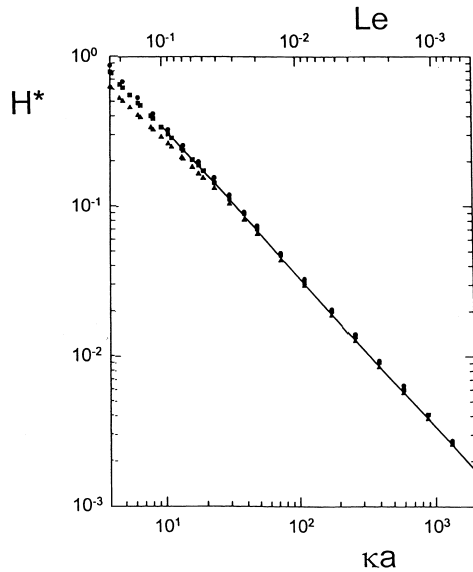


Fig. 17. The dependence of the effective interaction range H^* on the κa (Le) parameter [81]. The points represent exact numerical results for prolate spheroids characterised by various elongation: ●, $As = 1$ (spheres); ■, $As = 0.5$; ▲, $As = 0.2$; the solid lines show the analytical approximation calculated from the equation $H^* = 0.5 \bar{L}e \ln(\phi_0/\phi_{ch})$.

$$\theta_{mx} = \theta_{\infty} / (1 + H^*)^2 = \theta_{\infty} C_1 / C_1^* \quad (95)$$

The range of the validity of the EHP approximation, expressed by Eq. (95) can be estimated from data shown in Fig. 18 where the dependence of $\theta_{mx}/\theta_{\infty}$ vs. κa is plotted for spheres and spheroids (side on adsorption) characterised by $As = 0.5$ and $As = 0.2$, respectively. It can be observed that Eq. (95) reflects well the exact results obtained from the numerical MC RSA simulations (points), especially for $\kappa a > 10$ (thin double layer limit). The results shown in Fig. 18 suggest that the lateral electrostatic interactions (described by LSA model) will considerably influence the jamming (monolayer) coverage of colloid particles. Thus, for spheroidal particles with $As = 0.5$ the monolayer coverages drops to 50% of the hard particle value ($= 0.583$) for double layer thickness equal to 0.1 of the longer particle axis. Experimental results concerning an experimental verification of the theoretical data shown in Fig. 18 will be discussed later on.

The range of validity of the EHP approximation was discussed extensively in our previous reviews [48,67]. It was concluded that the RSA model extended for interacting particles proved useful for interpreting experimental results under moderate flow conditions. However, some deviations were observed for very low Re number flows [67], no flow conditions [174,175] and for adsorption at surfaces precovered with smaller particles [176]. The observed adsorption kinetics proved to be faster than the RSA model predicts. As pointed out in Adamczyk and co-workers

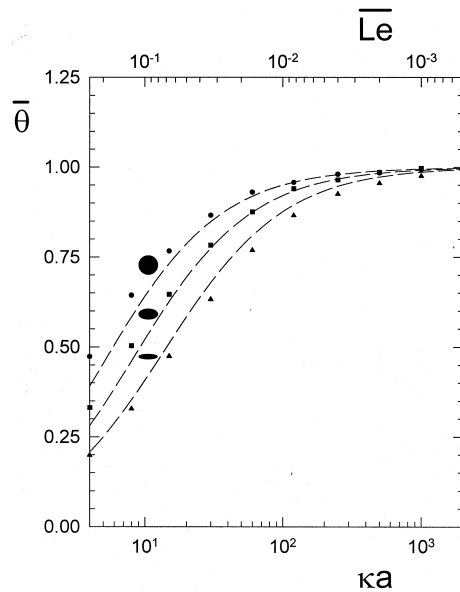


Fig. 18. The dependence of the normalised maximum surface concentration $\bar{\theta} = \theta_{max}/\theta_{\infty}$ on the κa parameter; the points denote the numerical results obtained for interacting prolate spheroids of various elongation, i.e. $As = 1$ (spheres), $As = 0.5$ and $As = 0.2$, the broken lines denote the analytical approximations calculated from Eq. (95).

[67,135] the deviations appeared because in the RSA model particle deposition is treated as a surface process independent of distance from the interface and particle diffusion. These limitations can be avoided in the recently developed diffusion RSA (DRSA) approach [134,135,177,178] which considers a one-dimensional transport of particles through the adsorbed particle layer. Thus, according to this approach the blocking effects due to adsorbed particles are not limited to the vicinity of the interface but they also influence particle transport in the bulk by decreasing the volume available for moving particles. For one-dimensional problems this exerts analogous effect as an decrease in the activity coefficient f which becomes dependent both on θ and the distance h . Physically, this would exert an analogous effect as an energy barrier extending over certain distance from the interface whose magnitude is growing with the coverage θ (time). Moreover, the height of the maximum can be closely related to the surface blocking parameter determined previously from the RSA model. It should be mentioned that a similar concept was developed in Warszyński [179] to interpret deposition kinetics (initial flux) for polymer coated particles.

4.2.1. The concept of the steric barrier

The starting point of our considerations is Eq. (77) expressed in the following form by noting that $\Phi = \phi + kT \ln f(\theta, h)$.

$$j = [n(\delta)f(\theta, \delta)e^{\phi/kT} - n(\delta_m)f(\theta, \delta_m)e^{\phi_m/kT}] / R_s(\theta) \quad (96)$$

where the steric barrier resistance $R_s(\theta)$ is given by Adamczyk et al. [135]

$$R_s(\theta) = R_{\text{exc}}(\theta) + R_0 \quad (97a)$$

with

$$R_{\text{exc}}(\theta) = \int_{\delta_m}^{\delta} [e^{\phi_s(\theta, h)/kT} - 1] \frac{e^{\phi/kT}}{D(h)} dh$$

$$R_0 = \int_{\delta_m}^{\delta} \frac{e^{\phi/kT}}{D(h)} dh \quad (97b)$$

$$\phi_s = kT \ln f(\theta, h)$$

It should be mentioned that the distance δ is defined as such where the activity coefficient becomes unity. Thus, δ is comparable with particle diameter (for hard particles δ equal to exactly $2a$). Since the convective transport in this layer was neglected, Eq. (96) is expected to become less accurate for deposition regimes characterised by larger Pe values, i.e. for larger particles, when this layer is penetrated by flow. As showed by Dąbrosz and van de Ven [180] this may happen for $Pe > 0.1$.

Assuming, in accordance with the PS model that ϕ_m tends to minus infinity, Eq. (96) can be formulated as

$$j = k_a n(\delta) \bar{B}(\theta) = j_0 \bar{B}(\theta) \quad (98)$$

where j_0 is the flux in the absence of adsorbed particles (initial flux) and

$$k_a = e^{\phi(\delta)/kT} / R_0$$

is the adsorption rate constant.

The function $\bar{B}(\theta)$ which can be treated as the generalised surface blocking parameter is defined as

$$\bar{B}(\theta) = \frac{R_0}{R_0 + R_{\text{exc}}(\theta)} = \left\{ 1 + \frac{\int_{\delta_m}^{\delta} [e^{\phi_s(\theta, h)/kT} - 1] \frac{e^{\phi/kT}}{D(h)} dh}{\int_{\delta_m}^{\delta} \frac{e^{\phi/kT}}{D(h)} dh} \right\}^{-1} \quad (99)$$

It should be mentioned that Eq. (98) constitutes the direct proof of the relationship used widely in previous works concerning the RSA governed adsorption kinetics [48,67].

It is difficult to evaluate $\bar{B}(\theta)$ explicitly in the general case because the activity coefficient is dependent not only on the distance h , the surface coverage θ but also

on the particle distribution over the surface. This distribution is in turn related to particle transport mechanism, i.e. diffusion, flow, external force [135]. However, some useful results can be derived from Eq. (99) for limiting adsorption regimes. Thus, in the case when the overall interaction potential ϕ (which can in general consist of the specific and external force contribution) exhibits a well defined maximum somewhere within $\delta_m < h < \delta$ then Eq. (99) can be approximated by

$$\bar{B}(\theta) \cong e^{-\phi_s(\theta, \delta_b)/kT} = f(\theta, \delta_b) \quad (100a)$$

where δ_b is the position of the maximum (barrier).

Eq. (100a) is valid for arbitrary shape of the barrier, provided that its extension (defined as the distance where the energy decreases by approx. $5 kT$ in comparison with its maximum value) is significantly smaller than the distance δ .

If the maximum is due to short ranged particle/interface electrostatic interactions or strong external force (gravity) acting outwards from the surface then the position of the maximum is close to the interface, so $\delta_b \sim \delta_m$, is a small fraction of particle dimensions. Then, the basic assumptions of the RSA model are fulfilled since all particles which overlap with adsorbed particles (at the surface) are removed due to presence of repulsive forces (energy barrier). Therefore, the activity coefficient $f(\theta, \delta_b)$ can well be approximated by its surface value given by the surface blocking function $B(\theta)$ originating from the RSA model [Eqs. (91)–(93)]. One may therefore write

$$\bar{B}(\theta) = e^{-\phi_s^0(\theta)/kT} = B(\theta) \quad (100b)$$

where ϕ_s^0 is the value of ϕ_s at P.M.

In this case, all the previous results derived from the RSA model for hard and interacting particles should retain their validity.

It seems also that these conditions were fulfilled in the experiments performed in [173,181,182] using the impinging jet cell when the gravity force was directed outwards from the interface.

Other useful results can be derived from Eqs. (97a,b) in the case of small colloid particles when the external forces become negligible and the specific interactions are described by the Type I profile close to the PS model. Then, the expression for $\bar{B}(\theta)$ simplifies to the form

$$\bar{B}(\theta) = \frac{\int_{\delta_m}^{\delta} \frac{dh}{D(h)}}{\int_{\delta_m}^{\delta} \frac{e^{-\phi_s(\theta, h)/kT}}{D(h)} dh} \quad (101)$$

where the ϕ_s/kT function can be expressed as the power series of θ [135]

$$\phi_s/kT = 1 - C_1'(h)\theta + C_2'(h)\theta_2 + 0(\theta)^3 \quad (102a)$$

where

$$C'_1 = 4\sqrt{1 - \xi^2}$$

$$C'_2 = \frac{8}{\pi} \left[2\xi^2(\xi^2 - 1) \arccos \frac{1}{2\sqrt{1 - \xi^2}} + \frac{1}{4} \sqrt{3 - 4\xi^2} (3 - 2\xi^2) \right] \quad (102b)$$

and $\xi = h/\delta$.

It can be easily noticed that for $\xi \rightarrow 0$ the C'_1 and C'_2 functions approach the RSA values, i.e. 4 and $(6\sqrt{3})/\pi$, respectively.

Using Eq. (102a) one can evaluate the expression for $\bar{B}(\theta)$, Eq. (101) as

$$\bar{B}(\theta) = 1 - \bar{C}_1\theta + \bar{C}_2(\theta)^2 + 0(\theta^3) \quad (103)$$

where the \bar{C}_1 coefficient is given by the analytical expression

$$\bar{C}_1 = [6 \ln \bar{\delta} - (1 - \bar{\delta})(5 - 7\bar{\delta} - 4\bar{\delta}^2)] / [1.5 \ln \bar{\delta} - 3(1 - \bar{\delta})] \quad (104)$$

$$\bar{\delta} = \delta_m / \delta$$

One can calculate from Eq. (104) that for $\bar{\delta} = 10^{-2}$, \bar{C}_1 is equal to 3.3 whereas for $\bar{\delta} = 10^{-3}$, \bar{C}_1 equals 3.5 which is only 12.5% less than the RSA value equal to 4. The \bar{C}_2 coefficient was found numerically to be 1.2 for $\bar{\delta} = 10^{-2}$ [135].

The expansion, Eq. (103) suggests that the DRSA model in which the hydrodynamic interactions sphere/interface were considered does not deviate considerably from the classical RSA model. Thus, for example for $\theta = 0.2$ one has $\bar{B}(\theta) = 0.33$ from the RSA model whereas $\bar{B}(\theta) = 0.37$ for the DRSA model. However, this hypothesis cannot be proven at present time due to mathematical difficulties in specifying the higher order terms in the expansion, Eq. (103).

Useful estimates of $\bar{B}(\theta)$ valid for higher coverages can be derived, however, by exploiting the properties of ϕ_s , i.e.

$$\phi_s(\theta, h) \rightarrow -kT \ln B(\theta) = \phi_s^0(\theta) \quad \text{for } h \rightarrow \delta_m$$

$$\phi_s(\theta, h) = 0 \quad \text{for } h > \delta \quad (105)$$

One can approximate the complicated distribution of $\phi_s(\theta, h)$ by the linear distribution, analogous to the triangular barrier discussed above, i.e.

$$\phi_s = \phi_s^0(\theta)(1 - \xi) \quad (106)$$

Substituting Eq. (106) into Eq. (99) one can derive for $\bar{B}(\theta)$ the formula

$$\bar{B}(\theta) = \frac{1 - \frac{1}{2} \ln \bar{\delta}}{kT \left(\frac{1}{\phi_s^0} - \frac{1}{2} \ln \bar{\delta} \right)} e^{-\phi_s^0/kT} \quad (107)$$

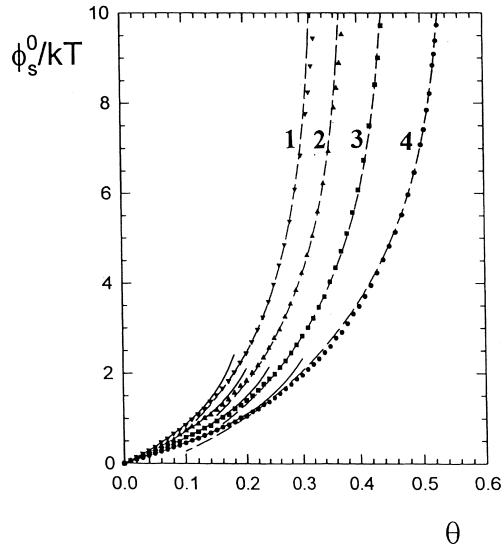


Fig. 19. The dependence of the steric interaction energy ϕ_s^0 on θ for interacting spheres; the points denote the numerical simulations performed for: (1) $H^* = 0.3$; (2) $H^* = 0.2$; (3) $H^* = 0.1$; (4) $H^* = 0$ (hard particles); the continuous lines denote the analytical results calculated from Eq. (90) and the broken line shows the asymptotic results calculated from Eq. (93).

For larger ϕ_s^0 the pre-exponential factor becomes practically independent on ϕ_s^0 and Eq. (107) simplifies to

$$\bar{B}(\theta) \cong \left(1 - \frac{2}{\ln \bar{\delta}}\right) e^{-\phi_s^0/kT} = \left(1 - \frac{2}{\ln \bar{\delta}}\right) B(\theta) \quad (108)$$

The dependence of the steric barrier height ϕ_s^0 on θ determined from the numerical MC simulations using the RSA model is plotted in Fig. 19 both for hard and interacting particles. The exact results (points) are compared with the approximate results stemming from the low coverage expansion, Eq. (90), when $\phi_s^0 = -kT \ln(1 - C_1\theta + C_2\theta^2)$ and the high coverage expansion when $\phi_s^0 = -m kT \ln(\theta_\infty - \theta) + C'$ (where C' is the dimensionless constant). One can see that these analytical models approximate well the exact numerical data both for hard and interacting spheres (characterised by $H^* = 0.1, 0.2$, and 0.3). From the data shown in Fig. 19 one may conclude that the steric barrier height increases rapidly when θ approaches the jamming (maximum) coverages. Since the accuracy of the steric barrier concept is expected to increase for larger barrier height (i.e. for $\theta \rightarrow \theta_\infty$) one can deduce that the previously calculated θ_∞ values (using the classical RSA model) will retain their significance as the most relevant parameters in the DRSA model.

It seems that extension of the DRSA model to non-spherical particles would be prohibitive mathematically since the $\bar{B}(\theta)$ function would depend not only on the

distance from the interface but also on particle orientation which in turn depends on local structure of adsorbed layer. However, the steric barrier concept could be used as a reasonable, first-order approximation at least for coverages close to jamming which are shown in Fig. 20 for hard prolate spheroids (derived from MC RSA simulations [81]). As one can observe, in the case of the side-on adsorption, the dependence of θ_∞ on the elongation parameter As exhibits a maximum around $As = 0.4$. On the other hand, in the case of unoriented adsorption θ_∞ increases monotonically when As is decreased, becoming proportional to $1/As$ for $As \rightarrow 0$ [81]. Note that the exact data for the unoriented adsorption deviate from the values calculated as an average of parallel and perpendicular orientation (shown by broken line in Fig. 20). This means that for later adsorption stages, due to topological constraints, the spheroids tend to adsorb under an orientation close to perpendicular [81]. This validates, at least to some extent the use of the steric barrier concept based on the one-dimensional diffusion equation. Due to complexity of the calculations, the jamming coverages for interacting spheroids (unoriented adsorption) were not calculated. It was shown in [81], however, that using the EHP concept θ for interacting particles which can be calculated from the approximate formula

$$\theta_{mx} = \theta_\infty \frac{(2.07 + 0.811As + 2.37As^2 - 1.25As^3)(1 + H^*)(1 + H^*/As)}{2.07 + 0.811As^* + 2.37As^{*2} - 1.25As^{*3}} \quad (109)$$

where $As^* = (As + H^*)/(1 + H^*)$

Knowing θ_{mx} one can then calculate the steric barrier ϕ_s^0 dependence on θ which is plotted in Fig. 21 both for hard and interacting spheroids, characterised by $H^* = 0.05, 0.1, 0.15$ and 0.25 . As one can observe the high coverage formula Eq. (93) with the exponent $m = 5$ which reflects well the exact numerical data. Thus, using Figs. 20 and 21 with the interpolating function given by Eq. (109) one can estimate the effect of the steric barrier on spheroidal particle adsorption.

All the results discussed hitherto were concerned with the transport through the layer of thickness δ with the convective effects neglected. In practice, for protein and colloid suspensions, δ is a small fraction of the overall diffusion boundary layer thickness only where the convection or external force dominate. In order to derive equations characterising the overall transport rate, one should couple the transfer rates through δ and the diffusion boundary layer, analogous to the SFBLA concept. In this way one can derive for the overall adsorption rate the formula [135]

$$j(\theta) = j_0 \frac{Ka}{Ka - 1 + \frac{1}{\overline{B}(\theta)}} \quad (110)$$

where

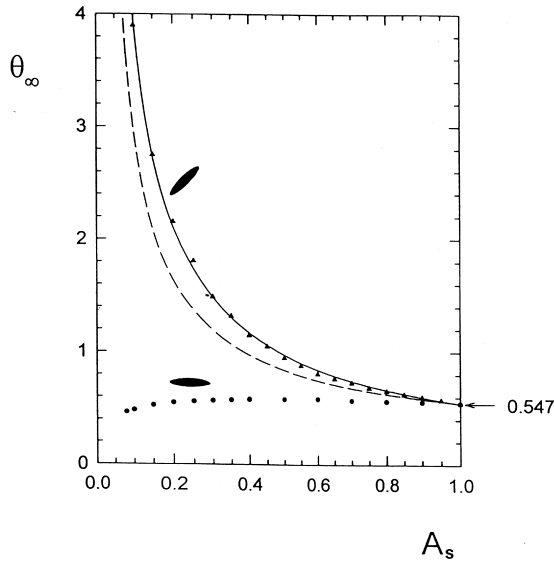


Fig. 20. The dependence of the jamming (maximum) surface coverage θ_∞ on the elongation parameter A_s determined numerically (points) for hard prolate spheroids under unorientated and side-on adsorption conditions: the solid line denotes the interpolation results [172] and the broken line shows the averaged from side-on and perpendicular orientation.

$$Ka = \frac{R_{\text{conv}}}{R_0} \tag{111}$$

Eq. (110) can be used for defining the overall blocking function $\tilde{B}(\theta)$

$$\tilde{B}(\theta) = \frac{j}{j_0} = \frac{Ka}{Ka - 1 + \frac{1}{\tilde{B}(\theta)}} \tag{112}$$

The Ka constant can explicitly be evaluated as

$$Ka = \frac{1}{2Sh_0q_0} \tag{113}$$

where $q_0 = \frac{D_\infty}{2a} \int_{\delta_m}^{\delta} \frac{e^{\phi/kT}}{D(h)} dh$.

Note that $Ka > 1$ because $R_{\text{conv}} \geq R_0$. When Ka assumes values much larger than unity (as is the case for protein and colloid particle transport) Eq. (112) simplifies to

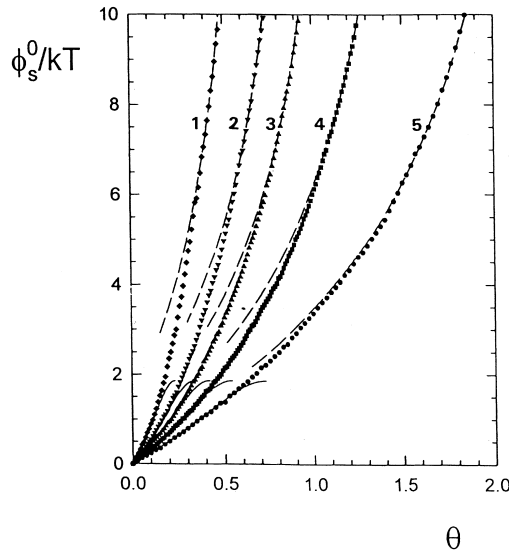


Fig. 21. The dependence of ϕ_s^0 on θ for interacting prolate spheroids ($As = 0.2$ unorientated adsorption); the points denote the numerical simulations performed for: (1) $H^* = 0.25$; (2) $H^* = 0.15$; (3) $H^* = 0.1$; (4) $H^* = 0.05$; (5) $H^* = 0$ (hard particles); the continuous lines denote the analytical results calculated from $\phi_s^0 = -kT \ln(1 - C_1\theta + C_2\theta^2)$ and the broken lines show the results calculated from Eq. (93).

$$\tilde{B}(\theta) = 1 - \left(\frac{1}{\bar{B}(\theta)} - 1 \right) / Ka \quad (114)$$

Substituting $\bar{B}(\theta) = 1 - C_1 \theta$ one obtains

$$\tilde{B}(\theta) = 1 - \frac{C_1}{Ka} \theta \quad (115)$$

Eqs. (114) and (115) clearly indicate that in the case of large diffusion boundary layer thickness (small particles) the influence of the surface blocking effects on particle adsorption rate will be negligible. In other words, the precise value of the $C_1 \div C_n$ constants becomes irrelevant since the adsorption rate remains unchanged (equal to the limiting flux j_0) as long as $1/\bar{B}(\theta) \ll Ka - 1$. However, the surface blocking effects become important when

$$\frac{1}{\bar{B}(\theta)} \gg Ka - 1 \quad (116)$$

Using Eqs. (93) and (108) this can be expressed as

$$\frac{1}{(\theta_\infty - \theta)^m} \gg Ka - 1 \quad (117a)$$

or

$$\theta_\infty - \theta \ll \sqrt[m]{\frac{1}{Ka - 1}} \quad (117b)$$

Eq. (117a) indicates that for θ approaching the jamming (or maximum) coverage this inequalities always fulfilled and the blocking effect described by the two-dimensional RSA model determine the overall transport rate.

Using the overall flux expression Eq. (110) one can formulate the kinetic equation for the deposited phase in the form of [135]

$$\frac{d\theta}{dt} = \pi a^2 j_0 \frac{Ka}{Ka - 1 + \frac{1}{\bar{B}(\theta)}} = \pi a^2 j_0 \tilde{B}(\theta) \quad (118)$$

By defining the dimensionless time $\tau = \pi a^2 j_0 t$ one can integrate Eq. (118) to the form of

$$(Ka - 1)\theta + \int_0^\theta \frac{d\gamma}{\bar{B}(\gamma)} = Ka \tau \quad (119a)$$

Substituting the DRSA expression for $\bar{B}(\theta)$ given by Eq. (103) one can convert Eq. (119a) to the implicit non-linear equation

$$(Ka - 1)\theta + \frac{1}{\bar{C}_2(\theta_1 - \theta_2)} \ln \frac{\theta_1(\theta_2 - \theta)}{\theta_2(\theta_1 - \theta)} = Ka \tau \quad (119b)$$

$$\text{where, } \theta_1 = \frac{\bar{C}_1}{2\bar{C}_2} [1 - q], \quad \theta_2 = \frac{\bar{C}_1}{2\bar{C}_2} [1 + q], \quad q = \sqrt{1 - \frac{4\bar{C}_2}{\bar{C}_1^2}}$$

For $Ka = 1$, Eq. (119b) can be explicitly evaluated as

$$\theta = \theta_1 = \frac{1 - e^{-q\bar{C}_1 Ka \tau}}{1 - \frac{\theta_1}{\theta_2} e^{-q\bar{C}_1 Ka \tau}} \quad (120a)$$

On the other hand, assuming $Ka = 1$ and using Eqs. (93) and (108), one can deduce from Eq. (119a) the limiting form

$$\theta_\infty - \theta \sim K' \tau^{-[1/(m-1)]} \quad (120b)$$

where K' is the dimensionless constant.

The steric barrier approach and the equations derived in this section are expected to describe adequately deposition of submicrometre sized particles for which the diffusional transport dominates at distances comparable with particle

diameter where there is no coupling between the specific and hydrodynamic force fields. For larger particles the hydrodynamic flow penetrates the surface layer and a significant coupling between the electrostatic and hydrodynamic force fields occurs. This is leading to the hydrodynamic scattering effect (HSE) enhancing the surface blocking phenomena. As discussed in Adamczyk and co-workers [48,67] these complex many-body interactions can to some extent be quantified in terms of the Brownian Dynamics simulations which are, however, very tedious, giving specific results of limited applicability [48,67]. Some approximate analytical expressions derived from the modified RSA model were reported in Adamczyk et al. [182]. For sake of brevity, in this review we do not address this problem in more detail.

5. Experimental results

The literature concerning experimental measurements of colloid particle deposition at solid/liquid interfaces is fairly extensive and has been reviewed in some detail in our previous works [48,67,78,132]. In this paper we present some selected experimental results obtained under well-defined transport conditions which elucidate the role of specific interactions in particle deposition processes. The data concerning limiting flux measurements (linear adsorption regime) are discussed first, whereas the last part of our paper will be focused on describing the effect of surface blocking effects (steric barrier).

5.1. Experimental methods — general remarks

There exists a large variety of experimental methods aimed at a quantitative determination of colloid particle adsorption kinetics which can be attributed to the indirect and direct category. The simplest to implement are the indirect methods when the suspension concentration changes in the bulk are measured prior and after contact with the adsorbent (interface). The depletion of the solution concentration is often determined by measuring optical density changes (turbidimetry) [183], by interferometry or nephelometry [184] or by applying the HPLC and FPLC methods coupled with appropriate detecting system [185,186]. Sometimes fluorescent [187] or radioactive [188] labelling of the adsorbate is used.

For larger colloid particles one can use the *on line* particle concentration detection based on the light scattering or Coulter counter principle. By using the depletion methods one implicitly assumes that the amount of the deposited (adsorbed) substance is equal to the amount disappeared from the solution. This sets certain limits on the accuracy of the depletion methods since adsorption on container walls or adsorbate trapping into pores cannot be a priori excluded. Another disadvantage of these methods is that one can usually gain a global information averaged from a considerable surface area of the interface. As in results, any detailed information about the local structure of the mono-layer (e.g. density fluctuations or inhomogeneities) is lost.

In this respect, these indirect methods are more accurate when the surface concentration of adsorbed particles is determined by measuring a physicochemical quantity which can unequivocally be assigned to the presence of deposited particles. Usually the change of optical or electrokinetic properties (streaming potential) due to adsorbed layer is exploited for surface concentration determination. Often the isotopically labelled particles are used to produce a well detectable signal stemming from the adsorbed layer.

Albery et al. [189,190] determined the concentration of adsorbed particles by measuring the intensity of the scattered light in the direction normal to the incident beam. The method was applied for studying the effect of electrode (prepared from a conductive glass) potential on adsorption kinetics of carbon black particles.

Ellipsometry is another optical technique widely used for studying bioparticle adsorption. The method is based on the principle that the state of polarisation of light changes upon reflection from an interface. Jonsson et al. [191] constructed the flow cell enabling the ellipsometric measurements to be performed with a support adsorbing surface exposed to the flow of well-defined geometry.

Refectometry is a new optical method gaining importance in studies on protein and nano-sized colloid particle deposition [174,192–194]. The method relies on the detection of reflectivity changes caused by the adsorbed layer having the refractive index different from the suspending medium. The polarised laser beam is focused on the surface to be studied at the angle close to the Brewster's angle. The ratio of reflected intensities of the perpendicular and the parallel polarisation components is measured and converted into an output signal. After a proper calibration and adopting some model assumptions for the configuration of the adsorbed layer the output signal can be related to the surface concentration of adsorbate. This method was further developed in Schaaf et al. [195] by allowing for changes in the incident angle of the beam around the value of the Brewster's angle in order to attain higher accuracy. This method, called scanning angle reflectometry (SAR), was successfully applied for determining the mean thickness and mean refractive index of the fibrinogen layer adsorbed at silica [196]. The main advantage of ellipsometry and reflectometry methods is that the optical signal can be detected directly without disturbing the system by introducing any labels such as radioisotopes or fluorescent dyes. On the other hand, one should remember that the sensitivity of the ellipsometry and reflectometry methods is rather limited, especially for low surface concentrations.

Another class of indirect methods aimed at studying particle adsorption is based on the radioactivity measurements of labelled particles [197–202]. The experiments are usually performed using a single capillary [199], hollow fibres [199] or parallel-plate channel [201]. Although the radioactivity method is rather sensitive it has limited accuracy due to presence of background radiation.

Other methods of determining particle adsorption exploit the fact that the electrokinetic potential of a solid/liquid interface in an electrolyte solution is very sensitive to the amount of adsorbed substance (both charged or uncharged). Usually the streaming potential of single capillaries is measured enabling one to

determine adsorbed amounts of polyelectrolytes [203], polymers [204] and proteins [193,194,205] in the range of a small fraction of a mono-layer. Thus, the accuracy of the electrokinetic method exceeds considerably that of the optical methods. However, there is no well-established theoretical basis for calculating quantitatively the surface concentration of adsorbate from the measured streaming potential changes, so the semi-empirical approaches are used [206]. Another disadvantage of the electrokinetic method is that its accuracy decreases considerably for high electrolyte concentrations (low signal) and for low concentrations (appearance of surface conductivity).

The indirect methods mentioned above are in principle applicable for arbitrary sized particles but they are especially well suited for semi-quantitative studies of protein, polymer and small colloid particle adsorption for surface coverage exceeding 10%.

It seems that an unequivocal determination of particle surface concentration as a function of various physicochemical parameters can only be achieved using the direct methods based on optical, AFM or electron microscope observations. For suspensions of larger sized colloids or bacteria the number of particles adsorbed can be determined in situ, in a continuous manner using the optical microscopy coupled with a micrograph [140–143,173,176,180] or image analysis technique [181,207,208]. Usually, the well-defined transport conditions are realized using the impinging-jet cells [140–143,173,175,176] or the parallel-plate channel [207–209]. Recently, the AFM tapping mode was used for direct in situ imaging of latex particle (diameter, 0.116 μm) adsorbed on mica [210]. However, the use of this technique is very awkward due to artifacts stemming from tip-induced aggregation of the suspension, convolution of the tip and particle signal, adhesion of particles to the tip, etc. [210]. A considerably better resolution can be achieved by imaging the particle in the air upon drying the sample. Such drying procedure must also be applied when adsorption at non-transparent surfaces is studied. This approach was used for determining particle deposition rate at the rotating disc [211–213]. However, this highly invasive procedure may lead to particle aggregation or removal due to strong capillary forces appearing upon drying. In order to eliminate this deficiency, Harley et al. [214] developed an ingenious experimental technique based on the thin film freeze drying principle followed by the scanning microscope examination of the interface with adsorbed particles. Using the method (referred to as TFFD-SEM) they have examined adsorption kinetics of small negatively charged polystyrene latex on larger positively charged particles.

Due to reliability and accuracy of the direct method, it seems to be the most appropriate for a quantitative verification of theoretical predictions, especially those concerning initial deposition rate when the surface coverage remains at a 1% order.

5.2. *The initial deposition rates*

The occurrence of the linear deposition regimes under barrier-less transport conditions in experiments involving colloid particles was often demonstrated

[140–144,210]. The quantity which was measured directly in these experiments was the number of particles N_p found over equally-sized surface areas ΔS . Since N_p is a statistical variable which obeys the Poisson fluctuation law [140] for low coverage, the accuracy of determining the average value of $\langle N_p \rangle$ is inversely proportional to N_t (where N_t is the total number of particles counted). In the above experiments N_t was usually above 1000 which gives the S.D. of $\langle N_p \rangle$ approximately 3%. For higher coverage the fluctuations in N_p are considerably reduced due to exclusion affects [140,215] which increases significantly the accuracy of measurements. On the other hand, for barrier-controlled deposition regimes the number of particles adsorbed is generally very low so N_p is subject to considerable fluctuations, increased by surface heterogeneity. In these cases the S.D. of $\langle N_p \rangle$ may well exceed 10%.

By knowing $\langle N_p \rangle$ the normalised adsorption rate is calculated using the definition, i.e.

$$j_0 = \frac{\Delta \langle N_p \rangle}{\Delta S \Delta t} = \frac{1}{\pi a^2} \frac{\Delta \theta}{\Delta t} \quad (121)$$

where $\Delta \langle N_p \rangle$ is the change in the averaged number of particles adsorbed over ΔS within the time interval Δt . In order to increase the accuracy of j_0/n_b determination averages from many experiments with different n_b are taken and the non-linear curve fitting procedure is applied [182].

The relatively high accuracy of the initial flux determined in this way was exploited for determining the range of validity of the convective diffusion theory, in particular the Smoluchowski–Levich approximation. The most interesting task was an experimental proof of the existence of minimum deposition rate predicted theoretically to appear for micrometer sized particles [72,153]. This was achieved in Adamczyk et al. [140] by using the impinging jet cell and mono-disperse polystyrene latex suspensions of negatively charged particles. Particle deposition occurred at modified mica surface (positively charged) which assured localised and irreversible adsorption conditions. The ionic strength in these experiments was kept relatively high (10^{-3} M) in order to eliminate the electrostatic interactions. The results shown in Fig. 22 suggest that for particles having a size $< 1 \mu\text{m}$, the adsorption rate j_0/n_b can well be reflected by the Smoluchowski–Levich theory depicted by the dashed line. This suggest that for colloid particles the initial flux decreases as $a^{-2/3}$ in accordance with Eq. (66) which indicates that the diffusion and convection were the dominated transport mechanisms. On the other hand, for particle sizes $> 1 \mu\text{m}$, the interception effect is playing an increasingly important role, especially for higher flow rates ($Re = 150$). This causes a considerable (manifold) deviation of the limiting flux from the Levich theory. Thus for $d > 1 \mu\text{m}$, j_0/n_b seems to increase parabolically with particle size in accordance with Eq. (74a). Note that the numerical solutions of the exact transport equation, Eq. (60) agrees well with the experimental data for the entire range of particle sizes studied.

In order to elucidate the role of the electrostatic interactions in colloid particle adsorption, a series of experiments has been performed in Adamczyk et al. [147] focused on measurements of the ionic strength effect. Typical results obtained in

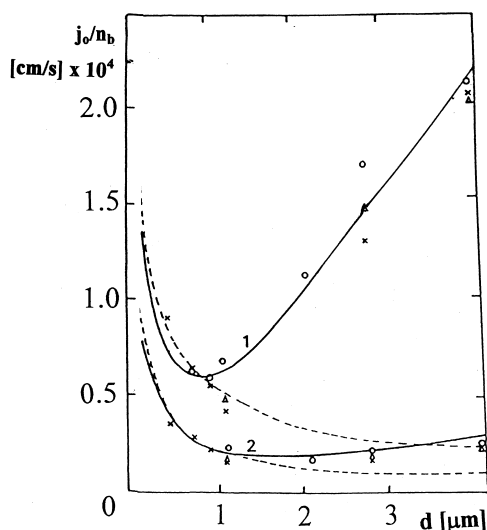


Fig. 22. The j_0/n_b dependence on particle diameter d . The points show the experimental results obtained in the impinging-jet cell using latex suspensions [140] ($I = 10^{-3}$ M). The solid lines are the exact numerical results and the broken lines represent theoretical results derived from the Smoluchowski-Levich approximation for $Re = 150$ (curve 1) and $Re = 30$ (curve 2).

the impinging jet cell using mono-disperse latex suspension (averaged particle diameter, $0.68 \mu\text{m}$) are shown in Fig. 23. As one can notice, for $I > 10^{-3}$ M, the electrostatic interactions seems to be effectively eliminated since the limiting flux j_0/n_b attains a plateau values for all Re numbers studied (8–150). This confirms that the results shown previously in Fig. 22 can be treated as the limiting values, characteristic for hard particles. On the other hand, for decreasing ionic strength the limiting flux is enhanced considerably over the hard particle values (for $Re = 150$ this increase is approximately four times). It should be observed that the flux increase remains fairly independent (within experimental error bounds) of the kind of electrolyte used, i.e. KCl, CsCl, LiCl, BaCl₂ and K₂SO₄ (at equal ionic strength). Thus, the flux enhancement for larger particle size and the indifference to electrolyte composition is in good agreement with the EHP concept described by Eq. (74a). Note also that the numerical results (continuous lines in Fig. 23) are in a quantitative agreement with the experimental data for the entire range of ionic strength investigated.

The limiting flux increase in dilute electrolyte solutions due to the interception effect is a universal phenomenon occurring for other flow configurations more related to practice. For example, Elimelech [156] carried out a series of throughout experiments on particle deposition (filtration) in columns packed with glass beads (having averaged diameters of 0.046 cm). The suspensions used was positively charged latex particles of various size ranging from 0.08 to $2.51 \mu\text{m}$ with the ionic strength varied between 5×10^{-6} M (de-ionized water) and 0.1 M. The number of

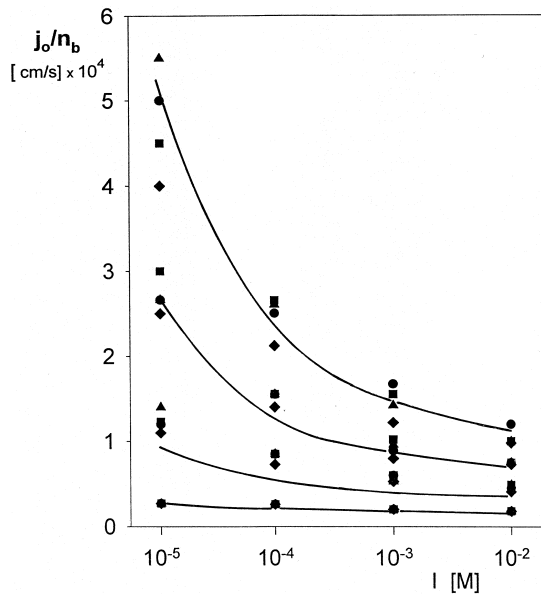


Fig. 23. The dependence of the normalised initial flux j_0/n_b on the ionic strength I regulated by various electrolytes; the points denote the experimental results obtained for latex particles (averaged particle size, $0.68 \mu\text{m}$) in the impinging-jet cell: (1) $Re = 150$; (2) $Re = 80$; (3) $Re = 28$; (4) $Re = 8$; the continuous lines are the theoretical results obtained from numerical solutions of the exact transport equation.

particles adsorbed was determined indirectly (depletion method) by monitoring the optical density change at the outlet of the column. Some selected results for a $1.15\text{-}\mu\text{m}$ particle suspension are shown in Fig. 24 in the form of the single collector removal efficiency (or reduced particle flux j_0/n_b) vs. the ionic strength I . As can be observed, the experimental results resembling closely those obtained in the impinging jet cell (see Fig. 23) indicate that the increase in initial particle flux can be as large as four times when using de-ionized water. This effect can quantitatively be interpreted in terms of the numerical solutions of the two-dimensional continuity equation [156]. Similar results were obtained for larger particle sizes although the measured particle deposition rates were generally smaller than predicted theoretically.

Other data confirming the significant role of the attractive double-layer interactions in particle deposition phenomena are presented in Fig. 25. These results were obtained in the slot impinging jet cell using a mono-disperse latex suspension (averaged particle size, $1.48 \mu\text{m}$) [144]. As can be observed the agreement between the experimental and theoretical data is satisfactory for the entire range of Re number studied (where the Re number was defined as $Re = Q/lv$, where Q is the volumetric flow rate and l the width of the rectangular capillary). It should be noted that for $Re < 4$ (which corresponds to $Pe < 10^{-2}$) the experimental results ap-

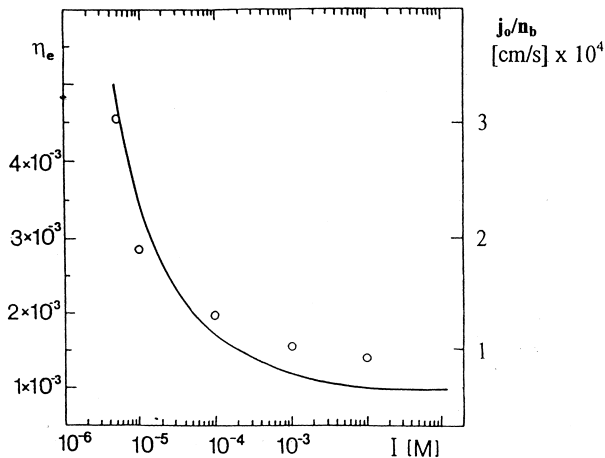


Fig. 24. The single collector removal efficiency η_e and j_0/n_b dependence on the ionic strength I ; the points show the experimental results obtained in the packed bed column using positively charged latex suspensions (averaged particle diameter of $1.15 \mu\text{m}$ [156]). The solid line denotes the theoretical results obtained numerically.

proach the same limiting curve which suggests that for low Reynolds number flows the attractive electrostatic interactions exert a negligible effect on particle deposition rate.

The above presented results and others discussed elsewhere [67,78] confirmed quantitatively the validity of the convective diffusion theory incorporating the specific force fields into the transport equations. It should be remembered, however, that the limiting flux measurements cannot be used for an unequivocal discrimination between various double-layer interaction models. This is so because the increase in particle flux is governed by the magnitude of interactions at distances comparable with the double-layer thickness and larger, where various models give similar results (see Figs. 11 and 12). Thus, the validity of the convective diffusion theory under barrier-less transport conditions can to some extent be attributed to low sensitivity of the measured deposition rate to these parameters which are difficult to control as, e.g. the spread of particle charge distribution, surface heterogeneity, etc. Thus, for example a uncertainty in particle zeta potential of 10 mV will result in a change of particle deposition rate of several percent.

A different situation is expected to occur for systems characterised by Type II energy profile, i.e. under the barrier-controlled deposition regimes. In such cases, a small perturbation in the governing parameters, such as zeta potentials, particle size, local interface geometry and charge heterogeneity will result in a large, usually non-linear, response of the system. As a result, the experiments carried out under barrier-controlled transport conditions are usually less reproducible and difficult for an unambiguous theoretical interpretation. A general feature observed in this type of experiment is that the measured limiting flux values are much larger

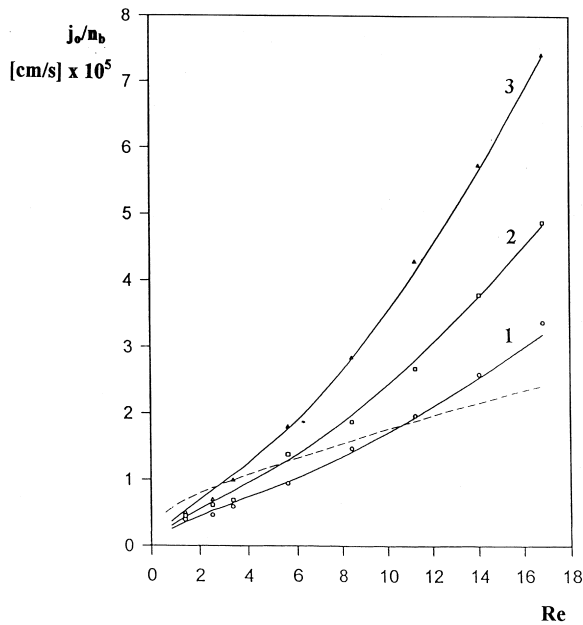


Fig. 25. The j_0/n_b vs. Re dependence. The points represent the experimental results obtained in the slot impinging-jet cell [144] using latex suspension of $1.48 \mu\text{m}$ averaged diameter. The solid lines are the exact numerical results and the broken line shows the Smoluchowski-Levich approximation: (1) $I = 10^{-3}$ M; (2) $I = 10^{-4}$ M; (3) $I = 10^{-5}$ M.

than theoretical predictions both for submicrometre [212] and larger [215] particle sizes.

Typical results obtained by the rotating disc technique followed by direct microscope determination of coverage are shown in Fig. 26 [212] (average size of latex particles used in these experiments was $0.3 \mu\text{m}$). As can be seen, the theoretical prediction based on the exact solution of the convective diffusion equation overestimate considerably the measured deposition rates for $I < 0.1$ M.

A similar behaviour was reported by Varennes and van de Ven [216] who used the impinging jet cell to determine deposition rate of latex suspension (averaged particle size, $3 \mu\text{m}$) at cover glass interfaces. They detected a measurable deposition rate for ionic strength as low as 10^{-5} M in contrast to the theory predicting in principle no deposition under these conditions. The discrepancy was attributed to polymer filaments protruding from the latex surface, responsible for the ‘hairiness’ of the particles.

It seems, however, that the positive deviation from theoretical flux values can be more naturally explained in terms of the surface heterogeneity hypothesis put forward in Adamczyk [78] and Song et al. [106]. The simplest possibility arises when due to natural fluctuation phenomena the charge on particles becomes non-uniformly distributed forming local micropatches characterised by more favourable

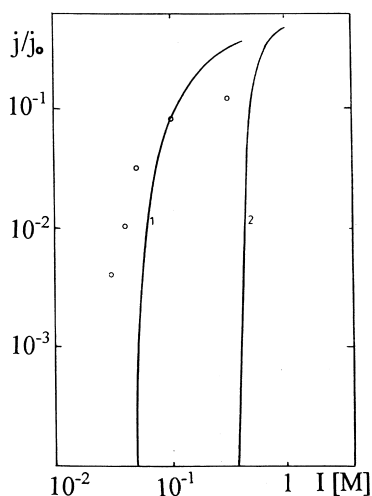


Fig. 26. The influence of ionic strength I on the relative initial flux j/j_0 (where j_0 is the flux value in the absence of electrostatic interactions); the points are the experimental results obtained for latex suspension using the rotating disc method [212]. The solid lines are the theoretical results predicted for a homogeneous charge distribution (curve 2) and a Gaussian charge distribution characterised by the relative S.D. of 0.35 (curve 1).

deposition condition than the average surface (this will correspond to the random heterogeneity hypothesis). Even if the fraction of these areas remains very low (of the order of 1% of the total area available) the overall deposition rate will be much larger than theoretically predicted for uniform surfaces due to its large sensitivity of particle flux to surface charge (potential). This hypothesis is strongly supported by the kinetic curves exhibiting saturation at low surface coverage of the order of percents [207–209] and a gross unevenness of the deposited layer.

Similarly, microphoretic measurements of zeta potential of particle suspensions suggests that there exists a natural spread of surface charge within a particle population. This will again lead to increased deposition rate since the particles bearing smaller charge will selectively be deposited from the suspension. This hypothesis was exploited to interpret the data shown in Fig. 26. As can be noticed, the theoretical calculations done by assuming a 0.35 relative S.D. of particle zeta potential are in significantly better agreement with the experimental data.

On the other hand, the surface heterogeneity concept was exploited by Song et al. [106] to interpret the experimental data of Litton and Olson [217] who determined deposition efficiency in packed bed columns (using soda glass beads, 0.275 mm in diameter and positively charged latex particles, 0.245 μm in diameter). In these experiments the ionic strength was kept constant, equal to 10^{-3} M, while the pH was varied within the limits 3.5–5.9 which resulted in a change of particle zeta potential from 0 to -66 mV. The results shown in Fig. 27 exhibit the same trend as previously, i.e. the measured deposition rates are much higher than theoretical predictions. Moreover, the results were found dependent on the clean-

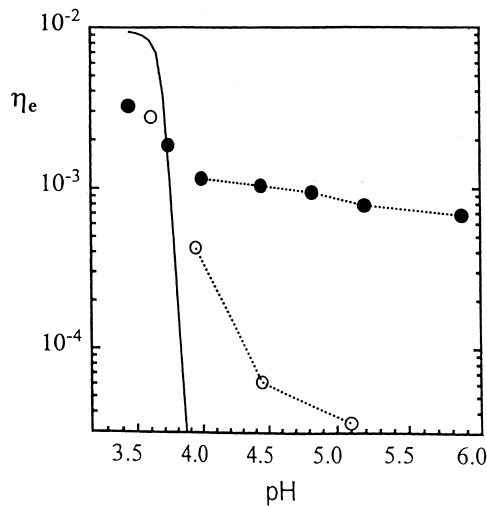


Fig. 27. The single collector removal efficiency η_e vs. pH of the suspension. The points represent the experimental results obtained for latex particles (averaged diameter, $0.245 \mu\text{m}$) adsorbing at glass beads (diameter, 0.0275 cm) [106]. The solid line represents the theoretical results derived for a homogeneous charge distribution and the dotted line shows the theoretical results predicted for a heterogeneous charge distribution.

ing procedure of glass beads. These facts were explained by Song et al. [106] by the existence of favourable surface sites on glass, probably composed of Al_2O_3 and Fe_2O_3 which are expected to bear a positive charge at this pH range. As one can notice in Fig. 27 the theoretical predictions calculated by assuming the surface heterogeneity hypothesis (dashed lines) are in good agreement with experimental data.

As can be concluded from the above results, in the case of barrier-controlled deposition, the classical DLVO energy profiles calculated for homogeneous surfaces are not sufficient for a theoretical interpretation of experimental data. However, a satisfactory agreement between theory and experiment can be attained by accepting the heterogeneity hypothesis postulating that the DLVO theory is valid in a local sense only, i.e. for a given surface area or a given particle. It seems therefore, that in order to unequivocally characterize a barrier-controlled system, more information is needed than just the averaged value of zeta potentials of particles and the interface.

Unfortunately, up to our knowledge, there exists no systematic studies in the literature concerning the influence of geometric heterogeneities (surface roughness) on the initial flux of colloid particles. The experiments which relatively closely match these conditions were reported in Adamczyk et al. [176]. These works were concerned with deposition kinetics of larger polystyrene latex particles (averaged diameter, $1.48 \mu\text{m}$) at mica surface precovered (in prior deposition experiments) with a given amount of smaller particles (averaged size, $0.68 \mu\text{m}$). The degree of

surface heterogeneity produced in this way was expressed in terms of smaller particle surface coverage $\theta_s = \pi a_s^2 N_s$, where a_s is the smaller particle radius and N_s is their surface concentration. The results shown in Fig. 28 indicate that the initial flux of larger particles falls abruptly when θ_s increases. This behaviour, analogous to the effect of the electrostatic barrier plotted in Figs. 26 and 27, is caused by the electrostatic repulsion between equally charged smaller and larger particles (the mica surface due to surface modification procedure described in Adamczyk et al. [140] was positively charged in these experiments). As can be noticed in Fig. 28, the numerical simulations performed according to the classical two-dimensional RSA model for interacting particles deviate significantly from the experimental data. This discrepancy, which could not be accounted for previously [176] can be interpreted in terms of the steric barrier due to the presence of preadsorbed smaller particles. However, in this case, the extension of the barrier determined by smaller particle size was markedly smaller than the thickness of the diffusion boundary layer of larger particles (equal to $1/Sh_0$ in dimensionless units). Hence Eq. (110) should be used for calculating the j/j_0 dependence for deposition at precovered surfaces. Indeed, one can observe in Fig. 28 that the theoretical results stemming from this equation (with $Ka = 2.5$ corresponding exactly to the experimental conditions) are in good agreement with experimental data.

Certainly, additional experiments are needed in order to derive conclusions of a general validity. Nevertheless, the data shown in Fig. 28 demonstrates that the presence of smaller particles at the surface can exert a profound effect on adsorption of larger particles. As discussed in Adamczyk et al. [218], the flux reduction is expected especially pronounced for large size ratio of particles. This suggests that in order to obtain reproducible results in particle deposition experiments the surface cleaning procedure should be carefully controlled and the presence of small colloid particles strictly avoided.

It should also be mentioned that in none of the above discussed experimental results, no evidence of additional repulsive interactions was found, except for the electrostatic interactions. This conclusion agrees with that formulated by Shubin and Kekekicheff [43] on the basis of direct force measurements.

The limiting flux measurements discussed in this section can be used for estimating the magnitude of the particle/interface interactions. The particle/particle energy profiles can be determined from kinetic measurements performed for later adsorption stages when the steric interactions appear. These experiments are discussed below.

5.3. Nonlinear adsorption kinetics

Most of the experimental results presented hereafter were obtained in the stagnation-point flow cells using mono-disperse latex suspension and by applying the direct optical microscope or AFM counting procedure. In an attempt to find the experimental conditions closely matching the RSA assumptions the cell was so oriented that gravity was acting opposite to the interface [140–144,147,173]. Moreover, the particle size range and flow rate were also carefully adjusted in order to

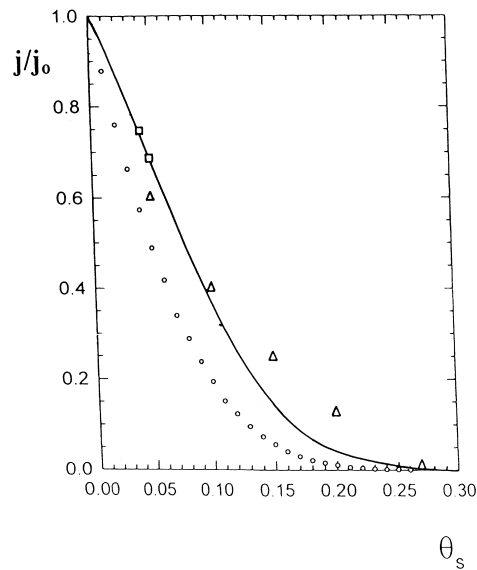


Fig. 28. The dependence of the reduced initial flux j/j_0 of larger particles on the surface coverage θ_s of smaller particles preadsorbed at mica. The triangles and squares denote experimental results obtained in the impinging jet cell [176] for polystyrene latex suspension (larger particle size, $1.48 \mu\text{m}$; smaller particle size, $0.68 \mu\text{m}$; $I = 10^{-4}$, $Re = 4$), the circles denote the simulation results stemming from the two-dimensional RSA model and the solid line represents the results calculated from Eq. (110) using the steric barrier concept.

reduce the diffusion boundary layer thickness and to avoid the hydrodynamic scattering effects. Typical kinetic curves measured under these circumstances for various ionic strength are shown in Fig. 29 (averaged particle size $0.88 \mu\text{m}$, $Re = 8$, bulk suspension concentration $n_0 = 4.4 \times 10^8 \text{ cm}^{-3}$, impinging-jet cell [48]).

One can observe that for initial deposition stages ($\theta < 0.1$) the slope of the kinetic curves (particle flux) decreases with ionic strength in accordance with previous discussions (see Fig. 23). On the other hand, for longer adsorption times an opposite situation can be observed, since the deposition rate is the smallest for $I = 10^{-5} \text{ M}$. In the latter case the adsorption rate becomes apparently negligible after reaching the surface coverage of 0.26. It should be noted that the two-dimensional RSA simulations performed by assuming the LSA model with energy additivity principle describe adequately the experimental adsorption kinetics for the entire range of deposition time and ionic strength.

Very similar trends were observed in the kinetic measurements of Johnson and Lenhoff [210] performed by the AFM method using the amidine latex particles (mean diameter, $0.116 \mu\text{m}$) adsorbing at freshly cleaved mica. The results shown in Fig. 30 demonstrate unequivocally that the coverage attained after longer adsorption time are considerably increased for higher electrolyte concentration. Due to limited accuracy for low coverage range the differences in kinetic curves for $\theta < 0.1$ cannot be easily distinguished.

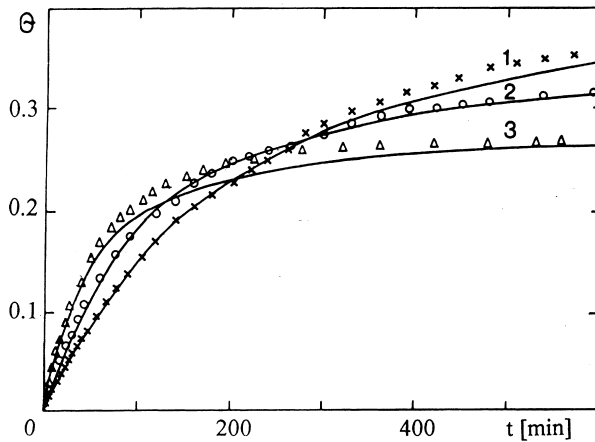


Fig. 29. Adsorption kinetics of latex particles (diameter, $d = 0.94 \mu\text{m}$) on mica measured experimentally using the impinging-jet cell for various ionic strength, i.e. (1) $I = 10^{-3} \text{ M}$; (2) $I = 10^{-4} \text{ M}$; $I = 10^{-5} \text{ M}$. The solid lines denote the smoothed MC-RSA simulations.

Analogous results were obtained by Johnson and Elimelech [219] who studied latex deposition in columns packed with soda glass beads (particle diameter, $0.48 \mu\text{m}$, $\text{pH} = 5$). It was deduced from kinetic break-through curves determined by the depletion method that the adsorption rate at initial stages was larger for lower ionic strength ($I = 10^{-5} \text{ M}$). However, the column break was attained much earlier for this ionic strength, than for $I = 10^{-3} \text{ M}$ which was interpreted by lower saturation coverage of the glass surface. It was shown that the experimental results

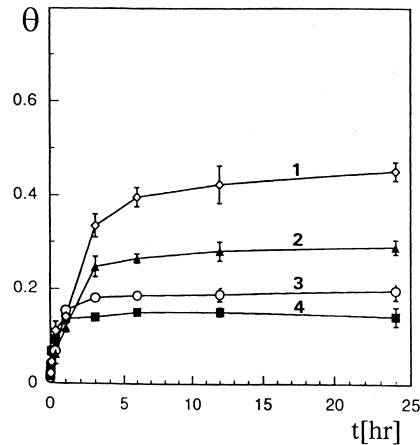


Fig. 30. Adsorption kinetics of positive latex particles (averaged diameter, $0.116 \mu\text{m}$) on mica under natural convection conditions measured using the tapping mode AFM [210]: (1) $I = 5 \times 10^{-3} \text{ M}$; (2) $I = 10^{-3} \text{ M}$; (3) $I = 10^{-4} \text{ M}$; (4) $I = 3 \times 10^{-6} \text{ M}$.

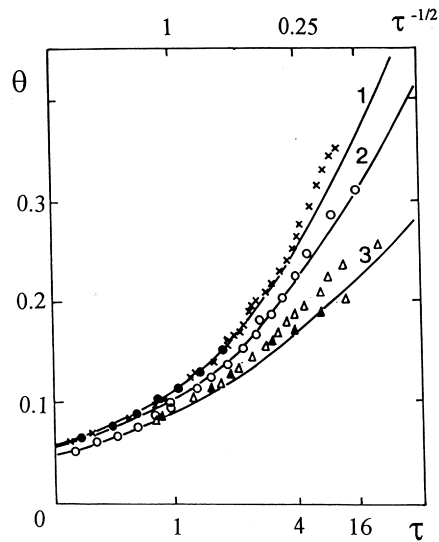


Fig. 31. Adsorption kinetics of latex particles (diameter, $0.94 \mu\text{m}$) on mica measured in the impinging-jet cell at $\text{Re} = 8$. The solid lines show the MC-RSA simulations performed for: (1) $I = 10^{-3} \text{ M}$; (2) $I = 10^{-4} \text{ M}$; (3) $I = 1.2 \times 10^{-5} \text{ M}$.

can well be interpreted in terms of the RSA model [with the $B(\Theta)$ blocking function] whereas the Langmuir model proved inadequate.

Further evidence of the validity of the RSA model for characterizing protein adsorption was reported by Ramsden [220].

One can conclude when analysing the data shown in Figs. 29 and 30 and other results [48] that the suspension ionic strength is exerting a profound affect on particle adsorption kinetics and surface coverage attained after long adsorption time. However, one should remember that according to the RSA model, the maximum coverage are attained very slowly, i.e. as $\tau^{-1/2}$ (cf. Eq. (120b)). One should expect, therefore, that for longer times the θ vs. $\tau^{-1/2}$ transformation (where $\tau = \pi a^2 j_0 t$, and j_0 being the experimentally determined limiting flux) should be more appropriate for expressing the experimental data if the RSA mechanism is valid. The experimental results obtained for ($0.94 \mu\text{m}$ in diameter) latex particles [48] are plotted using this transformation in Fig. 31. As can be seen, the θ vs. $\tau^{-1/2}$ dependencies become indeed linear for $\tau \gg 1$ with the slope decreasing monotonically with the decrease in ionic strength. Note also that the numerical RSA simulations are in good agreement with the experimental data for all ionic strength studied.

The good agreement of the experimental data shown in Figs. 29 and 31 with the classical RSA model is probably due to the fact that due to forced convection the diffusion boundary layer thickness was fixed at a value comparable with particle diameter, hence Ka was close to unity. Under such circumstances the overall

blocking function $\tilde{B}(\theta)$ can be expressed according to Eq. (110) as

$$\tilde{B}(\theta) = Ka\bar{B}(\theta) \cong B(\theta) \quad (122)$$

Since $\bar{B}(\theta)$ stemming from the DRSA model is slightly smaller the $B(\theta)$ (calculated from the RSA model) and Ka is slightly larger than unity, the product of the quantities can be close to the blocking function of the classical RSA model, given by Eqs. (90)–(93).

However, for lower Re flows or for small particles the deviations from the RSA model are expected to become more pronounced. They should be the largest for small coverage (short adsorption time) where the experimental accuracy is limited. Thus, a precise determination of these deviations seems rather difficult although they were observed qualitatively in Adamczyk et al. [221] for $Re = 0.6$ (micrometer size particles) and in Bohmer et al. [174] for nanometer sized particles.

The θ vs. $t^{-1/2}$ transformation was also used in the above mentioned work of Johnson and Lenhoff [210]. The data shown in Fig. 32 suggest that for deposition time exceeding 1 h, the θ vs. $t^{-1/2}$ kinetic curves resemble straight line dependencies. This behaviour is rather unexpected since in these experiments, carried out under diffusion controlled regime the bulk flux is supposed to decrease with time as $t^{-1/2}$. Then, by combining this with Eq. (120b) one can expect that for long times

$$\theta_\infty - \theta \sim t^{-1/4} = \sqrt{t^{-1/2}}$$

This indicates that the θ vs. $t^{-1/2}$ dependence should be non-linear (parabolic) for long times. The discrepancy between this result and the Johnson and Lenhoff

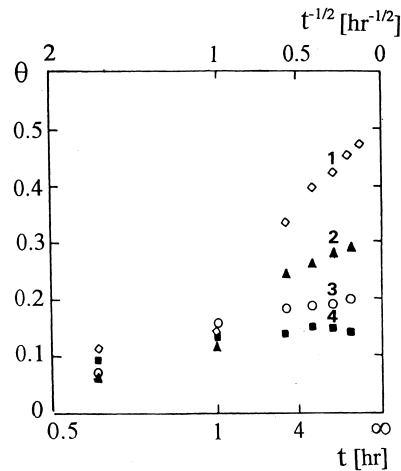


Fig. 32. Adsorption kinetic of latex particles on mica determined by AFM under the natural convection transport conditions [210]: (1) $I = 5 \times 10^{-3}$ M; (2) $I = 10^{-3}$ M; (3) $I = 10^{-4}$ M; (4) $I = 3 \times 10^{-6}$ M.

data is probably due to the appearance of natural convection for long deposition times. This will fix the thickness of the diffusion boundary layer and prevent the bulk flux from decreasing indefinitely with time.

It seems that furthermore, more precise experiments are needed for an unambiguous determination of deposition kinetics under diffusion-controlled regime and for assessing the range of validity of the RSA and DRSA models in these processes.

5.4. *The maximum coverage*

From a practical viewpoint, more interesting than these subtle differences in deposition kinetics, are the maximum coverage θ_{mx} attained after longer deposition times, which can be used for estimating an interface ‘capacity’ per unit area. One can, however, deduce when carefully examining the results shown in Figs. 31 and 32 that determining θ_{mx} for colloid particles without knowing any theoretical model would be difficult. This is so because deposition times needed to attain the surface coverage close to θ_{mx} become prohibitively long, e.g. in the experiments shown in Fig. 31 the maximum times exceeded 16 h. Experiments carried out for such long times are less reliable due to likely contamination of the surface due to impurities present in the suspensions. Obviously one can reduce this value by using more concentrated suspensions. However, the accuracy of experiments will be significantly reduced in this case, especially when the indirect methods are used with the drying procedure.

Another complication associated with θ_{mx} determination is of a more fundamental nature. One should remember that unlike θ_{mx} for hard particles which has a unique value, in the case of interacting particles, θ_{mx} is dependent not only in electrostatic interactions but also on particle transport mechanism and particle distribution over an interface. Also the polydispersity of the colloid suspension would significantly increase the θ_{mx} values [222]. All these effects lead to deviation of the θ vs. τ dependencies from linearity, hence a direct extrapolation of the kinetic data to infinite time may not be accurate enough. Even with this limitations, which are expected to be of the order of percent, the extrapolation procedure is more accurate than the usually adopted method of treating the coverage attained after a long (but undefined) time as true θ_{mx} value.

The determination of θ_{mx} for proteins was first attempted by Feder and Giaever [223] who used ferritin (globular protein having almost spherical shape of diameter of approx. 10 nm). Even by using highly concentrated saline solution (0.15 M) the authors were unable to reach the limiting value of 0.547, characteristic for hard spheres. They have determined θ_{mx} within the range 0.2–0.5. This discrepancy can be accounted for by the RSA model since according to Eq. (95), θ_{mx} should be 0.35 for $\kappa a = 12.5$, corresponding to the experimental conditions of Feder and Giaever.

Experimental results concerning colloid particle adsorption are more abundant. Onoda and Liniger [224] determined θ_{mx} for large polystyrene particles (diameter, 2.95 μm) adsorbing on glass slides, modified by adsorption of cationic polyacrylamide. Particle deposition occurred under gravity (sedimentation) and the drying

procedure was used before particle counting. The jamming coverage was found to be 0.55, in an ideal agreement with theoretical predictions for the RSA model for hard particles. However, if one considers the gravity effect, the theoretical θ_∞ value should increase to 0.61 [225,226]. It seems, therefore, that the agreement with the RSA model is due to compensation of the sedimentation, ionic strength (which was not controlled) and polydispersity effects as discussed in Adamczyk et al. [222]. Similar, gravity driven deposition was studied in Adamczyk et al. [227] using the sedimentation cell and polymeric (melamine) particles with a size of 1.68 μm and specific density 1.5 g cm^{-3} . The influence of the ionic strength, varied between 5×10^{-6} and 10^{-3} M, when $\theta_{m,x}$ was systematically studied. It was found that the maximum coverage dependence on I can well be described by Eq. (95) with the hard particle value θ_∞ equal to 0.61.

There are numerous experimental results concerning the $\theta_{m,x}$ determination for diffusion controlled transport conditions like the above mentioned work of Bohmer [175] who studied various latex suspensions (with particle diameter varied between 9 and 90 nm) using the reflectometric method and Johnson and Lenhoff [210] who used the AFM method. The effect of the ionic strength varied between 3×10^{-6} and 5×10^{-3} M on $\theta_{m,x}$ was systematically studied in this work. On the other hand, the micrograph technique was used for studying diffusion-controlled adsorption of 0.3- and 1- μm latex particles on mica [228] for ionic strength changes between 10^{-2} and 2×10^{-5} M.

Harley et al. [214] used the above TFFDSEM method to determine the effect of the ionic strength of suspension on $\theta_{m,x}$ in the case of deposition of small, negatively charged particles (diameter ranging from 0.116 to 0.696 μm) on positively charged latex, 2.17 μm in diameter. They measured a systematic decrease in $\theta_{m,x}$ from 0.1 for the smallest particles and lowest ionic strength to 0.45 for the largest particles. However, $\theta_{m,x}$ was expressed as the ratio of the number of particles adsorbed to the maximum number of particles which can be accommodated at the surface of the larger sphere assuming a close hexagonal packing. This may lead to an ambiguous interpretation since for the particle/particle problem the undeformed hexagonal packing is not possible due to curvature effects.

A similar problem of determining $\theta_{m,x}$ as a function of ionic strength for the small/large sphere configuration was experimentally studied by Vincent et al. [183] by using the indirect, concentration depletion method.

For the sake of convenience most of the above discussed data were collected in Fig. 33. In order to facilitate the comparison between results obtained under various deposition conditions (when θ_∞ was also varied) the universal coordinate system $\theta_{m,x}/\theta_\infty$ vs. κa was chosen. The theoretical results stemming from the RSA simulations performed using the LSA model are also shown in Fig. 33 together with the analytical results calculated from Eq. (95) by assuming the EHP concept (solid line). It should be noted that in the latter case the theoretical data for $\kappa a < 5$ can only be treated as an approximate since the large κa assumption pertinent to the EHP model breaks down for this range of κa . One can observe in Fig. 33 that the experimental data are in fairly good agreement with theoretical predictions although, for $\kappa a > 5$, the $\theta_{m,x}$ derived from experiments are generally

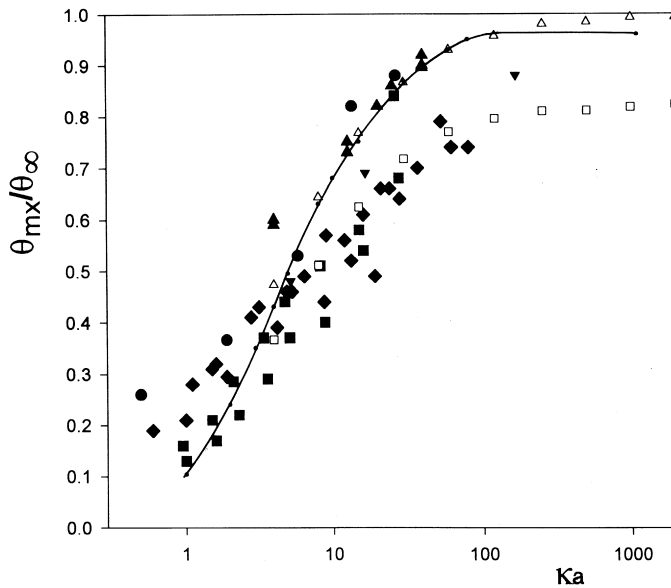


Fig. 33. The ‘master’ graph showing the collection of experimental data concerning the maximum coverage ($\theta_{m_x}/\theta_\infty$) dependence on κa : ●, Johnson and Lenhoff data [210] obtained by AFM under natural convection; ▲, Adamczyk et al. [227] obtained in situ optical microscopy under gravity (sedimentation); ▼, Adamczyk and Szyk data [228] obtained by in situ microscopy under natural convection; ■, Bohmer et al. data [174] obtained by reflectometry in impinging-jet cell; ◆, Harley et al. data [214] obtained by electron microscopy (TFFDSEM method), the empty symbols show the theoretical simulation data (obtained by the Monte-Carlo RSA method for $\tau = 10$ — squares and $\tau = 10^5$ — triangles). The solid line represents the analytical approximation given by Eq. (95).

smaller than theoretically predicted. These deviations are most likely due to limited experimental time of deposition measurements and lack of the extrapolation procedure discussed above. This hypothesis is supported by the fact that theoretical data obtained from simulations after $\tau = 10$ (which would correspond to physical deposition times of the order of hours) reflect the lower branch of experimental results well.

On the other hand, a proper theoretical interpretation of experimental results for $\kappa a < 5$ would require a true three-dimensional modelling of particle deposition process with appropriate expressions for the many-body electrostatic interactions. An attempt in this direction was undertaken by Oberholtzer et al. [89] who considered the true three-dimensional particle transport in a force field stemming from adsorbed particles and the interface. Since the authors still used the LSA approach (generalised for the two particle/interface configuration as previously mentioned) the deviation from the two-dimensional RSA simulations in respect to θ_{m_x} was found not to be significant.

Obviously there is need for additional theoretical studies in this field although a

proper consideration of the many-body electrostatic interaction at interfaces may pose considerable difficulties.

In any case, the classical RSA approach seems to work well from a practical point of view [range of κa (5–100)] agrees well with the experimentally found effect of considerable decrease in the θ_{mx} for lower κa (low ionic strength).

6. Conclusions

The analysis of experimental evidences collected under well-defined conditions confirmed the thesis that electrostatic interactions play an essential role in adsorption and deposition phenomena of colloid particles. For the low coverage regime the limiting flux of particles, j_0 is considerably increased by the attractive electrostatic interactions, especially for low ionic strength and larger Pe number. This behaviour can quantitatively be interpreted in terms of the convective diffusion theory using the DLVO Type I energy profiles. One can expect, therefore, that the measurements of the limiting flux can be used for estimating the magnitude of the particle/interface interactions.

For Type II energy profiles (an energy barrier present), significant deviations from theoretical predictions were found in experimental works. The discrepancy can be accounted for by assuming the surface heterogeneity hypothesis or by considering the spread of surface properties within particle populations. This enabled one to conclude that for barrier-controlled systems the DLVO theory is applicable in a local sense only, i.e. for a given surface area or for a concrete particle. Therefore, in order to unequivocally characterize these systems one should not only know the averaged surface potential values but also their distribution over the surface or within particle population.

Particle deposition kinetics for later stages can be quantitatively interpreted in terms of the exclusion effects (called traditionally blocking effects) enhanced by the electrostatic repulsion between adsorbed and moving particles. In contrast to previous approaches, these blocking effects are treated as true three-dimensional phenomena extending into the bulk. Thus, the effect of particles deposited (irreversibly adsorbed) at the surface becomes analogous to the presence of an energy barrier of extension comparable with particle diameter whose magnitude increases with coverage. This concept enables one to formulate proper boundary conditions for the bulk transport problems and to introduce the generalised surface blocking function $\bar{B}(\theta)$ defined by Eq. (99). It was predicted that $\bar{B}(\theta)$ should become similar to the previously used $B(\theta)$ function (derived, e.g. RSA simulations) for Type II energy profiles (which can also be realized by external force acting outwards from the interface).

Additionally, the concept of three-dimensional blocking phenomena proved advantageous for describing the coupling between the near-surface transport affected by deposited particles and the bulk transport. The overall transport rate in this case is characterised by the function $\tilde{B}(\theta)$ defined by Eq. (112) with the $Ka = 1/2Sh_0q_0$ rate constant being a crucial parameter (cf. Eq. (113)). It was

deduced that for $Ka \gg 1$ (small Sh_0 corresponding to small colloid particles or proteins), the influence of the blocking effects on particle deposition can be neglected until the maximum coverage θ_{mx} is approached. Then, the overall blocking function $\tilde{B}(\theta)$ becomes equal to $Ka\tilde{B}(\theta)$. Thus, for practical purposes the θ_{mx} values, affected by the electrostatic interactions, are of primary significance. It was also predicted that the influence of the blocking effects and electrostatic interactions is the most important for Ka close to unity, which can be realized in practice for micrometer-sized particles under moderate flow conditions.

These theoretical predictions were confirmed quantitatively by experimental data obtained for model latex suspensions. It was found that the classical RSA model remains useful for describing deposition kinetics of particle sizes of around micrometres under not very vigorous flows. The deviations from the RSA model occurring for smaller particles or very low Re (diffusion controlled deposition) can be accounted for by the coupling effect, expressed by the $\tilde{B}(\theta)$ function.

It was also found that the RSA approach reflects well the experimentally found decrease in the maximum coverage θ_{mx} due to lateral electrostatic interactions (described approx. by Eq. (95)).

It should be mentioned that in none of the experimental results discussed above, any evidence of additional repulsive interactions was found, except for the electrostatic interactions. This conclusion agrees with that formulated by Shubin and Kekekicheff [43] on the basis of direct force measurements.

Acknowledgements

The authors thank Prof. P. Schaaf and Dr P. Warszyński for stimulating discussions. Also the invaluable technical help from many co-workers, especially G. Para, E. Porębska and M. Noworyta is heartily acknowledged. One of the authors (Z. Adamczyk) would like to express his gratitude to the Jaworski family for creating the stimulating environment for the work to be started. This work was financially supported by the ERBIC-COPERNICUS Grant No. 14-CT98-0121 and the KBN Grant No. 7 T08B 039 14.

References

- [1] B.V. Derjaguin, B.V. Kolloid Z. 69 (1934) 155.
- [2] B.V. Derjaguin, Trans. Faraday Soc. 36 (1940) 203.
- [3] E.J.W. Verwey, J.Th.G. Overbeek, Theory of the Stability of Lyophobic Colloids, Elsevier, Amsterdam–New York, 1948.
- [4] G. Gouy, J. Physique 9 (1910) 457.
- [5] D.L. Chapman, Philos. Mag. 25 (1913) 475.
- [6] O. Stern, Z. Electrochem. 30 (1924) 508.
- [7] E. Hückel, G. Krafft, Z. Phys. Chem. N.F. 3 (1955) 135.
- [8] S. Levine, G.M. Bell, J. Phys. Chem. 64 (1960) 1188.

- [9] F.H. Stillinger, J.G. Kirkwood, *J. Chem. Phys.* 33 (1960) 1282.
- [10] V.S. Krylov, V.G. Levich, *Russ. J. Phys. Chem.* 37 (1960) 106.
- [11] F.P. Buff, F.H. Stillinger, *J. Chem. Phys.* 39 (1963) 1911.
- [12] C.W. Outwaite, *Chem. Phys. Lett.* 7 (1970) 636.
- [13] L. Blum, *J. Phys. Chem.* 81 (1977) 136.
- [14] S. Levine, C.W. Outwaite, *Trans. Faraday. Soc.* 74 (1978) 1670.
- [15] A.B. Schmidt, E. Ruckenstein, *J. Colloid Interface Sci.* 150 (1992) 169.
- [16] E. Ruckenstein, A.B. Schmidt, *J. Colloid Interface Sci.* 155 (1993) 37.
- [17] X. Chu, D.T. Wasan, *J. Colloid Interface Sci.* 184 (1996) 264.
- [18] E. Ruckenstein, *Adv. Colloid Interface Sci.* 75 (1998) 169.
- [19] I. Sogami, *Phys. Lett. A* 96 (1983) 190.
- [20] I. Sogami, N. Ise, *J. Chem. Phys.* 81 (1984) 6320.
- [21] J.Th.G. Overbeek, *J. Chem. Phys.* 87 (1987) 4406.
- [22] C.E. Woodward, *J. Chem. Phys.* 89 (1988) 5149.
- [23] S. Levine, D.G. Hall, *Langmuir* 8 (1992) 1090.
- [24] J.Th.G. Overbeek, *Mol. Phys.* 80 (1993) 685.
- [25] H. Brodowsky, H. Strehlow, *Z. Electrochem.* 63 (1950) 262.
- [26] E. Wicke, M. Eigen, *Z. Electrochem.* 56 (1952) 551.
- [27] E. Wicke, *J. Phys. Chem.* 58 (1954) 702.
- [28] M.J. Spaarnay, *Rec. Trav. Chem. Pay-Bas* 77 (1958) 872.
- [29] F. Booth, *J. Chem. Phys.* 19 (1951) 391.
- [30] A.D. Bucknigham, *J. Phys. Chem.* 25 (1956) 428.
- [31] Y. Gur, I. Ravina, A.J. Babchin, *J. Colloid Interface Sci.* 64 (1978) 326.
- [32] I. Ravina, A.J. Babchin, *J. Colloid Interface Sci.* 64 (1978) 333.
- [33] I. Prigogine, P. Mazur, R. Defay, *J. Chim. Phys.* 50 (1953) 146.
- [34] S. Levine, G.M. Bell, *J. Phys. Chem.* 67 (1963) 1408.
- [35] S. Levine, G.M. Bell, *J. Colloid Interface Sci.* 17 (1962) 838.
- [36] S. Levine, G.M. Bell, *Discuss. Faraday. Soc.* 42 (1966) 69.
- [37] P.L. Levine, *J. Colloid Interface Sci.* 51 (1975) 72.
- [38] W.E. Williams, *Proc. Phys. Soc. A* 66 (1953) 372.
- [39] Z. Adamczyk, P. Belouschek, D. Lorenz, *Ber. Bunsenges. Phys. Chem.* 94 (1990) 1483.
- [40] Z. Adamczyk, P. Belouschek, D. Lorenz, *Ber. Bunsenges. Phys. Chem.* 94 (1990) 1492.
- [41] Z. Adamczyk, P. Belouschek, D. Lorenz, *Ber. Bunsenges. Phys. Chem.* 95 (1991) 566.
- [42] Z. Adamczyk, P. Belouschek, D. Lorenz, *Bull. Pol. Ac. Chem.* 38 (1991) 424.
- [43] V.E. Shubin, P. Kekekicheff, *J. Colloid Interface Sci.* 155 (1993) 108.
- [44] N.E. Hoskin, S. Levine, *Philos. Trans. R. Soc. London Ser. A* 248 (1956) 449.
- [45] G.M. Bell, S. Levine, *Trans. Faraday. Soc.* 53 (1957) 143.
- [46] G.M. Bell, S. Levine, *Trans. Faraday. Soc.* 54 (1958) 785.
- [47] G.M. Bell, S. Levine, *Trans. Faraday. Soc.* 54 (1958) 975.
- [48] Z. Adamczyk, P. Warszyński, *Adv. Colloid Interface Sci.* 63 (1996) 41.
- [49] G. Frens, J.Th.G. Overbeek, *J. Colloid Interface Sci.* 38 (1972) 335.
- [50] G. Kar, S. Chander, T.S. Mika, *J. Colloid Interface Sci.* 44 (1973) 347.
- [51] D.J.C. Chan, D.J. Mitchel, *J. Colloid Interface Sci.* 95 (1983) 193.
- [52] D. McCormak, S.L. Carnie, D.Y.C. Chan, *J. Colloid Interface Sci.* 169 (1995) 177.
- [53] S. Levine, A. Suddaby, *Proc. Phys. Soc.* 64 (1951) 287.
- [54] S. Levine, A. Suddaby, *Proc. Phys. Soc.* 64 (1951) 431.
- [55] J.E. Jones, S. Levine, *J. Colloid Interface Sci.* 30 (1969) 241.
- [56] E.P. Honig, P.M. Mul, *J. Colloid Interface Sci.* 36 (1971) 259.
- [57] O.F. Devereux, P.L. de Bruyn, *Interactions of Plane-parallel Layers*, M.I.T. Press, Cambridge, MA, 1963.
- [58] R. Hogg, T.W. Healy, D.W. Furstenuau, *Trans. Faraday Soc.* 62 (1966) 1638.

- [59] G.R. Wiese, T.W. Healy, *Trans. Faraday Soc.* 66 (1970) 490.
- [60] S. Usui, *J. Colloid Interface Sci.* 44 (1973) 107.
- [61] J. Gregory, *J. Colloid Interface Sci.* 51 (1975) 44.
- [62] D.C. Prieve, E. Ruckenstein, *J. Colloid Interface Sci.* 63 (1978) 317.
- [63] H. Oshima, *Colloid Polym. Sci.* 252 (1974) 158.
- [64] H. Oshima, *Colloid Polym. Sci.* 253 (1975) 150.
- [65] H. Oshima, *Colloid Polym. Sci.* 254 (1976) 484.
- [66] H. Oshima, *Colloid Polym. Sci.* 257 (1979) 630.
- [67] Z. Adamczyk, B. Siwek, M. Zembala, P. Belouschek, *Adv. Colloid Interface Sci.* 48 (1994) 151.
- [68] T. Sugimoto, *Adv. Colloid Interface Sci.* 28 (1987) 65.
- [69] J.J. Peters, *J. Colloid Interface Sci.* 50 (1975) 296.
- [70] E. Matijević, R.S. Sapienszko, J.B. Melville, *J. Colloid Interface Sci.* 50 (1975) 567.
- [71] E. Matijević, P. Schreiner, *J. Colloid Interface Sci.* 63 (1978) 509.
- [72] S. Hamado, E. Matijević, *J. Chem. Soc. Faraday I* 78 (1982) 2147.
- [73] M. Ozaki, S. Kratochvil, E. Matijević, *J. Colloid Interface Sci.* 102 (1984) 146.
- [74] D. Wilhelmy, E. Matijević, *Colloids Surf.* 16 (1985) 1.
- [75] M. Oceana, M. Anders, M. Martinez, C.J. Serna, E. Matijević, *J. Colloid Interface Sci.* 163 (1994) 262.
- [76] C.C. Ho, A. Keller, J.A. Odell, R.H. Otewill, *Colloid Polym. Sci.* 271 (1993) 469.
- [77] A.M. Wirenga, A.P. Philipse, *J. Colloid Interface Sci.* 180 (1996) 360.
- [78] Z. Adamczyk, *Colloids Surf.* 39 (1989) 1.
- [79] L.R. White, *J. Colloid Interface Sci.* 95 (1983) 286.
- [80] Z. Adamczyk, P. Weroński, *Langmuir* 11 (1995) 4400.
- [81] Z. Adamczyk, P. Weroński, *J. Colloid Interface Sci.* 189 (1997) 348.
- [82] S. Bhattacharjee, M. Elimelech, *J. Colloid Interface Sci.* 193 (1997) 273.
- [83] G.M. Bell, S. Levine, L.N. McCartney, *J. Colloid Interface Sci.* 33 (1970) 335.
- [84] H. Oshima, T.W. Healy, L.R. White, *J. Colloid Interface Sci.* 90 (1982) 17.
- [85] A.L. Loeb, J.Th.G. Overbeek, P. Wiersema, *The Electrical Double Layer Around a Spherical Particle*, Press, Cambridge, MA, 1961.
- [86] W.C. Chew, P.N. Sen, *J. Chem. Phys.* 77 (1982) 2042.
- [87] D. Henderson, S.G. Davison, *Physical Chemistry, vol. II, An Advanced Treatise*, Academic Press, New York, 1967.
- [88] C.A. Castillo, R. Rajagopalan, S.C. Hirtzel, *Rev. Chem. Eng.* 2 (1984) 237.
- [89] M.R. Oberholtzer, J.M. Stankovitch, S.L. Carnie, D.Y.C. Chan, A.M. Lenhoff, *J. Colloid Interface Sci.* 194 (1997) 138.
- [90] J.A. Barker, D. Henderson, *J. Chem. Phys.* 47 (1967) 4714.
- [91] S. Levine, *Proc. R. Soc. Ser. A* 70 (1939) 165.
- [92] S. Levine, G.P. Dube, *Trans. Faraday Soc.* 35 (1939) 1125.
- [93] S. Levine, G.P. Dube, *Trans. Faraday Soc.* 35 (1939) 1141.
- [94] S. Levine, G.P. Dube, *Philos. Mag.* 29 (1940) 105.
- [95] H. Oshima, T. Kondo, *J. Colloid Interface Sci.* 155 (1993) 499.
- [96] H. Oshima, T. Kondo, *J. Colloid Interface Sci.* 157 (1993) 504.
- [97] H. Oshima, T. Kondo, *J. Colloid Polym. Sci.* 271 (1991) 1993.
- [98] H. Oshima, T. Kondo, *J. Colloid Interface Sci.* 170 (1995) 432.
- [99] L.N. McCartney, S. Levine, *J. Colloid Interface Sci.* 30 (1969) 345.
- [100] J.E. Sader, S.L. Carnie, D.Y.C. Chan, *J. Colloid Interface Sci.* 171 (1995) 46.
- [101] N.E. Hoskin, *Philos. Trans. R. Soc., London Ser. A* 48 (1956) 433.
- [102] S.L. Carnie, D.Y.C. Chan, J. Stankovich, *J. Colloid Interface Sci.* 65 (1994) 116.
- [103] P. Warszyński, Z. Adamczyk, *J. Colloid Interface Sci.* 187 (1997) 283.
- [104] P. Richmond, *JCS Faraday Trans. II* 70 (1974) 1066.
- [105] P. Richmond, *JCS Faraday Trans. II* 71 (1975) 1154.
- [106] L. Song, P.R. Johnson, M. Elimelech, *Environ. Sci. Technol.* 28 (1994) 1164.
- [107] H. Krupp, *Adv. Colloid Interface Sci.* 1 (1967) 111.

- [108] M. Elimelech, C.R.O. Melia, *Langmuir* 6 (1990) 1153.
- [109] J. Czarnecki, *Adv. Colloid Interface Sci.* 24 (1986) 282.
- [110] J. Czarnecki, P. Warszyński, *Colloids Surf.* 22 (1987) 207.
- [111] M.C. Herman, K.D. Papadopolous, *J. Colloid Interface Sci.* 136 (1990) 385.
- [112] M.C. Herman, K.D. Papadopolous, *J. Colloid Interface Sci.* 142 (1991) 331.
- [113] L. Suresh, K.Y. Walz, *J. Colloid Interface Sci.* 183 (1996) 199.
- [114] L. Suresh, K.Y. Walz, *J. Colloid Interface Sci.* 196 (1997) 177.
- [115] M. Kostaglou, A.J. Karabelas, *J. Colloid Interface Sci.* 151 (1992) 34.
- [116] J. Mahanty, B.V. Ninham, *Dispersion Forces*, Academic Press, New York, 1976.
- [117] R.J. Hunter, *Foundations of Colloid Science*, V.I. Clarendon Press, Oxford, 1986.
- [118] J.N. Israelachvili, *Intermolecular and Surface Forces*, Academic Press, London, 1985.
- [119] J.H. de Boer, *Trans. Faraday Soc.* 2 (1936) 10.
- [120] H.C. Hamaker, *Physica* 4 (1937) 1058.
- [121] E.M. Lifshitz, *Soviet. Phys. JETP* 2 (1956) 73.
- [122] F. London, *Trans. Faraday Soc.* 33 (1937) 8.
- [123] J.H. Schenkel, J.A. Kitchener, *Trans. Faraday Soc.* 35 (1960) 161.
- [124] H.B. Casimir, D. Polder, *Phys. Rev.* 73 (1948) 86.
- [125] A. Suzuki, N.F.H. Ho, W.I. Higuchi, *J. Colloid Interface Sci.* 29 (1969) 552.
- [126] J. Czarnecki, *J. Colloid Interface Sci.* 72 (1979) 361.
- [127] J. Czarnecki, T. Dąbroś, *J. Colloid Interface Sci.* 78 (1980) 25.
- [128] R. Rajagopalan, J.S. Kim, *J. Colloid Interface Sci.* 83 (1981) 428.
- [129] J.S. Kim, R. Rajagopalan, *Colloids Surf.* 4 (1982) 17.
- [130] M. Smoluchowski, *Phys. Z.* 17 (1916) 585.
- [131] Z. Adamczyk, T.G.M. van de Ven, *J. Colloid Interface Sci.* 97 (1984) 68.
- [132] Z. Adamczyk, T. Dąbroś, J. Czarnecki, T.G.M. van de Ven, *J. Colloid Interface Sci.* 97 (1984) 91.
- [133] Z. Adamczyk, T. Dąbroś, J. Czarnecki, T.G.M. van de Ven, *Adv. Colloid Interface Sci.* 19 (1983) 183.
- [134] P. Wojtaszczyk, B. Avalos, J.M. Rubi, *Europhys. Lett.* 40 (1997) 299.
- [135] Z. Adamczyk, B. Senger, J.C. Voegel, P. Schaaf, *J. Chem. Phys.*, in press.
- [136] V.G. Levich, *Physicochemical Hydrodynamics*, Prentice Hall, Engelwood Cliffs, NJ, 1962.
- [137] Z. Adamczyk, J. Petlicki, *J. Colloid Interface Sci.* 118 (1987) 20.
- [138] Z. Adamczyk, *J. Colloid Interface Sci.* 78 (1980) 559.
- [139] Z. Adamczyk, *J. Colloid Interface Sci.* 79 (1981) 381.
- [140] Z. Adamczyk, M. Zembala, B. Siwek, J. Czarnecki, *J. Colloid Interface Sci.* 10 (1986) 188.
- [141] T. Dąbroś, T.G.M. van de Ven, *Colloid Polym. Sci.* 261 (1983) 694.
- [142] T. Dąbroś, T.G.M. van de Ven, *Physicochem. Hydrodyn.* 8 (1987) 161.
- [143] Z. Adamczyk, L. Szyk, P. Warszyński, *Colloids Surf.* 75 (1993) 185.
- [144] Z. Adamczyk, L. Szyk, P. Warszyński, *J. Colloid Interface Sci.* 209 (1999) 350.
- [145] G.L. Natanson, *Dokl. Nauk. SSSR* 112 (1957) 100.
- [146] M. Leveque, *Ann. Mines* 13 (1928) 201.
- [147] Z. Adamczyk, B. Siwek, M. Zembala, P. Warszyński, *J. Colloid Interface Sci.* 130 (1989) 578.
- [148] E. Ruckenstein, D.C. Prieve, *J. Chem. Soc. Faraday II* 69 (1973) 1522.
- [149] L.A. Spielman, S.K. Friedlander, *J. Colloid Interface Sci.* 46 (1974) 22.
- [150] B.D. Bowen, S. Levine, N. Epstein, *J. Colloid Interface Sci.* 54 (1976) 375.
- [151] E. Ruckenstein, *J. Colloid Interface Sci.* 66 (1978) 531.
- [152] T. Dąbroś, Z. Adamczyk, *Chem. Eng. Sci.* 34 (1979) 1041.
- [153] Z. Adamczyk, T.G.M. van de Ven, *J. Colloid Interface Sci.* 80 (1981) 340.
- [154] Z. Adamczyk, T.G.M. van de Ven, *J. Colloid Interface Sci.* 84 (1981) 497.
- [155] M. Elimelech, *L. Song, Sep. Technol.* 2 (1992) 2.
- [156] M. Elimelech, *J. Colloid Interface Sci.* 164 (1994) 190.
- [157] D.C. Prieve, M.J. Lin, *J. Colloid Interface Sci.* 76 (1980) 32.
- [158] L.A. Spielman, J.A. Fitzpatrick, *J. Colloid Interface Sci.* 42 (1973) 607.
- [159] B. Widom, *J. Chem. Phys.* 58 (1973) 4043.
- [160] J. Feder, *J. Theor. Biol.* 87 (1980) 237.

- [161] Y. Pomeau, *J. Phys. A* 13 (1980) 193.
- [162] R.H. Swendsen, *Phys. Rev. A* 24 (1981) 504.
- [163] E.L. Hinrichsen, J. Feder, T. Jossang, *J. Stat. Phys.* 11 (1986) 793.
- [164] P. Schaaf, J. Talbot, *J. Chem. Phys.* 91 (1989) 4401.
- [165] P. Schaaf, J. Talbot, *Phys. Rev. Lett.* 62 (1989) 175.
- [166] J. Talbot, G. Tarjus, P. Schaaf, *Phys. Rev. A* 40 (1989) 4808.
- [167] J. Talbot, P. Schaaf, G. Tarjus, *Mol. Phys.* 72 (1991) 1397.
- [168] G. Tarjus, P. Viot, S.M. Ricci, J. Talbot, *Mol. Phys.* 73 (1991) 773.
- [169] P. Viot, G. Tarjus, S.M. Ricci, J. Talbot, *J. Chem. Phys.* 97 (1992) 5212.
- [170] S.M. Ricci, J. Talbot, G. Tarjus, P. Viot, *J. Chem. Phys.* 97 (1992) 5219.
- [171] J.W. Evans, *Rev. Modern Phys.* 65 (1993) 1281.
- [172] Z. Adamczyk, P. Weroński, *J. Chem. Phys.* 105 (1996) 5562.
- [173] Z. Adamczyk, M. Zembala, B. Siwek, P. Warszyński, *J. Colloid Interface Sci.* 140 (1990) 123.
- [174] M.R. Bohmer, E.A. van der Zeeuw, G.J.M. Koper, *J. Colloid Interface Sci.* 197 (1998) 242.
- [175] M.R. Bohmer, *J. Colloid Interface Sci.* 197 (1998) 251.
- [176] Z. Adamczyk, B. Siwek, M. Zembala, *J. Colloid Interface Sci.* 195 (1997) 261.
- [177] P. Schaaf, A. Johner, J. Talbot, *Phys. Rev. Lett.* 66 (1991) 1603.
- [178] B. Senger, P. Schaaf, J.C. Voegel, A. Johner, A. Schmitt, J. Talbot, *J. Chem. Phys.* 97 (1992) 3813.
- [179] P. Warszyński, *Colloids Surf.* 39 (1989) 79.
- [180] T. Dąbroś, T.G.M. van de Ven, *Colloids Surf.* B75 (1993) 95.
- [181] Z. Adamczyk, B. Siwek, M. Zembala, *J. Colloid Interface Sci.* 151 (1992) 351.
- [182] Z. Adamczyk, B. Siwek, L. Szyk, *J. Colloid Interface Sci.* 174 (1995) 130.
- [183] B. Vincent, C.A. Young, Th.F. Tadros, *JCS Faraday I* 76 (1980) 665.
- [184] G.R. Joppien, *J. Phys. Chem.* 82 (1978) 2210.
- [185] T. Arai, W. Norde, *Colloids Surf.* 51 (1990) 1.
- [186] A.V. Engersma, R.L.J. Zsom, W. Norde, J. Lyklema, *Colloids Surf.* 54 (1991) 89.
- [187] A.C. Juriaanse, J. Arends, J.J. Ten Bosch, *J. Colloid Interface Sci.* 76 (1980) 212.
- [188] J.D. Aptel, J.C. Voegel, A. Schmitt, *Colloids Surf.* 29 (1988) 359.
- [189] W.J. Albery, G.R. Kneebone, A.W. Foulds, *J. Colloid Interface Sci.* 108 (1985) 193.
- [190] W.J. Albery, R.A. Fredlein, G.R. Kneebone, G.J. O'Shea, A.L. Smith, *Colloids Surf.* 44 (1990) 337.
- [191] U. Jonsson, I. Ronnberg, M. Malquist, *Colloids Surf.* 13 (1985) 333.
- [192] J.C. Dijt, M.A. Cohen Stuart, J.E. Hofman, G.J. Fleer, *Colloids Surf.* 51 (1990) 141.
- [193] H. Shirahama, J. Lyklema, W. Norde, *J. Colloid Interface Sci.* 139 (1990) 177.
- [194] A.V. Elgersma, R.L.J. Zsom, J. Lyklema, W. Norde, *Colloids Surf.* 65 (1992) 17.
- [195] P. Schaaf, P. Dejardin, A. Schmit, *Rev. Phys. Appl.* 21 (1986) 741.
- [196] P. Schaaf, Ph. Dejardin, A. Schmitt, *Langmuir* 3 (1988) 1128.
- [197] N. de Baillou, J.C. Voegel, A. Schmitt, *Colloids Surf.* 16 (1985) 271.
- [198] J.D. Aptel, J.M. Thomann, J.C. Voegel, A. Schmitt, E.F. Bress, *Colloids Surf.* 32 (1988) 159.
- [199] P. Wojciechowski, J.L. Brash, *J. Biomater. Sci. Polym. Edn.* 2 (1991) 203.
- [200] F. Yan, Ph. Dejardin, *Langmuir* 7 (1991) 2230.
- [201] B.D. Bowen, N. Epstein, *J. Colloid Interface Sci.* 72 (1979) 81.
- [202] M. Zembala, J.C. Voegel, P. Schaaf, *Langmuir* 14 (1998) 2167.
- [203] R. Wehn, D. Woermann, *Ber. Bunsenges. Phys. Chem.* 90 (1986) 121.
- [204] M.A. Cohen Stuart, J.W. Mulder, *Colloids Surf.* 15 (1985) 49.
- [205] W. Norde, E. Rouwendel, *J. Colloid Interface Sci.* 139 (1990) 169.
- [206] M. Zembala, Ph. Dejardin, *Colloids Surf. B* 3 (1994) 119.
- [207] J. Siollema, H.J. Busscher, *Colloids Surf.* 47 (1990) 323.
- [208] J. Siollema, H.J. Busscher, *Colloids Surf.* 47 (1990) 337.
- [209] J.M. Meinders, J. Noordmans, H.J. Busscher, *J. Colloid Interface Sci.* 152 (1992) 265.
- [210] C.A. Johnson, A.M. Lenhoff, *J. Colloid Interface Sci.* 179 (1996) 587.
- [211] J.K. Marshall, J.A. Kitchener, *J. Colloid Interface Sci.* 22 (1966) 342.
- [212] M. Hull, J.A. Kitchener, *Trans. Faraday Soc.* 65 (1969) 3093.
- [213] Z. Adamczyk, A. Pomianowski, *Powder Technol.* 27 (1980) 125.
- [214] S. Harley, D.W. Thompson, B. Vincent, *Colloids Surf.* 62 (1992) 163.

- [215] Z. Adamczyk, B. Siwek, L. Szyk, M. Zembala, J. Chem. Phys. 105 (1996) 5552.
- [216] S. Varennes, T.G.M. Van de Ven, Physicochem. Hydr. 9 (1987) 537.
- [217] G.M. Litton, T.M. Olson, Environ. Sci. Technol. 27 (1992) 185.
- [218] Z. Adamczyk, B. Siwek, P. Weroński, M. Zembala, Progress Colloid Polym. Sci. 111 (1998) 41.
- [219] P.R. Johnson, M. Elimelech, Langmuir 11 (1995) 801.
- [220] J.J. Ramsden, Phys. Rev. Lett. 71 (1993) 295.
- [221] Z. Adamczyk, B. Siwek, M. Zembala, P. Weroński, Langmuir 8 (1992) 2605.
- [222] Z. Adamczyk, B. Siwek, M. Zembala, P. Weroński, J. Colloid Interface Sci. 185 (1997) 236.
- [223] J. Feder, J.J. Giaever, J. Colloid Interface Sci. 78 (1980) 144.
- [224] G.Y. Onoda, E.G. Liniger, Phys. Rev. A 33 (1986) 715.
- [225] A.P. Thompson, E.D. Glandt, Phys. Rev. A 46 (1992) 4639.
- [226] H.S. Choi, J. Talbot, G. Tarjus, P. Viot, J. Chem. Phys. 99 (1993) 9296.
- [227] Z. Adamczyk, B. Siwek, M. Zembala, J. Colloid Interface Sci. 198 (1998) 193.
- [228] Z. Adamczyk, L. Szyk, J. Colloid Interface Sci. to be published.